Structured Reactors for Deactivating Systems in Fine Chemistry?

Nakul Thakar

Structured Reactors for Deactivating Systems in Fine Chemistry? Nakul Thakar

Stellingen behorende bij het proefschrift

Gestructureerde reactoren voor deactiverende systemen in de fijn-chemische industrie?

door Nakul Thakar

1. Helaas zijn de juiste reactiepaden voor aromatische keton hydrogenaties slechts zelden opgehelderd, terwijl ze cruciaal zijn om betrouwbare kinetische modellen te verkrijgen.
   Hoofdstuk 2, 3 en 4 van dit proefschrift.
   S. P. Mathew, M.V. Rajashekharam en R. V. Chaudhari, Catal. Today 49 (1999) 49.

2. Het gebruik van alleen kinetische data en modellen om zo het mechanisme van de directe hydrogenolyse van de carbonyl groep van acetofenon naar ethylbenzeen te bepalen is onjuist, directe experimentele bevestiging is essentieel.
   M. Bejblová, P. Zámostny, L. Červeny en J. Čejka, Collect. Czech. Chem.Commun. 68 (2003) 1969.

3. De verschillende reactiepaden die worden waargenomen over Pd/C en Pd/SiO_2 tonen aan dat het effect van de drager nooit vergeten moet worden bij het onderzoeken van de deactivering en kinetiek van heterogeen gekatalyseerde reacties.
   Hoofdstuk 2, 3 en 4 van dit proefschrift.

4. Tenzij rekening gehouden wordt met de aanwezigheid van de katalysator in de nauwelijks toegankelijke macroporiën van cordieriet monolieten, zullen complexe mathematische vergelijkingen om de katalysatoreffectiviteit te schatten voor niet-uniforme kanaal geometriën nog steeds leiden tot verkeerde resultaten.
   R. E. Hayes, B. Liu en M. Votsmeier, Chem. Eng. Sci. 60 (2005) 2037.

5. Alhoewel het gebruikelijk is om het effect op het tussenproduct te bestuderen tijdens kinetische studies aan serie reacties in hydrogenering (A→ B→ C) zou, om misinterpretatie te voorkomen, ook experimenteel bevestigd moeten worden dat het tussenproduct (B) niet dehydrogeneert naar het originele reactant (A) bij de reactie temperatuur.
   Hoofdstuk 4 van dit proefschrift.

6. Het verbeteren van de bestaande extrusietechnologie om direct cordieriet monolieten met ronde kanalen en zonder macroporiën te produceren zou veel praktischer zijn dan de huidige praktijk om vulmiddelen te gebruiken voor het dichten van macroporiën en het rondmaken van de vierkante kanaalgeometrie in commercieel verkrijgbare cordieriet monolieten.
   Hoofdstuk 5 van dit proefschrift.

7. Alhoewel monolieten theoretisch gebruikt kunnen worden voor deactiverende systemen in de fijnchemische industrie, suggereert de huidige proceseconomie dit vaak van niet.

8. Katalysatordeactivering in chemische processen is een probleem analoog aan dat van illegale immigratie waarmee vele landen worden geconfronteerd; het is bijna onmogelijk het probleem kwijt te raken. Men kan alleen proberen het probleem te minimaliseren door de juiste remedies toe te passen.

9. Algemeen gesproken, de instroom van ongeschoolde migranten naar Nederland vertoont een nulde-orde afhankelijkheid met de steeds strengere immigratie politiek.

10. Ook informele discussies in de koffiekamer kunnen op een belangrijke manier bijdragen aan de ontwikkeling van nieuwe wetenschappelijke ideeën.

Deze stellingen worden opponeerbaar en verdedigbaar geacht en zijn als zodanig goedgekeurd door de promotoren, prof. dr. J.A. Moulijn en prof. dr F. Kapteijn.

Propositions accompanying the thesis

Structured Reactors for Deactivating Systems in Fine Chemistry?

by Nakul Thakar

1. Unfortunately, accurate reaction pathways for aromatic ketone hydrogenation are rarely elucidated although they are crucial in obtaining reliable kinetic models.
   Chapters 2, 3 and 4 of this thesis.
   S. P. Mathew, M.V. Rajashekharam and R. V. Chaudhari, Catal. Today 49 (1999) 49.

2. The use of only kinetic data and models to conclude the mechanism of the direct hydrogenolysis of the carbonyl group of acetophenone to ethylbenzene is incorrect, direct experimental confirmation is vital.
   M. Bejblová, P. Zámostny, L. Červeny and J. Čejka, Collect. Czech. Chem. Commun. 68 (2003) 1969.

3. The different reaction pathways observed over Pd/C and Pd/SiO_2 demonstrate that the effect of the support should never be ignored when researching the deactivation and kinetics of heterogeneously catalyzed reactions.
   Chapters 2, 3 and 4 of this thesis.

4. Unless the presence of catalyst inside the hardly accessible macropores of the cordierite monoliths is accounted for, complex mathematical equations to estimate catalyst effectiveness for non-uniform channel geometries will still lead to erroneous results.
   R. E. Hayes, B. Liu and M. Votsmeier, Chem. Eng. Sci. 60 (2005) 2037.

5. Though it is common practice to study the effect of the intermediate product during kinetic studies for the series hydrogenation reactions (A→ B→ C), to avoid misinterpretation, it should also be confirmed experimentally that the intermediate product (B) does not dehydrogenate to the original reactant (A) at the reaction temperature.
   Chapter 4 of this thesis.

6. Improving the existing extrusion technology to directly manufacture round channel cordierite monoliths without macropores would be more practical as opposed to the current practice of using fillers to plug macropores and round off the square channel geometry of commercially available cordierite monoliths.
   Chapter 5 of this thesis.

7. Although monoliths can theoretically be used for deactivating systems in fine chemical industry, the present process economics often suggest otherwise.

8. Catalyst deactivation in chemical processes is a problem analogous to illegal immigration that many countries face, in that it is next to impossible to get rid of the problem. One can only try to minimize the problem by taking suitable remedies.

9. Generally speaking, the influx of unskilled migrants into the Netherlands shows a zero order dependence on the increasingly stringent immigration policies.

10. Informal discussions in the coffee room can also contribute in an important way towards generating new scientific ideas.

These propositions are considered opposable and defendable and as such have been approved by the supervisors, prof. dr. J.A. Moulijn and prof. dr. F. Kapteijn.

STRUCTURED REACTORS FOR DEACTIVATING SYSTEMS IN FINE CHEMISTRY?

STRUCTURED REACTORS FOR DEACTIVATING SYSTEMS IN FINE CHEMISTRY?

PROEFSCHRIFT

ter verkrijging van de graad van doctor
aan de Technische Universiteit Delft
op gezag van de Rector Magnificus prof. dr. ir. J. T. Fokkema,
voorzitter van het College voor Promoties,

in het openbaar te verdedigen op 25 September 2007 om 15:00 uur

door

Nakul THAKAR

Bachelor of Engineering (Polymer), University of Pune, India
geboren te Pune, India

Dit proefschrift is goedgekeurd door de promotoren:
Prof. dr. J. A. Moulijn
Prof. dr. F. Kapteijn

Samenstelling promotiecommissie:

Rector Magnificus	voorzitter
Prof. dr. J. A. Moulijn	Technische Universiteit Delft, promotor
Prof. dr. F. Kapteijn	Technische Universiteit Delft, promotor
Prof. dr. B. Weckhuysen	Universiteit Utrecht
Prof. dr. I. W. C. E. Arends	Technische Universiteit, Delft
Dr. A. J. A. van der Weerdt	Quest International
Dr. A. E. W. Beers	BASF Nederland B.V.
Dr. G. Mul	Technische Universiteit Delft
Prof. dr. S. J. Picken	Technische Universiteit Delft (reservelid)

This research was financially supported by STW, BASF Nederland B.V. and Quest International through project DPC 5772.

Keywords: Fine chemistry, Deactivation, Palladium, Structured Reactors

ISBN 9789064641701

Contents

Preface

1. Aim of the research

The original aim of this research was to develop a flexible multi-step reactor system for the fine chemicals industry. In the fine chemicals and pharmaceuticals industry, syntheses of complex molecules consist of a number of different reaction steps, which are commonly performed in series in batch (slurry) reactors. The disadvantage of this manner of production is that in between reactions, costly (catalyst) separations have to be carried out and intermediate products may need to be stored. The development of a multi-functional structured (monolithic) reactor, in which all the reaction steps are carried out in series in a single pass (one-through flow operation) without intermediate catalyst separation, is therefore highly advantageous.

Monolithic catalysts are an interesting alternative for conventional slurry catalysts in heterogeneous catalysis since the catalyst is coated onto the monolithic support and in effect, a fixed bed reactor can be developed using slurry catalyst particles. The novel monolithic reactor system to be developed would consist of monoliths coated with different catalysts, simply to be taken off the shelf (as one now does for a number of 'standard' slurry catalysts) and linked in the correct order to carry out complete conversion. This concept was to be demonstrated for the synthesis of Ibuprofen, a well-known non-steroidal anti-inflammatory drug. The synthesis of Ibuprofen consists of a liquid-liquid reaction as well as a gas-liquid reaction and both homogeneously and heterogeneously catalyzed reactions, thereby covering the most relevant catalytic systems.

This project was a joint effort between the Catalysis Engineering group at the Delft University of Technology and the Metal Mediated Synthesis group at the Utrecht University. The knowledge of chemistry and heterogenization of homogeneous catalysts of Utrecht was to be integrated with the Delft knowledge on monolithic catalysts and reaction engineering, together covering all aspects of the project. This project was sponsored by STW under project code DPC 5772 and by BASF Nederland B.V. and Quest International (ICI).

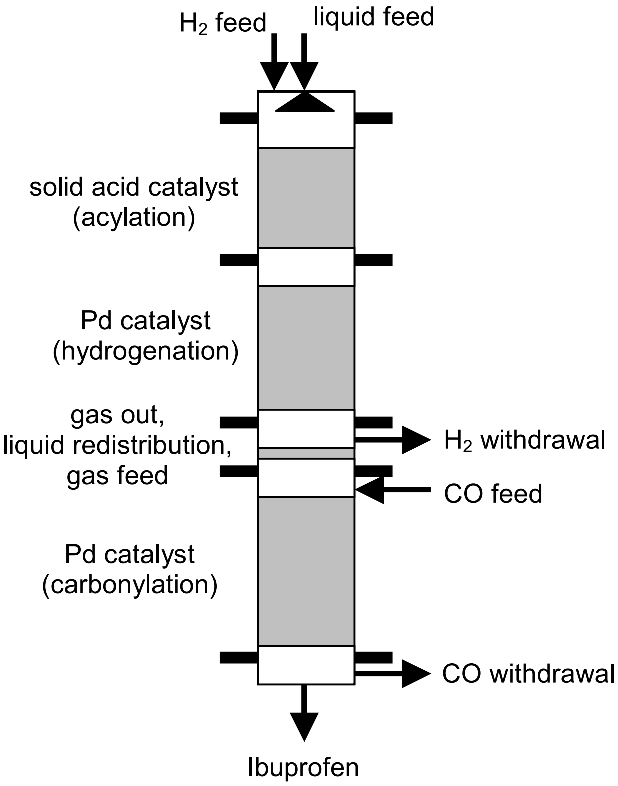

Figure 1: Schematic of a multi-functional monolithic reactor

2. Novel monolith reactor

Figure 1 gives an impression of how a down flow monolithic multi-step reactor can be assembled out of different flanged segments. As down flow operation is most convenient for gas-liquid reactions in a monolith, the high flow rates (and consequently the lower residence times) in this type of operation requires high catalytic activities. Different temperatures for the different reactions can easily be obtained by using heat-exchanger segments. Intermediate feeding of reactants can be possible by pumping them into the reactor at a side-connection. The total reactor system will look like small building blocks containing heaters/coolers/feed/catalyst segments, simply flanged together allowing for a maximum flexibility.

3. Project Execution

Most of the pharmaceutical drugs are chiral molecules and it is the (*S*)-enantiomer that is responsible for the desired therapeutic effect, whereas the (*R*)-enantiomer can have a fatal effect. However, Ibuprofen can be administered as a racemate because the inactive (*R*)-enantiomer is not harmful as it undergoes *in vivo* inversion of configuration to form the active (*S*)-enantiomer. The choice of Ibuprofen synthesis as a model reaction system was based on the fact that the chirality of the molecule would not be a critical issue.

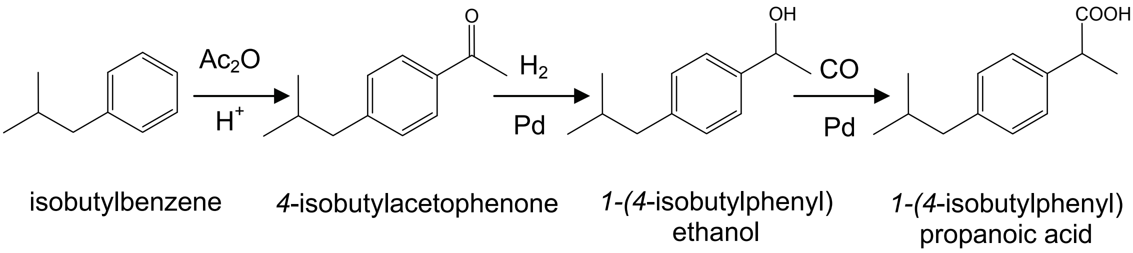

Scheme 1: Multi-step synthesis of *1*-(*4*-isobutylphenyl) propanoic acid (Ibuprofen)

The synthesis of Ibuprofen consists of three sequential reaction steps (Scheme 1) (*i*) acylation of isobutylbenzene to *4*-isobutylacetophenone (*ii*) selective hydrogenation of *4*-isobutylacetophenone to *1*-(*4*-isobutylphenyl) ethanol and (*iii*) hydroxycarbonylation of *1*-(*4*-isobutylphenyl) ethanol to yield Ibuprofen.

A thorough literature survey on the three reaction steps indicated that a one-through flow operation without integrated product separation and reactant addition steps was unfeasible for several reasons.

(i) If the acetic acid by-product formed during the acylation of isobutylbenzene with acetic anhydride (step 1) was not separated from the reaction mixture, prior to the hydrogenation of *4*-isobutylacetophenone (step 2), it would surely have a negative effect on the yield of the *1*-(*4*-isobutylphenyl) ethanol (formed by hydrogenation of *4*-isobutylacetophenone) by promoting the dehydration of the alcohol.

(ii) An alkaline medium would maximize the yield of the desired hydrogenation product *1*-(*4*-isobutylphenyl) ethanol, but acidic promoters (tosylic acid) are known to tremendously enhance the catalytic activity for the subsequent carbonylation step.

So, clearly a tuned process design would be required.

A crucial requirement to justify the use of a one-through flow system consisting of any fixed bed reactor, e.g. monoliths, over slurry catalysts is the stability of the catalyst. Preliminary experiments were performed using slurry catalysts to investigate the acylation of isobutylbenzene (step 1) over a wide variety of zeolites (HBEA and HY of varying Si/Al ratios, nafion silica). Apart from severe catalyst deactivation, a very poor yield of less than 20 % of the desired *4*-isobutylacetophenone was observed in all the cases. Reports in the literature also confirmed the poor performance of zeolites for non-activated (non-phenolic) substrates. Similarly, severe catalyst deactivation was also observed after a single run during the hydrogenation of *4*-isobutylacetophenone. The Utrecht group focussed on the immobilisation of a palladium picolinic acid complex, which has been shown to be the best catalyst for the regioselective hydroxycarbonylation of aryl ethanol and a number of its derivatives. However, immobilizing of this homogeneous catalyst was not feasible.

So, it was concluded that the development of a monolithic one-through flow reactor for the multi-step synthesis of Ibuprofen would be impractical.

The first two steps in the multi-step synthesis of Rossitol (a 3-alkylcycloalkanol used as a fragrance compound) were also investigated as a potential model reaction to demonstrate the concept of a novel monolithic reactor. This reaction involved the sequential acylation of 2-methylanisole (**1**) followed by the complete reduction of the resulting aromatic ketone (**2**) to the substituted methylcyclohexane (**4**) (Scheme 2). An attractive aspect was that the reaction was chemically compatible (the acid by-product of the acylation step could promote the dehydration of the aromatic alcohol to give the desired intermediate product (**3**). However, severe catalyst deactivation was observed after a single hydrogenation run for this system also. The use of monoliths for such a severely deactivating system is unattractive.

It was realized that there were similarities between the two multi-step syntheses presented here. Both these systems involved hydrogenation of

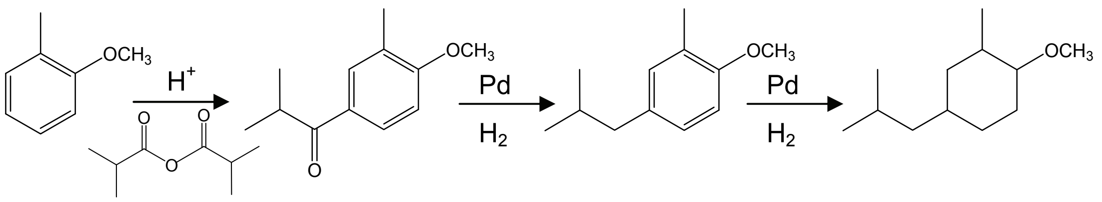

2-methyl anisole
(1)

1-(4-methoxy-3-methylphenyl) 2-methyl -1- propanone
(2)

4-(2-methylpropyl)-1-methoxy -2-methylbenzene
(3)

4-(2-methylpropyl)-1-methoxy-2-methylcyclohexane
(4)

Scheme 2: Multi-step synthesis of intermediates in Rossitol production aromatic ketones and suffered severe catalyst deactivation after a single hydrogenation run. Thus for this class of reactions, catalyst stability is the key issue and it became clear that the investigation of the deactivation behaviour during the hydrogenation of aromatic ketones in general was interesting both from a scientific and a practical point of view and the first step towards utilizing monoliths for such reactions.

There were a number of other aspects in the hydrogenation of 4-isobutylacetophenone (step 2 of Ibuprofen synthesis) such as the accurate reaction pathway, catalyst deactivation and kinetic modelling that were not dealt with in the literature. So one of the modified objectives of this research was to elucidate the above-mentioned aspects for the hydrogenation of 4-isobutylacetophenone using slurry catalysts.

A few important aspects need to be addressed to enable the efficient use of monoliths for reactions in fine chemistry. Due to the low surface area of the monoliths ($< 4\ m^2/g$), a high surface area support is wash coated onto the monolith structure prior to deposition of the active metal. The application of the washcoat to the commercially available square channel monoliths leads to a non-uniform thickness of the coat layer (Figure 2). The longer effective diffusion length in the corners (L′) can have a negative effect by theoretically lowering the desired intermediate product yield by internal diffusion limitations, especially for fast, diffusion-limited reactions. Although the use of monoliths eliminates the catalyst separation step, it is nevertheless important to optimize the channel geometry of the monoliths to maximize the desired product yield. Thus, another objective of this research was to optimize the

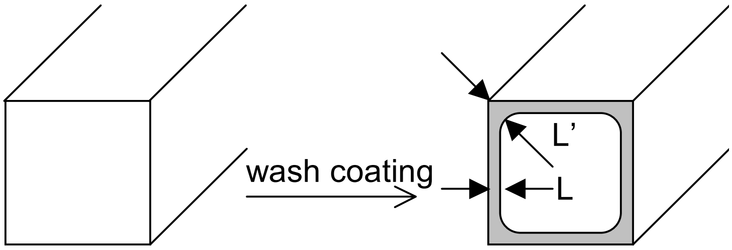

Figure 2: Unequal wash coat thickness on a conventional monolith channel ($L \neq L'$)

channel geometry of the conventional monoliths to improve their performance in the selective hydrogenations. These optimized monoliths were then compared with the conventional ones for the fast, diffusion-limited selective hydrogenation of a non-deactivating alkyne system.

4. Outline of the thesis

The two major goals of this research were investigating the catalyst deactivation and related aspects for the hydrogenation of *4*-isobutylacetophenone, and optimizing the channel geometry and catalyst coating technique on monoliths.

Two reaction systems were investigated (*i*) selective hydrogenation of *4*-isobutylacetophenone using slurry catalysts and (*ii*) selective hydrogenation of *3*-methyl-*1*-pentyn-*3*-ol using optimized monolithic catalytic reactors. A parallel research was performed focussing on both, the catalyst deactivation occurring during the hydrogenation of *4*- isobutylacetophenone using slurry catalysts and on optimizing the catalyst coating technique on the monoliths for improved efficiency for the hydrogenation of *3*-methyl-*1*-pentyn-*3*-ol.

Chapter 1 contains a general introduction to selective catalytic hydrogenation, an overview of the various metal catalysts that are commonly used for the hydrogenation of aromatic functional groups and the different catalyst deactivation mechanisms observed in the bulk and fine chemical reactions.

The pathway of transformation of *1*-(*4*-isobutylphenyl) ethanol to *4*-isobutylethylbenzene (either by direct hydrogenolysis or by dehydration-hydrogenation) over Pd/SiO_2, Pd/C and unsupported Pd black is investigated in ***Chapter 2***. A deuteration study coupled with multinuclear NMR analysis allowed us to conclusively state the pathway of C-O bond scission of *1*-(*4*-isobutylphenyl) ethanol. The knowledge of the exact reaction pathway was important to understand the catalyst deactivation, which is studied in depth in the subsequent chapter.

Chapter 3 deals with testing various supported Pd catalysts for the hydrogenation of *4*-isobutylacetophenone. A Pd/SiO_2 catalyst was prepared and compared with commercially available Pd/C, Pd/$CaCO_3$ and Pd black. The highest activity and selectivity in a reasonable time period were obtained with a Pd/SiO_2 catalyst. Severe catalyst deactivation was observed over Pd/SiO_2 as well as over Pd/C and Pd/$CaCO_3$. The fresh and spent Pd/SiO_2 catalysts were thoroughly characterized by a number of thermal (TGA, TPO-MS), microscopic (TEM) and spectroscopic (DRIFT, LEIS) techniques and the cause of catalyst deactivation was proposed.

Having an in-depth knowledge of the reaction pathway and the deactivation mechanism, a comprehensive kinetic model was developed that incorporated the loss of catalytic activity due to deactivation. This is presented in ***Chapter 4***. The experiments were performed over a broad temperature and pressure range and a number of Langmuir-Hinshelwood type models were discriminated using Athena Visual Studio (www.Athenavisualstudio.com). The model was used to predict optimum batch operating conditions to maximize the product *1*-(*4*-isobutylphenyl) ethanol yield for a pure *4*-isobutylacetophenone feed with a deactivating catalyst system.

Chapter 5 deals with the optimization of the channel geometry and catalyst deposition technique on commercially available monoliths to obtain a uniform coating thickness. The effect of the presence of catalyst in the macropores on the catalyst effectiveness is demonstrated by finite element calculations (FEM). The optimized monoliths are then compared with the conventional monoliths for the selective hydrogenation of *3*-methyl-*1*-pentyn-*3*-ol.

Chapter 6 is a wrap up of the thesis, which includes a summary and evaluation of the results obtained. Conceptual reactor designs for operation on an industrial scale are also discussed.

1

Introduction

A general introduction is presented on catalytic hydrogenation reactions and the operating parameters that influence the reaction performance. An overview on the various metal catalysts used for the hydrogenation of various functional groups and commonly observed deactivation mechanisms in the bulk and fine chemical industry is given. An introduction to the batch slurry reactor; the 'workhorse' of the fine chemical industry, and monolithic reactors is also presented.

1. Introduction

The name 'catalysis' was coined by Berzelius in 1836. Towards the end of the eighteenth and the beginning of the nineteenth century, scientists observed that contacting substances in the presence of different metals or oxides led to the formation of different products. An example is the decomposition of alcohol: in the presence of copper or iron, carbon and an inflammable gas were produced, while in the presence of pumice stone, decomposition into ethylene and water was observed [1]. In other words, selectivity was demonstrated.

Amongst the first industrial catalytic processes were the Deacon process (oxidation of HCl into Cl_2) [2] and the production of sulphuric acid [1]. Only after the formulation of the theory of chemical equilibria by Van 't Hoff, a framework for catalyst development became available. This initiated the development of chemical process engineering, as we know it today. Many reasons underlie the development of the science and technology of catalysis. One of the driving forces that should not be overlooked is the availability of the raw materials. Originally, biomass was predominant. Later, coal became the most important industrial feedstock. Subsequently, oil took over the place of coal and the technological scene changed profoundly. More recently, natural gas resources appear to have become much more important than had been expected. In recent years, environmental and sustainability considerations have been the major driving force for novel (often catalytic) processes.

2. Catalyzed Selective Hydrogenations

In organic chemistry, it is common practise to refer to so-called functional groups, which are specific groups of atoms within molecules that are responsible for the characteristic chemical reactions of those molecules. The same functional group will undergo the same or similar chemical reaction(s) regardless of the size of the molecule it is a part of. The commonly occurring functional groups are alkynes, alkenes, aromatics, carbonyls, alcohols, esters, ethers, lactones, carboxylic acids, amines, amides, nitro groups and nitriles. Catalytic hydrogenation involves the addition of hydrogen to a functional group (either in gas or liquid phase), usually in the presence of a solid catalyst, and is one of the most common industrial processes. An overview of the commonly hydrogenated functional groups and the metal catalysts used is presented in Table 1. Catalytic hydrogenation is observed in processes performed in the crude oil refining, petrochemicals as well as fine chemicals and pharmaceuticals industry. A majority of the industrial processes are consecutive liquid-phase hydrogenations in which the liquid reactant is hydrogenated to a desired product, which can undergo further hydrogenation to the undesired product. The goal of selective hydrogenations is thus to maximize the formation of the desired product.

Chemoselective hydrogenation can be defined as the preferential reaction of hydrogen with one of two or more different functional groups, whereas enantioselective hydrogenation is defined as the preferential formation of one enantiomer over another (enantiomers are isomers that are mirror images of one another). Chiral catalysis plays a major role in the synthesis of optically active enantiomers, which is of utmost importance to the pharmaceutical industry. Although chiral (enantioselective) catalysis is generating tremendous academic and industrial interest, this topic is outside the scope of the work presented in this thesis. The selectivity referred to henceforth in this thesis is chemoselectivity, unless specified otherwise.

Two types of selective hydrogenations can further be distinguished (*i*) selective hydrogenation of one particular functional group in the presence of multiple functional groups (e.g. hydrogenation of cinnamaldehyde or citral, that contain an aromatic, a carbonyl and an alkene functional group [3] or hydrogenation of aromatic ketones containing an aromatic as well as a carbonyl functional group [4]) (chemoselectivity) and (*ii*) selective hydrogenation of a functional group to the desired intermediate functional

Table 1: Commonly hydrogenated functional groups and catalysts used

Structure	Functional group	Hydrogenation catalysts	Reference
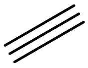	Alkyne	Pd, Pd-Pb, Ni	[5-8]
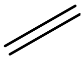	Alkene	Pd	[8]
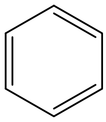	Aromatic	Rh, Ru, Pt, Ni, Pd	[9-12]
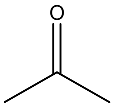	Carbonyl	Pt, Rh, Ru, Ni, Cu	[3,4,8,13,14]
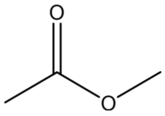	Ester	Cu, Raney Ni	[14]
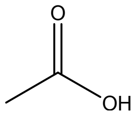	Carboxylic acid	Cr, Pt, Ru-Sn	[15-17]
$-NO_2-$	Nitro	Pt, Pd, Ni, Au	[18-20]
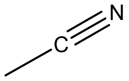	Nitrile	Pt, Rh, Ru, Raney Ni	[21-23]

group (e.g. selective hydrogenation of alkynes to alkenes or dienes to monoenes [24]).

The noble metals (ruthenium, rhodium, palladium and platinum) are exceptionally active hydrogenation catalysts, and most functional groups can be reduced under mild conditions over one or another of these catalysts.

3. The toolbox of the catalytic chemist

Blaser and Studer [25] have defined the 'toolbox' of the catalytic chemist as the set of various tools available for developing catalysts that make a desired transformation technically feasible.

3.1. Design parameters for heterogeneous catalytic systems

The two important types of heterogeneous catalysts are supported and unsupported, with the former being further divided into those for use in slurry processes and those for use in fixed-bed operations. Unsupported metal catalysts (e.g. Pd black) are used less efficiently than supported metal catalysts and recovery losses are likely to be higher. It is not surprising that most unsupported catalysts are low-cost materials (Ni). One the one hand, the advantage of unsupported catalysts is that they exhibit good settling properties, important in slurry operations. On the other hand, supported metal catalysts have an advantage over unsupported metal catalysts, in that the support permits greater efficiency in use of the active metal by increasing the active metal surface area and provides flexibility with respect to the active phase (e.g. egg-shell catalysts for fast, diffusion-limited reactions and egg yolk catalysts if catalyst attrition is an important issue). The most commonly used support materials are activated carbon, SiO_2 and γ-Al_2O_3, which offer a high surface area to create a high dispersion of the noble metal catalyst [26]. However, low surface area supports (α-Al_2O_3, $CaCO_3$) have also been applied for selective hydrogenations of acetylene and diene impurities in alkene streams [6,27,28]. Supports may also have an effect on the catalytic performance of the active component or induce reactions themselves (e.g. in hydrocracking reactions, the scission of the C-C bond of heavy aromatic fractions present in crude oil takes place on the acidic support, whereas the hydrogenation occurs on the metal function).

Of the many parameters of a heterogeneous hydrogenation catalyst that affect its performance, the following are the most important ones.

(i) *Type of metal*: The metals used most often are Pd, Pt, Ni, Cu, Rh and Ru. The important parameters for the active metal are the metal surface area, dispersion (typically only 10 – 60% of the metal atoms are exposed), the crystallite size (typically in the range of 2 to 20 nm), the location in the pores of the support and the oxidation state (reduced or unreduced).

(ii) *Metal loading* of supported catalysts: These are typically in the range of 0.1 – 5 wt.%, although higher loadings have been used in exceptional cases (e.g. the Pearlman catalyst ($Pd(OH)_2/C$) often used for debenzylation reactions has a Pd content of 20 wt.%, or high (> 20 wt.%) Pt loadings in fuel cells)

(iii) *Type of support (active carbon, silica, alumina)*: The important support parameters are the particle size (for slurry catalysts typically 1 – 100 μm), the surface area (typically in the range of 100 – 1500 m^2/g), pore structure (pore volume, pore size distribution) and acid-base properties.

3.2. Catalyst modifiers or promoters

In cases where a commercially available catalyst lacks a desired property or selectivity, the addition of a modifier is an interesting option. Both organic molecules (e.g. amines, chiral modifiers such as cinchona alkaloids) and inorganic salts/metals are known for this purpose. The modifier can either be added to the catalysts before it is introduced into the reaction (e.g. Lindlar catalyst where Pd is alloyed with Pb [6]) or can be added directly to the reaction mixture as process modifier [29,30].

3.3. Reaction Conditions

The catalyst performance can be optimized by choosing a suitable reaction system for the particular catalyst and optimal reaction conditions. Important parameters are the solvent, reaction temperature, hydrogen pressure (in case of hydrogenations), substrate and catalyst concentration, and process modifiers.

(*i*) *Solvent choice*

Very often, the choice of the solvent is the most important of these parameters since an optimal solvent can improve catalyst performance. Mukherjee and Vannice [31] recently studied the solvent effects during the liquid phase citral hydrogenation over Pt/SiO_2 by comparing the specific activity and selectivity in eight different solvents (having significantly different physical and electronic properties) and observed a three-fold variation in the initial turn over frequencies (TOF) over the studied temperature range. The rate dependence on citral also fell between one-half to first order, emphasizing the importance of selecting the appropriate solvent. An improper solvent choice (non-inert) can also have a negative effect on product selectivity (e.g. esters may be formed during catalytic hydrogenation of carboxylic acids in an alcoholic solvent). The solvent can also be used to moderate a temperature rise for highly exothermic reactions by its evaporation.

(*ii*) *Reaction temperature, hydrogen pressure and catalyst concentration*

For exothermic reactions, the hydrogenation rate increases with an increase in temperature. However, there is also an increased possibility of catalyst deactivation, lower product selectivity or an increase in the number of side reactions.

The dependence of the reaction rate on hydrogen pressure is usually between 0 and 1. A higher hydrogen pressure nearly always results in higher rates.

The amount of catalyst affects the reaction rate, productivity and in commercial operations, the economics of the process. Sometimes, overhydrogenation of the desired intermediate product maybe decreased and selectivity improved by the use of small amounts of catalyst.

These three process variables are usually inter-related and the optimization order is usually hydrogen pressure, reaction temperature and amount of catalyst (noble metals or less active catalysts).

3.4. Reaction control (end point)

Monitoring the progress of a catalytic reaction can be difficult, especially if the catalyst is air-sensitive or if the reaction is carried out in a sealed reactor. Nevertheless, in the laboratory it is usually possible to find a suitable solution (e.g. use of a gas chromatograph, monitoring H_2 consumption using a mass flow meter, or reaction calorimetry). This is by no means the case under the conditions of large-scale production, where one has to rely on relatively inaccurate measurements or defined reaction times. On-line monitoring of the substrate and/or product concentrations could be of great help, especially for reactions where a precise end point control is crucial for high product yields. Here, ATR–FTIR probes can sometimes be very useful for on-line spectroscopy [32].

4. Catalyst Deactivation

Although a high selectivity along with a reasonably high activity are the hallmarks of a good catalyst, it is important that the catalyst retains these properties for some time. In practise however, this is not always the case. Depending on the process used the catalyst cycle life may vary from a few seconds, as in fluid catalytic cracking (FCC), to several years, as in ammonia synthesis. The importance of catalyst stability is often underestimated, not only in academia but also in certain sectors of the industry, notably in the fine chemicals industry. In bulk chemicals production, its importance has generally been acknowledged due to the general preference for a continuous mode of process operation. However, in fine chemicals production, chemists often look upon the catalyst as a reactant: when it does not function anymore, it is disposed and a new catalyst is added. So, it is understandable that catalyst stability is not always a point of strong concern. This attitude is expected to change with increasing environmental awareness.

The five main causes of catalyst deactivation are *poisoning*, *fouling*, *thermal degradation (sintering)*, *mechanical damage* and *corrosion/leaching* by the reaction mixture [33]. It should be noted that the causes listed are often not independent. A good example is the adsorption of sulphur on a platinum catalyst; sulphur poisons the Pt sites, and at the same time causes the Pt clusters to become more mobile leading to sintering [34].

(*i*) *Poisoning*

Poisoning is defined as catalyst deactivation by strong adsorption of reactants, products and usually by impurities in the feed. It is important to distinguish between temporary and permanent poisoning. In the former situation, the poison can be removed, whereas this is not the case in the latter situation. The distinction between temporary and permanent poisoning is not always straightforward as compounds that are strong poisons at low temperatures are less harmful in high-temperature processes (e.g. although acetylenes and dienes readily polymerize to form carbonaceous deposits on catalysts at low temperatures, higher temperatures help to remove these deposits by depolymerization). It is quite common for poisoning to occur by strong adsorption of traces of feed impurities. Poisoning by sulphur compounds is encountered in many large-scale processes using metal catalysts (H_2S formation in hydrodesulphurization reactions).

Poisoning can also be advantageous in that the addition of a poison gives the option to enhance selectivity by alleviating diffusion limitations, although this usually is at the expense of some activity. The addition of a small amount of Co on a Pd catalyst can improve the selectivity of acetylene hydrogenation relative to ethylene [35]. In such cases, the term modifier better describes the process than poison. It is also possible that a strongly adsorbing species leads to an increase in activity. For instance, in the production of amines by nitrile hydrogenation, the addition of a small amount of an alkali hydroxide to the reactant feed improves the activity of the metal catalyst and the selectivity to the desired primary amine [35].

(*ii*) *Fouling*

Fouling covers all phenomena where the catalyst surface is covered with a deposit whose origin is not always related to processes on the catalyst. An example is the deposition of dust (e.g. from mechanical wear of upstream equipment). In high temperature processes, large molecules can be formed by free radical mechanisms and subsequent deposition on the catalyst particles. In the aforementioned examples, although the catalyst probably does not play a major role, the catalyst itself is responsible for fouling by undesired by-products that lead to deposits. In most of the catalytic processes in the petroleum refinery, fouling by 'coke' deposition plays a major role. Coke is a term that is used in many meanings. In fact, classification of coke under fouling can be disputed. Poisoning or self-poisoning are better terms. The coke associated with high temperature reactions is produced by unwanted polymerization and dehydrogenation of organic molecules present in the feed or formed as a product. These reactions leave a layer of highly hydrogen deficient carbonaceous material on the catalyst surface, rendering the active sites inaccessible.

Coke formation is not limited to petroleum processing. For instance, in alkene reactions over acid sites oligomerization and alkylation reactions will occur. When the products do not desorb, deactivation is observed and the deposit might be referred to as 'coke'. Such type of deactivation (due to oligomerization) is also commonly observed in the fine chemicals industry. In this thesis, a strict distinction is made between 'coke' and oligomers, with 'coke' being defined as the polyaromatic, graphitic compounds formed at elevated temperatures due to polymerization and dehydrogenation reactions and 'oligomers' being defined as large molecular units formed due to condensation type reactions, but not deficient in hydrogen.

A special type of deactivation is due to carbon fiber formation [36]. Depending on the gas phase composition, the active phase decomposes hydrocarbons or CO and forms carbon nanofibers. This process continues until the active phase becomes either encapsulated or the catalyst being completely mechanically destroyed by the expansion process, comparable with polymerization processes. Especially Ni is known to form carbon nanofibers.

(*iii*) *Thermal degradation*

Thermal degradation is a physical process leading to catalyst deactivation because of sintering or evaporation. Sintering is the loss of catalyst active surface area due to crystallite growth of either the support material or the active phase. The most important mechanism for sintering of small particles often is the movement of atoms rather than particles [33]. Sintering resembles crystallization in that the larger particles grow at the expense of smaller ones. Sintering is strongly temperature dependent and the melting point plays a critical role. The so-called Tamman and Hüttig temperatures, indicative for the temperature at which sintering may occur, are directly related to the melting temperature ($T_{\text{Hüttig}} = 0.3T_{\text{melting}}$, $T_{\text{Tamman}} = 0.5\ T_{\text{melting}}$). On reaching the Hüttig temperature, atoms at defects will become mobile. If the Tamman temperature is reached, atoms from the bulk will exhibit mobility, and at the melting temperature the mobility will be so high that liquid phase behaviour is observed. Actually, the temperature at which the solid becomes mobile depends on several factors such as texture, size, morphology and interaction with a support in the case of catalysts. γ-Al_2O_3 (highly porous) is much more sensitive to sintering than α-Al_2O_3 (low porosity). Thermal degradation can occur in all stages of the life cycle of the catalyst. It might occur due to local heating during preparation (calcination), reduction (fresh or passivated catalyst), reaction (hot spots), or regeneration (coke burn-off).

In practice though, mobility is not always undesired and can be advantageously applied to regenerate catalysts in certain cases. An elegant example is the redispersion of Pt in reforming catalysts. During reaction, the dispersion of Pt decreases. Addition of chlorine components maintains a certain mobility of the Pt, keeping it dispersed to a certain extent under reaction conditions. Additionally, by a high temperature regeneration treatment (up to 920 K) in an oxygen containing gas, Pt is slightly vaporized due to the formation of Pt-oxides. Adsorption on active sites of the support takes place and the dispersion is restored.

(*iv*) *Mechanical deactivation*

Mechanical strength is important in giving the catalyst resistance against crushing, e.g. during transport and loading of the catalyst in the reactor. A packed bed of catalyst particles will experience strong stresses in its life cycle: during start-up, it will be heated and thermal expansion of the tube will occur, whereas during cooling down, the opposite will happen. So, it is no surprise that mechanical degradation is observed: during its life cycle, the catalyst is often experiencing harsh conditions.

(*v*) *Corrosion/Leaching*

The reaction medium can sometimes be quite corrosive, which can have a detrimental effect on the catalyst. Considering that the amphoteric alumina dissolves at $pH > 12$ and $pH < 3$, it is not surprising that corrosion/leaching will occur when the pH of the reaction medium approaches 12 or 3. For extremely low or high pH, carbon should be considered as a support, not alumina.

Leaching of active phase into reaction medium is often observed in liquid-phase catalysis. A good example of leaching is the leaching of nickel during solid-catalyzed fat hydrogenation or glucose hydrogenation. This does not apply to palladium, which might be a good reason to replace nickel with palladium [33]. However, hydrogen atoms are known to enter the bulk crystal, forming a palladium hydride phase. The mechanical and electronic properties of palladium are strongly affected by the lattice expansion during the formation of palladium hydride from a dilute α phase (low hydrogen concentrations) to the fully loaded β phase [37]. Formation of β hydride is most likely one of the main causes of leaching during hydrogenation reactions involving Pd as the catalyst. This can be linked to the Pd crystallite size: larger Pd crystallites form hydrides more easily [38].

5. Reactor configurations in fine chemicals production

In the fine chemicals industry, rather complex molecules with limited thermal stability are produced via multi step synthesis (5-10 steps for pharmaceuticals and 3-7 steps for agrochemicals). Production is usually carried out in solution at mild pressures and low to medium temperature in relatively small (0.5 – 10.0 m^3) multi-purpose batch equipment. Products are typically in the range between 1 and 1000 tonnes per year (pharmaceuticals) and 500 – 10,000 tonnes per year (agrochemicals), respectively [39]. As a result, batch processing in multi-purpose plants still remains the 'workhorse' in fine/specialty chemicals processing.

5.1. Mechanically agitated slurry reactors

In this reactor type, the catalyst particles are in a suspended state. The mechanically agitated slurry reactor is the workhorse in the fine chemical industry due to relatively low production volumes. The main advantages of slurry reactors are high catalyst utilization, uniform temperature, good external mass transfer and flexibility. The main disadvantages are catalyst attrition and the need for catalyst separation. Selective hydrogenation, which may be applied in one or more synthesis steps, is carried out in mechanically agitated slurry batch reactors, too.

Stirred 'slurry' batch reactors and jet-loop 'venturi' reactors are commercially offered by companies such as Biazzi, Davy Process Technology (Buss loop reactor), DeDietrich, Lurgi and others [40]. Stirred tank reactors in combination with hollow-shaft turbines for high internal hydrogen recirculation and improved hydrogen dispersion into the liquid are very efficient. Even more efficient are jet-loop (venturi) reactors in which the slurry is circulated back at high flow in a loop connected to a venturi where hydrogen is sucked in due to a local underpressure. The intense turbulence achieves a very large interfacial area between tiny bubbles and the slurry. An external heat exchanger on the loop enables an almost unlimited heat removal, convenient for highly exothermic reactions in order to reach isothermal operation. On the other hand, jet-loop reactors are restricted to attrition resistant catalysts [41].

5.2. Bubble Column Slurry Reactors

In bubble column slurry reactors, the reactant gas is dispersed due to the upflow operation through the liquid reactant, thereby also suspending the catalyst particles present. This reactor configuration is suited for medium to large-scale production. This reactor configuration offers advantages over mechanically agitated slurry reactors such as the absence of any moving parts (mechanical agitation) and lower power consumption. The main disadvantage is the considerable amount of back mixing in the liquid phase, resulting in poorer reactor performance.

5.3. Monolith Reactors

Monoliths are extruded ceramic structures consisting of straight, parallel channels. The diameter of each channel is typically of the order of one millimetre and the wall thickness is typically one-tenth of the channel diameter. The open structure without bends hardly obstructs the flow, thereby leading to a very low pressure drop, and with small channels a high

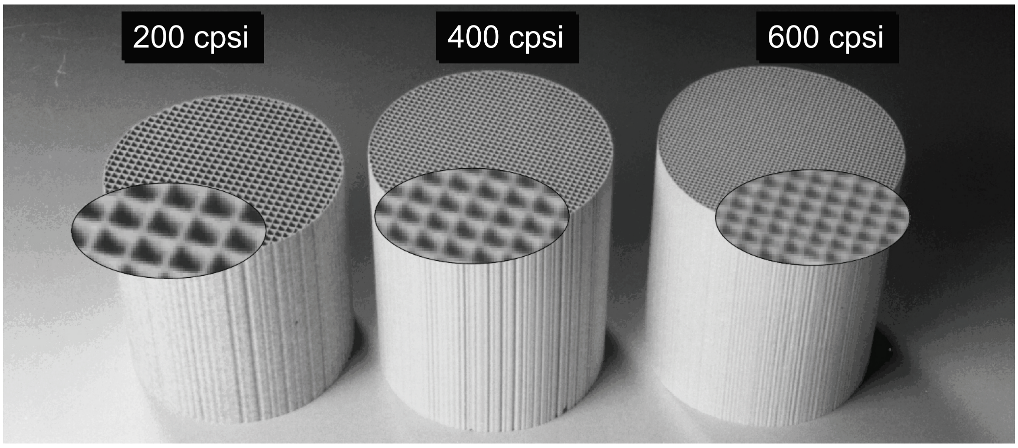

Figure 1: Examples of commercially available cordierite monoliths

surface area of catalyst is obtained to ensure fast mass transfer. The size of the channels is usually indicated by the number of the channels per square inch (cpsi) of frontal area of the structure. The most commonly used monoliths have a cell density of 200, 400, 600 or 1100 cpsi. The cross-sectional shape of most bare monolith channels is square (Figure 1). Typical values of some important geometric dimensions of ceramic monoliths are listed in Table 2.

Since the bare monoliths have a very low surface area (< 4 m^2/g), the walls of the inert channels are usually coated with a high surface area support [42,43]. Subsequently, the catalytically active material is deposited to obtain a homogeneously distributed active phase along the monolith length, where the catalyst layer thickness is similar to that of a particulate egg-shell catalyst. However, maldistribution of the active phase along the monolith length is also possible during the drying step, as observed by Vergunst *et al.* [44]. For an overview of the preparation of monolith catalysts, see the reviews by Nijhuis *et al.* [45] and Vergunst *et al.* [46]. In principle, structuring the catalyst allows decoupling of the pressure drop and mass transport. The small catalyst particles (of the same order of magnitude as those used in slurry reactors) eliminate the diffusion problems associated with fixed bed reactors and due to the straight parallel channels, a very low pressure drop is obtained. Thus monoliths offer the possibility to develop fixed-bed reactor technology using 'immobilized' slurry catalysts.

Kapteijn *et al.* [47] and Cybulski and Moulijn [48,49] have reviewed the

Table 2: Properties of square channel monoliths with different cell density

Cell density (cpsi)	Wall thickness (μm)	Channel diameter (mm)	Surface area (m^2/m^3)	Void fraction (-)
200 (31 cm^{-2})	270	1.53	1890	0.72
400 (62 cm^{-2})	165	1.11	2740	0.76
600 (93 cm^{-2})	112	0.93	3440	0.80
1100 (170 cm^{-2})	64	0.71	4790	0.84

applicability of monolithic reactors in multiphase processes. Edvinsson Albers *et al*. [50] have proposed the use of a novel monolithic stirred reactor for the synthesis of fine chemicals. In 'Structured Catalysts and Reactors' [51], a comprehensive review of the available literature on monolithic reactors is given.

6. Monolithic reactors in fine chemical industry

The use of monoliths as catalytic converters in automobiles and in deNOx reactors that remove nitrous oxides from power plant emissions is well known. The pharmaceutical and fine chemical industry is typified by high value and low volume reactions, which are usually performed in slurry batch reactors. Although these reactors are versatile, the catalyst used is in the powder form and needs to be separated from the product after reaction. This catalyst separation step is energy intensive and can also lead to loss of expensive catalyst. Although the fine chemical industry has traditionally been associated with high profits due to the high value added products, due to stricter environmental legislation and increased competition, the profit margins are shrinking. Thus, replacing the slurry catalyst with a fixed catalyst on e.g. a monolith or a ceramic foam structure and thereby eliminating the expensive catalyst separation step seems to be a promising alternative.

A monolith reactor also offers a volumetric rate advantage over a slurry reactor due to the superior rate of mass transfer of reactants from the gas and bulk liquid phase to the catalytic surface [52,53]. This rate advantage holds when the hydrogenation process is limited by the rate of hydrogen mass transfer (i.e. for fast reactions). High mass transfer rates allow the amount of catalyst required to be small, so that overall economics are favourable [54]. If the reaction is so slow that it renders the process kinetically controlled, this advantage disappears since the overall throughput is then set directly by the amount of catalyst in the system. Due to the limitation of the catalyst amount that can be incorporated on a monolith (usually < 5 wt. %), a slurry reactor with a higher catalyst loading may offer a better performance. In every case, an economical analysis has to be made to assess feasibility, although safety is not easily expressed in economic numbers.

A commercial large-scale application (~200 kilo tonnes/year) of monoliths as multiphase reactors is the hydrogenation of anthraquinone to hydroquinone in the production of hydrogen peroxide (anthraquinone auto-oxidation process) by Akzo Nobel [55]. In the 1990s, some other companies were also actively developing monolithic hydrogenation processes. One of these was the Austrian Chemie Linz, which has been taken over by DSM. According to their patents, they worked on at least a small pilot scale with catalyst volumes in the range of 14 l and they have developed several processes that involve hydrogenation of ozonolysis products using Pt, Pd and Lindlar type monolithic catalyst [56,57].

Air Products has been and still is very active in filing patent applications on the use of monolithic catalysts and have explored the possibility of replacing conventional slurry reactors with monoliths for glucose hydrogenation [58] as well as for the hydrogenation of dinitrotoluene to toluenediamine [59]. Air Products has teamed up with Johnson-Matthey for investigating hydrogenation reactions based on monoliths.

To operate a monolithic reactor, several configurations are possible. In the following paragraphs, four options of monolithic reactors that are already used at the lab-scale are introduced; Screw Impelled Stirred Reactor (SISR), Monolithic Turbine Reactor (MTR), the Monolith Loop Reactor (MLR), and the Monolithic Stirrer Reactor (MSR).

6.1. Monolithic Turbine Reactor (MTR)

The monolithic turbine reactor (MTR) used in our laboratory, shown in Figure 2 a, is an autoclave of 500 ml capacity that can be used to test monoliths either 1 cm or 5 cm in diameter and having a maximum length of 5 cm. The reactor is equipped with a stirrer with blades, which has a maximum rotation speed of 3000 rpm.

6.2. Screw Impelled Stirred Reactor (SISR)

The Screw Impelled Stirred Reactor (SISR) consists of a helical screw surrounded by monolith pieces. A mixture of gas and liquid is forced through the monoliths (in our design having a diameter of 1 cm) in an internal recirculation mode. The set-up is shown in Figure 2 b. The reactor can be operated in two- or three- phase mode at elevated pressure. Because of the small volume, this reactor is a very convenient lab-scale reactor to compare monoliths with conventional slurry catalysts.

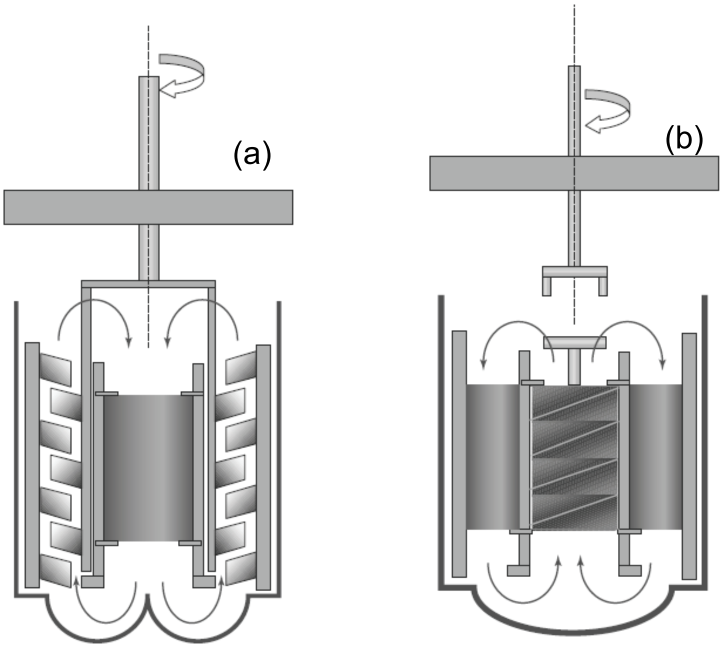

Figure 2: Schematic of **(a)** MTR and **(b)** SISR for monolith performance testing

6.3. Monolith Loop Reactor (MLR)

The monolith loop reactor (Figure 3) can be used as an alternative for conventional three-phase reactors. The monolith is placed vertically in a recycle with a tank. The reactor can be operated in a continuous or batch mode. The monolith section can be placed on an existing vessel. The MLR consists of a storage tank from which the liquid is pumped towards the liquid distributor. At the distributor, the liquid is evenly spread over the monolith cross-section, and subsequently flows back down to the storage tank. The size of this tank depends upon the application; for batch operation the tank

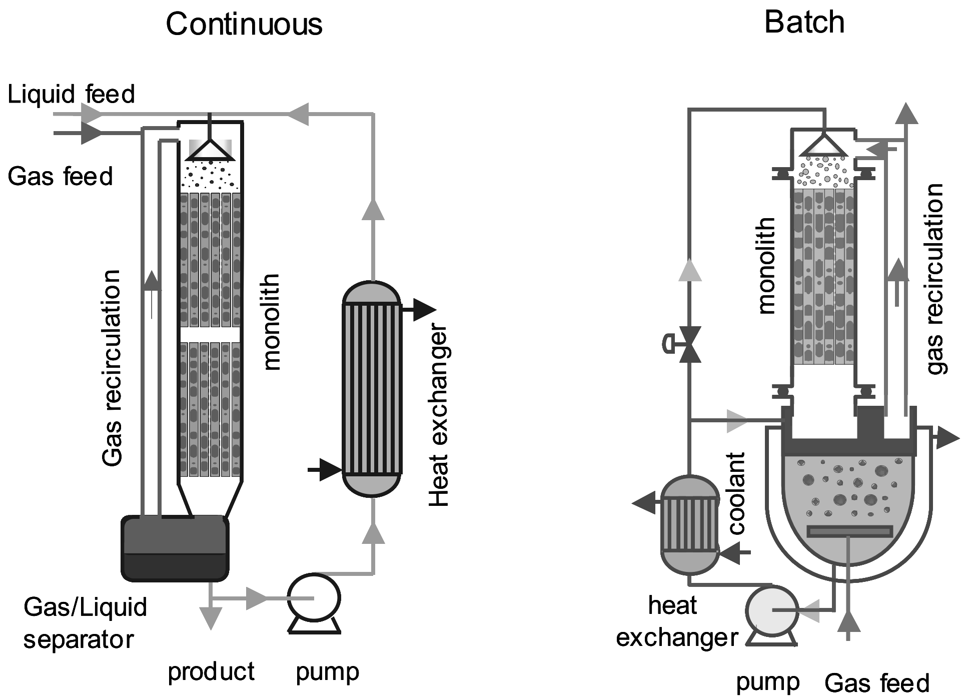

Figure 3: Monolith loop reactor in two possible configurations

volume can be large compared to the monolith volume, for continuous operation the tank serves only to separate the gas and liquid phases and should be kept small. In this case, it can be a retro fit option for a slurry reactor. The suction that is created by the liquid distributor, combined with gravity ensures that the gas is introduced in all the channels at the top-section. As a result, no compressor is required.

6.4. Monolithic Stirrer Reactor (MSR)

The monolithic stirrer reactor (Figure 4) uses monoliths as stirrer blades. When the stirrer is rotated through the liquid, a pressure drop is created over the monolith structures. The pressure drop is the driving force for flow through the monolith channels. An MSR is a convenient way to transform a slurry reactor into a structured reactor type. Using a catalytic stirrer that contains structured catalysts as stirrer blades combines the advantages of a structured reactor and a catalytic stirrer, in the sense that the support is a large structure that is readily separated from the liquid medium, and that convenient batch operation and rapid mixing/contacting is facilitated. This system can also be used for deactivating catalysts. After loss of catalytic

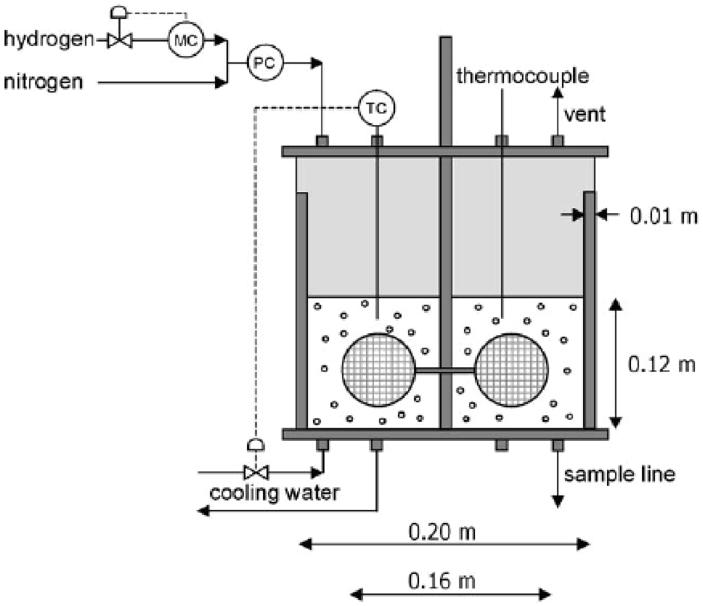

Figure 4: Schematic overview of a monolithic stirrer reactor as used in our laboratory

activity, the monoliths on the stirrer can simply be replaced with fresh monoliths. Some disadvantages of this reactor include the limited operational experience and the limited catalyst loading. The amount of catalyst can be tuned by changing the number, length and cell density of the monoliths.

7. Problems associated with the use of monoliths

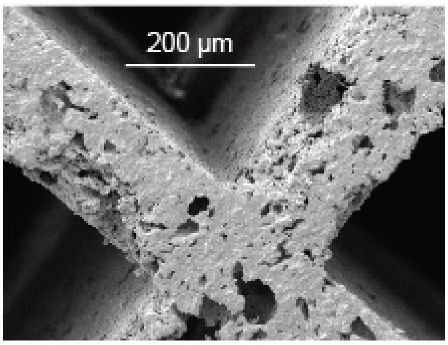

Figure 5: SEM image of a cordierite monolith (400 cpsi)

Although monolithic reactors seem an attractive replacement for slurry reactors in the fine chemical industry, their use presents considerable challenges. In particular, usually time-consuming optimized preparation procedures have to be developed. The ceramic monoliths consist of macro-porous square channels (Figure 5) and have a low surface area. On coating the monolith with a high surface area support, the support and consequently the active metal enters the macropores. As a result, the active metal might not be fully accessible to the reactants thereby leading to non-optimal usage of the active metal. It is also important to ensure that the active metal is uniformly present throughout the length of the monolith. It has been shown earlier by Vergunst *et al.* [44] that the drying step is critical in this respect and that maldistribution of the active metal can occur during this stage. Furthermore, the square geometry of the channels also leads to a non-uniform coating thickness and consequently to longer diffusion lengths on coating with the high surface area support. Although it is desirable to operate a monolith reactor in diffusion limited regime to exploit the high gas-liquid mass transfer rates and optimally use the active catalyst [54], the longer and non-uniform diffusion length can lead to further loss of selectivity of the desired product, especially for selective hydrogenations. It would therefore be beneficial to have a nearly uniform diffusion length for the reactants. Thus developing a coating procedure for optimum catalyst distribution on the monolith and testing the optimized monolith for industrially important reactions was one of the goals of this research.

8. Outline of the thesis

The hydrogenation of aromatic ketones is an important class of reaction in the fine chemical industry. In particular, the selective hydrogenation of *4*-isobutylacetophenone (*4*-IBAP) to *1*-(*4*-isobutylphenyl)ethanol (*4*-IBPE) (Scheme 1) is an intermediate step in the multistep synthesis of Ibuprofen.

The aromatic functionality of an aromatic ketone activates the carbonyl bond, thereby allowing for its hydrogenation at relatively milder conditions. This activation allows facile selective reduction of aromatic carbonyls with Pd [40,60]. Although the hydrogenation of 4-IBAP is an industrially important

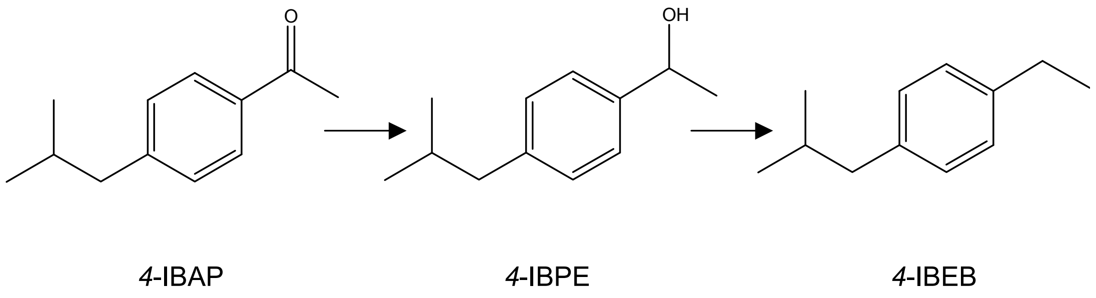

Scheme 1: Reaction scheme for *4*-IBAP hydrogenation

reaction, surprisingly it has not been reported in detail in the open literature. Since it was important to understand the reaction behaviour under different operating conditions, we performed preliminary experiments using slurry Pd catalyst in a batch reactor system. Severe catalyst deactivation was observed after a single batch run for the hydrogenation of *4*-IBAP over supported Pd catalysts. There are only a few literature reports dealing with the hydrogenation of *4*-IBAP [61,62] and only one mentions the catalyst deactivation over a supported Ni catalyst [63]. The severe catalyst deactivation made the hydrogenation of *4*-IBAP in a monolith reactor unattractive. Elucidation of the mechanism is crucial for the development of a process based on a fixed bed reactor. It appeared that there were many important issues related to the hydrogenation of *4*-IBAP that had still not been addressed in the literature. The C-O bond scission of *4*-IBPE (Scheme 2) can occur via two pathways; one of them leading to the formation of a styrene intermediate (4-IBSty), which could be the cause of catalyst deactivation. In order to suggest suitable remedies to prevent catalyst deactivation, it was concluded to be highly desired to understand the cause of catalyst deactivation.

Although Pd is the catalyst of choice in the existing patents [64-66], no kinetic modelling has been performed over supported Pd catalysts. The knowledge of intrinsic kinetics enables one to design industrial scale reactors. The few kinetic models existing in the literature do not account for the loss of catalytic activity due to deactivation [61,62]. Thus we decided to focus our efforts on

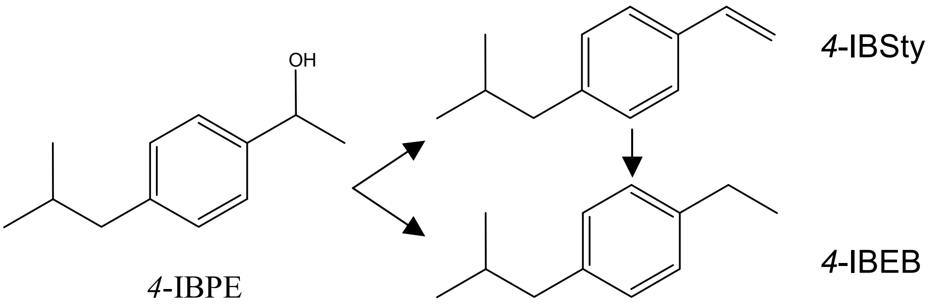

Scheme 2: Possible pathways for C-O bond scission of *4*-IBPE

elucidating the reaction pathway and deactivation mechanism for the hydrogenation of *4*-IBAP, and develop a comprehensive kinetic model using this information, which is also one of the goals of this research.

A parallel research was performed; on the one hand investigating the reaction pathway, deactivation mechanisms and kinetic modelling of *4*-IBAP hydrogenation over Pd/SiO_2 and on the other hand developing optimized monoliths and testing their performance for the hydrogenation of *3*-methyl-*1*-pentyn-*3*-ol. The selective hydrogenation of *3*-methyl-*1*-pentyn-*3*-ol to *3*-methyl-*1*-penten-*3*-ol (Scheme 3) over Pd/SiO_2 was chosen as a model reaction system to test the optimized monoliths, since a Pd/SiO_2 catalyst was reported to be stable for this reaction [67,68] and this is an example of a fast diffusion limited reaction.

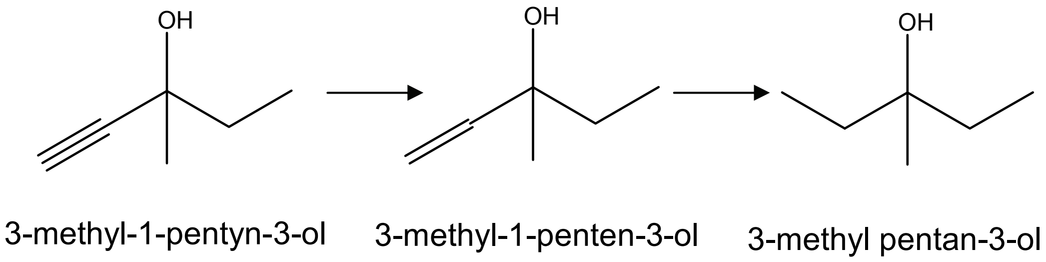

Scheme 3: Reaction scheme for 3-methyl-1-pentyn-3-ol hydrogenation

9. Objectives of the thesis

The main objectives of this thesis are summarized below.

(i) To identify the exact pathway of the C-O bond scission of *4*-IBPE.

(ii) To investigate the causes of catalyst deactivation during the hydrogenation of *4*-IBAP.

(iii) To model the kinetics of 4-IBAP hydrogenation over Pd/SiO_2 including the loss of catalytic activity due to deactivation.

(iv) To optimize the channel geometry of the commercially available monoliths and test them for the selective hydrogenation of a fast, diffusion-limited reaction.

Reference List

1. 'Catalysis: An Integrated Approach', 2nd Ed., Elsevier, Amsterdam (**1999**).

2. H. Deacon, 'Improvement in Manufacture of Chlorine', US 165,802 (**1875**).

3. P. Gallezot and D. Richard, 'Selective Hydrogenation of α, β Unsaturated Aldehydes', *Catalysis Reviews - Science and Engineering*, 40 (**1998**) 81.

4. P. Maki-Arvela, J. Hajek, T. Salmi and D. Yu. Murzin, 'Chemoselective Hydrogenation of Carbonyl Compounds Over Heterogeneous Catalysts', *Applied Catalysis A: General*, 292 (**2005**) 1.

5. B. W. Hoffer, A. D. van Langeveld, J. P. Janssens, R. L. C. Bonne, C. M. Lok and J. A. Moulijn, 'Stability of Highly Dispersed Ni/Al_2O_3 Catalysts: Effects of Pretreatment', *Journal of Catalysis*, 192 (**2000**) 432.

6. H. Lindlar, 'A New Catalyst for Selective Hydrogenations', *Helvetica Chimica Acta*, 35 (**1952**) 446.

7. N. Marin-Astorga, G. Pecchi, J. L. G. Fierro and P. Reyes, 'Alkynes Hydrogenation Over Pd-Supported Catalysts', *Catalysis Letters*, 91 (**2003**) 115.

8. S. Nishimura, 'Handbook of Heterogeneous Catalytic Hydrogenation for Organic Synthesis', Wiley, New York (**2001**).

9. G. G. Joris and J. Vitrone Jr., 'The Catalytic Hydrogenation of Phenol', US 2,828,166 (**1958**) to Allied Signal.

10. W. Kuhn, ‘Method for producing cis-2-tertbutylcyclohexanol by catalytically hydrogenating 2-tertbutylphenol’ WO 0248079 A2 (**2002**) to Haarmann and Reimer.

11. O. Mitsui and Y. Fukuoka, 'Process for Producing Cycloolefins', US 4,678,861 (**1987**) to Asahi Chemicals.

12. A. M. Liu, K. Hidajat and S. Kawi, 'Combining the Advantages of Homogeneous and Heterogeneous Catalysis: Rhodium Complex on Functionalized MCM-41 for the Hydrogenation of Arenes', *Journal of Molecular Catalysis A: Chemical*, 168 (**2001**) 303.

13. R. S. Rao, R. T. K. Baker and M. A. Vannice, 'Furfural Hydrogenation Over Carbon Supported Copper', *Catalysis Letters*, 60 (**1999**) 51.

14. R. L. Augustine, 'Heterogeneous Catalysis for the Synthetic Chemist', Dekker, New York (**1996**).

15. T. Yokoyama and N. Fujita, 'Hydrogenation of Aliphatic Carboxylic Acids to Corresponding Aldehydes Over Cr_2O_3 Based Catalysts', *Applied Catalysis A: General*, 276 (**2004**) 179.

16. K. Tahara, E. Nagahara, Y. Itoi, S. Nishiyama, S. Tsuruya and M. Masai, 'Liquid Phase Hydrogenation of Carboxylic Acid on Supported Bimetallic Ru-Sn Alumina Catalysts', *Applied Catalysis A: General*, 154 (**1997**) 75.

17. W. Rachmady and M. A. Vannice, 'Acetic Acid Hydrogenation Over Supported Platinum Catalysts', *Journal of Catalysis*, 192 (**2000**) 322.

18. A. Corma and P. Serna, 'Chemoselective Hydrogenation of Nitro Compounds With Supported Gold Catalysts', *Science*, 313 (**2006**) 332.

19. P. Baumeister, H. U. Blaser and M. Studer, 'Strong Reduction of Hydroxylamine Accumulation in the Catalytic Hydrogenation of Nitroarenes by Vanadium Promoters', *Catalysis Letters*, 49 (**1997**) 219.

20. M. Studer, S. Neto and H. U. Blaser, 'Modulating the Hydroxylamine Accumulation in the Hydrogenation of Substituted Nitroarenes Using Vanadium Promoted RNi Catalysts', *Topics in Catalysis*, 13 (**2000**) 205.

21. J. Pfeffinger, M. Huellmann, A. Hoehn, F. Funke, F. Ohlbach and T. Gerlach, 'Hydrogenation Process and Supported Rhodium Catalysts for the Preparation of Secondary Amines From Nitriles', EP 1221436 A2 (**2002**) to BASF A. G.

22. B. W. Hoffer, P. H. J. Schoenmakers, P. R. M. Mooijman, G. M. Hamminga, R. J. Berger, A. D. van Langeveld and J. A. Moulijn, 'Mass

Transfer and Kinetics of the Three Phase Hydrogenation of a Dinitrile Over a Raney-Type Nickel Catalyst', *Chemical Engineering Science*, 59 (**2004**) 259.

23. C. De Bellefon and P. Fouilloux, 'Homogeneous and Heterogeneous Hydrogenation of Nitriles in a Liquid Phase: Chemical, Mechanistic and Catalytic Aspects', *Catalysis Reviews - Science and Engineering*, 36 (**1994**) 459.

24. A. Molnar, A. Sarkany and M. Varga, 'Hydrogenation of Carbon–Carbon Multiple Bonds: Chemo-, Regio- and Stereo-Selectivity', *Journal of Molecular Catalysis A: Chemical*, 173 (**2001**) 185.

25. H. U. Blaser and M. Studer, 'The Role of Catalysis for the Clean Production of Fine Chemicals', *Applied Catalysis A: General*, 189 (**1999**) 191.

26. P. N. Rylander, 'Catalytic Hydrogenation Over Platinum Metals', Academic Press, New York (**1967**).

27. A. Sarkany, 'Semi-Hydrogenation of 1,3-Butadiene Over Pd-Ag/α-Al_2O_3 Poisoned by Hydrocarbonaceous Deposits', *Applied Catalysis A: General*, 165 (**1997**) 87.

28. R.-J. Liu, P. A. Crozier, C. M. Smith, D. A. Hucul, J. Blackson and G. Salaita, 'Metal Sintering Mechanisms and Regeneration of Palladium/Alumina Hydrogenation Catalysts', *Applied Catalysis A: General*, 282 (**2005**) 111.

29. A. Gotti and R. Prins, 'Effect of Metal Oxide Additives on the CO Hydrogenation to Methanol Over Rh/SiO_2 and Pd/SiO_2', *Catalysis Letters*, 37 (**1996**) 143.

30. P. N. Rylander and L. Hasbrouck, 'Studies in Selectivity: Hydrogenation of Acetophenone', *Engelhard Industries, Technical Bulletin*, 8 (**1968**) 148.

31. S. Mukherjee and M. A. Vannice, 'Solvent Effects in Liquid-Phase Reactions I. Activity and Selectivity During Citral Hydrogenation on Pt/SiO_2 and Evaluation of Mass Transfer Effects ', *Journal of Catalysis*, 243 (**2006**) 108.

32. G. Mul, G. M. Hamminga and J. A. Moulijn, 'Operando ATR-FTIR Analysis of Liquid Phase Catalytic Reactions: Can Heterogeneous Catalyst Be Observed?', *Vibrational Spectroscopy*, 34 (**2004**) 109.

33. J. A. Moulijn, A. E. van Diepen and F. Kapteijn, 'Catalyst Deactivation: Is It Predictable? What to Do?', *Applied Catalysis A: General*, 212 (**2001**) 3.

34. C. H. Bartholomew, 'Mechanisms of Catalyst Deactivation', *Applied Catalysis A: General*, 212 (**2001**) 17.

35. C. S. Satterfield, 'Heterogeneous Catalysis in Industrial Practice (Chapter 6)', 2nd Ed. McGraw Hill, New York (**1991**).

36. K. P. De Jong and J. W. Geus, 'Carbon Nanofibers: Catalytic Synthesis and Applications', *Catalysis Reviews - Science and Engineering*, 42 (**2000**) 481.

37. P. Albers, J. Pietsch and S. F. Parker, ‘Poisoning and deactivation of Pd catalysts’, *Journal of Molecular Catalysis A: Chemical,* 173 (**2001**) 275.

38. J. Panpranot, K. Pattamakomsan and P. Praserthdam, ‘Deactivation of silica supported catalysts during liquid-phase hydrogenation’, *Reaction Kinetics and Catalysis Letters,* 86 (**2005**) 141.

39. H. U. Blaser, 'Heterogeneous Catalysis for Fine Chemicals Production', *Catalysis Today*, 60 (**2000**) 161.

40. B. Chen, U. Dingerdissen, J. G. E. Krauter, H. G. J. Lansink Rotgerink, K. Mobus, D. J. Ostgard, P. Panster, T. H. Riermeier, S. Seebald, T. Tacke and H. Trauthwein, 'New Developments in Hydrogenation Catalysis Particularly in Synthesis of Fine and Intermediate Chemicals', *Applied Catalysis A: General*, 280 (**2005**) 17.

41. J. F. Jenck, 'Gas-Liquid-Solid Reactors for Hydrogenation in Fine Chemical Synthesis', *Studies in Surface Science and Catalysis*, 59 (**1991**) 1.

42. X. Xu and J. A. Moulijn, 'Preparation of Monolithic Catalysts by Dip Coating', *Studies in Surface Science and Catalysis*, 118 (**1998**) 845.

43. E. Garcia-Bordeje, F. Kapteijn and J. A. Moulijn, 'Preparation and Characterization of Carbon-Coated Monoliths for Catalyst Supports', *Carbon*, 40 (**2002**) 1079.

44. T. Vergunst, F. Kapteijn and J. A. Moulijn, 'Monolithic Catalysts- Non-Uniform Active Phase Distribution by Impregnation', *Applied Catalysis A: General*, 213 (**2001**) 179.

45. T. A. Nijhuius, A. E. W. Beers, T. Vergunst, I. Hoek, F. Kapteijn and J. A. Moulijn, 'Preparation of Monolithic Catalysts', *Catalysis Reviews*, 42 (**2001**) 345.

46. T. Vergunst, M. J. G. Linders, F. Kapteijn and J. A. Moulijn, 'Carbon Based Monolithic Structures', *Catalysis Reviews - Science and Engineering*, 43 (**2001**) 291.

47. F. Kapteijn, J. J. Heiszwolf, T. A. Nijhuis and J. A. Moulijn, 'Monoliths in Multiphase Catalytic Processes - Aspects and Prospects', *CATTECH*, 3 (**1999**) 24.

48. A. Cybulski, A. Stankiewicz, R. J. Edvinsson Albers and J. A. Moulijn, 'Monolithic Reactors for Fine Chemical Industries: a Comparative Analysis of a Monolithic Reactor and a Mechanically Agitated Slurry Reactor', *Chemical Engineering Science*, 54 (**1999**) 2351.

49. A. Cybulski and J. A. Moulijn, 'Monoliths in Heterogeneous Catalysis', *Catalysis Reviews - Science and Engineering*, 36 (**1994**) 179.

50. R. Edvinsson Albers, M. J. J. Houterman, T. Vergunst, E. Grolman and J. A. Moulijn, 'Novel Monolithic Stirred Reactor', *AIChE Journal*, 44 (**1998**) 2459.

51. A. Cybulski and J. A. Moulijn, 'Structured Catalysts and Reactors', 2nd Ed. CRC Taylor & Francis, Boca Raton (**2006**).

52. M. T. Kreutzer, F. Kapteijn and J. A. Moulijn, 'Shouldn't Catalysts Shape Up? Structured Reactors in General and Gas-Liquid Monoliths in Particular.', *Catalysis Today*, 111 (**2006**) 111.

53. M. T. Kreutzer, P. Du, J. J. Heiszwolf, F. Kapteijn and J. A. Moulijn, 'Mass Transfer Characteristics of Three-Phase Monolithic Reactors', *Chemical Engineering Science*, 56 (**2001**) 6015.

54. R. M. Machado, R. R. Broekhuis, A. F. Nordquist, B. P. Roy and S. R. Carney, 'Applying Monolith Reactors for Hydrogenations in the Production of Specialty Chemicals—Process and Economic Considerations', *Catalysis Today*, 105 (**2005**) 305.

55. R. Edvinsson Albers, M. Nystrom, M. Siverstrom, A. Sellin, A. C. Dellve, U. Andersson, W. Herrmann and T. Berglin, 'Development of a Monolith-Based Process for H_2O_2 Production: From Idea to Large Scale Implementation', *Catalysis Today*, 69 (**2001**) 247.

56. S. Pollhammer, J. Schaller and W. Winetzhammer, 'Hydrogenolytic Reduction of Organic Peroxidic Ozonolysis Compounds to Aldehydes', EP 614869 A1 (**1994**) to Chemie Linz.

57. C. Kos, W. Winetzhammer, S. Pollhammer, J. Schaller, F. Hebesberger, E. Lust and R. Haar, 'Process and Monolithic Catalysts for the Hydrogenation of Aldehydes to Alcohols', EP 672643 A2 (**1995**) to Chemie Linz.

58. R. R. Broekhuis, B. M. Budhlall and A. F. Nordquist, 'Monolithic Catalytic Process for Producing Sorbitol: Catalyst Development and Evaluation', *Industrial & Engineering Chemistry Research*, 43 (**2004**) 5146.

59. R. M. Machado, D. J. Parrillo, R. P. Boehme and R. R. Broekhuis, 'Improved Process for Hydrogenation of Dinitrotoluene to Toluenediamine by Monolith Catalyst Containing Nickel and Palladium', US 6,005,143 (**1999**) to Air Products and Chemicals.

60. H. U. Blaser, A. Indolese, A. Schnyder, H. Steiner and M. Studer, 'Supported Palladium Catalysts for Fine Chemical Synthesis', *Journal of Molecular Catalysis A: Chemical*, 173 (**2001**) 3.

61. M. V. Rajashekharam and R. V. Chaudhari, 'Kinetics of Hydrogenation of *p*-Isobutyl Acetophenone Using a Supported Ni Catalyst in a Slurry Reactor', *Chemical Engineering Science*, 51 (**1996**) 1663.

62. S. P. Mathew, M. V. Rajashekharam and R. V. Chaudhari, 'Hydrogenation of *p*-Isobutyl Acetophenone Using a Ru/Al_2O_3 Catalyst: Reaction Kinetics and Modeling of a Semi-Batch Slurry Reactor', *Catalysis Today*, 49 (**1999**) 49.

63. M. V. Rajashekharam and R. V. Chaudhari, 'Improved Stability of a Bimetallic Ni-Pt Catalyst for Hydrogenation of Acetophenone and Substituted Derivatives', *Catalysis Letters*, 41 (**1996**) 171.

64. V. Elango, 'Method for Producing Ibuprofen', EP 0400 892 A2 (**1990**) to Hoechst Celanese Corp.

65. D. A. Ryan, 'Method of Producing *1*-(*4*-Isobutylphenyl) Ethanol', EP 0358 420 A2 (**1990**) to Hoechst Celanese Corp.

66. K. Saeki and K. Shima, 'Preparation of Aromatic Carbinols From Aromatic Ketones', JP 0262 837 (**1990**) to Daicel Chemical Ltd.

67. T. A. Nijhuis, G. van Koten and J. A. Moulijn, 'Optimized Palladium Catalyst Systems for the Selective Liquid-Phase Hydrogenation of Functionalyzed Alkynes', *Applied Catalysis A: General*, 238 (**2003**) 259.

68. I. Hoek, T. A. Nijhuis, A. I. Stankiewicz and J. A. Moulijn, 'Performance of the Monolithic Stirrer Reactor: Applicability in Multi-Phase Processes', *Chemical Engineering Science*, 59 (**2004**) 4975.

2

Deuteration study to elucidate hydrogenolysis of benzylic alcohols over supported palladium catalysts

Deuteration in combination with multinuclear NMR spectroscopy was applied to elucidate the pathway of the C-O bond scission of *1*-(*4*-isobutylphenyl) ethanol (*4*-IBPE) to *4*-isobutylethylbenzene (*4*-IBEB) over Pd/SiO_2, Pd/C and unsupported Pd black. Information about the pathway was obtained by determination of the positions at which deuterium was incorporated by means of ^1H, ^2H and ^{13}C NMR spectroscopy. The C-O bond scission of *4*-IBPE over Pd/SiO_2 and Pd black occurred exclusively by direct hydrogenolysis, whereas both hydrogenolysis and the dehydration-hydrogenation route were observed over Pd/C. The latter was attributed to the acidic nature of the carbon support. Spillover of dissociatively adsorbed hydrogen from the metal surface to the support does not play an important role in the direct hydrogenolysis of *4*-IBPE over Pd.

This chapter is published in the *Journal of Catalysis*, 246 (**2007**) 344-350.

1. Introduction

The selective hydrogenation of aromatic ketones to the corresponding alcohols is an important reaction in the fine chemicals industry. Supported Pd catalysts are usually the catalysts of choice for these reactions due to their ability to selectively hydrogenate the carbonyl functional group under mild operating conditions [1,2]. The selective hydrogenation of *4*-isobutylacetophenone (*4*-IBAP) to *1*-(*4*-isobutylphenyl) ethanol (*4*-IBPE) (Scheme 1) is an intermediate reaction step in the multistep synthesis of Ibuprofen [3]. The desired product *4*-IBPE is further carbonylated to yield Ibuprofen. Ibuprofen can be administered as a racemate because the inactive (R)-enantiomer undergoes *in vivo* inversion of configuration, providing the active (S)-enantiomer [4]. Though *4*-IBPE is the desired product, the formation of the undesired *4*-isobutylethylbenzene (*4*-IBEB) is also observed, especially when using acidic supports or at higher hydrogen pressures. Whereas Pd/C is the most commonly used catalyst as mentioned in many patents [3,5,6], also Ru/Al_2O_3 [7] and Ni/HY [8] have been reported for this system. We recently reported on the performance of Pd/SiO_2 for this particular reaction [9]. The formation of the undesired *4*-IBEB was observed in all these reports [7-9]. There are two possible routes for the transformation of *4*-IBPE to *4*-IBEB (Scheme 2) (*i*) dehydration-hydrogenation or (*ii*) direct hydrogenolysis [10] of the C-O bond of *4*-IBPE. The first route proceeds via the formation of an intermediate *4*-isobutylstyrene (*4*-IBSty), followed by further hydrogenation to yield *4*-IBEB. Chaudhari *et al.* [7,8] postulated the dehydration-

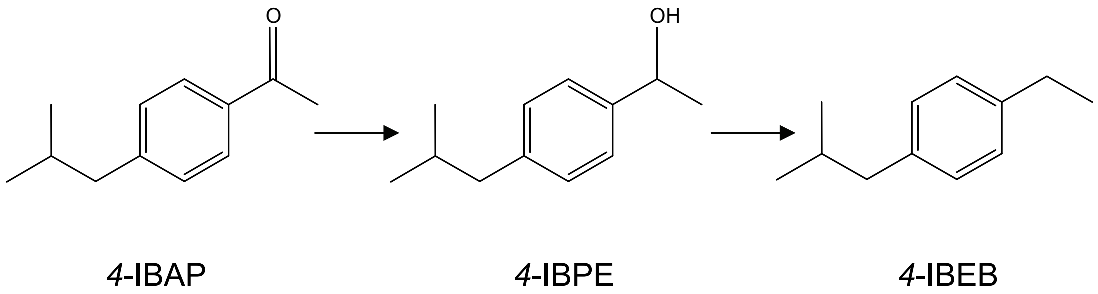

Scheme 1: Reaction scheme for the hydrogenation of *4*-isobutylacetophenone over supported Pd catalysts

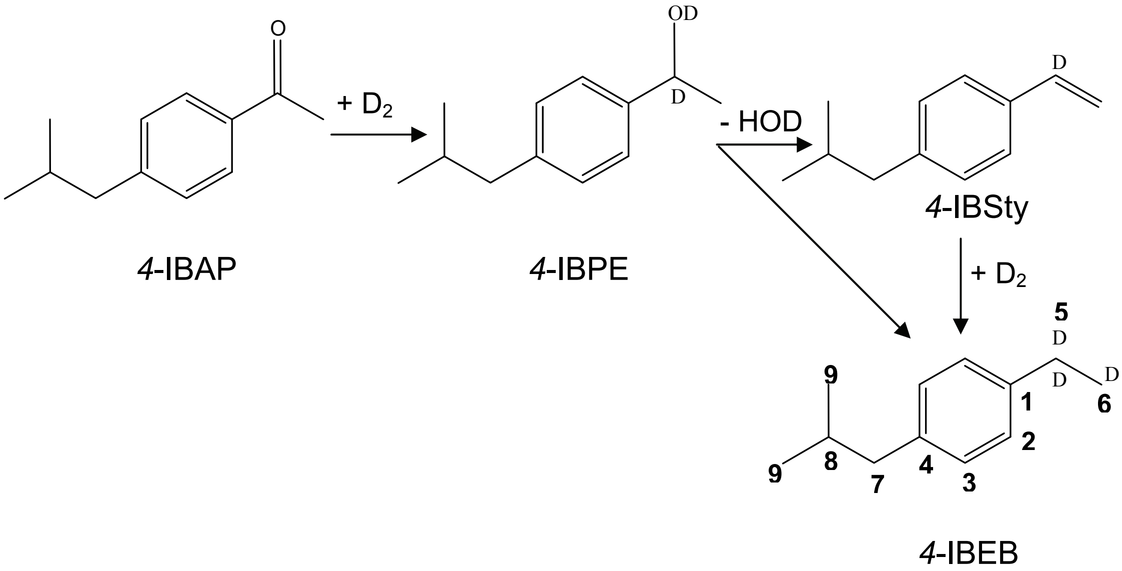

Scheme 2: Pathways to C-O bond cleavage of *1*-(*4*-isobutylphenyl)ethanol

hydrogenation route for the formation of *4*-IBEB over Ru/Al_2O_3 and Ni/HY catalysts, although no evidence of the intermediate *4*-IBSty was observed by the GC analysis. The elucidation of the exact pathway is important from the viewpoint of accurate kinetic modelling, since the acidic support also participates if the transformation of *4*-IBPE to *4*-IBEB is by the dehydration-hydrogenation pathway and consequently must be accounted for in the kinetic rate expression. Furthermore, for this reaction system, the catalyst is known to deactivate [8,9], and one of the reasons could be the polymerization of the intermediate *4*-IBSty formed if the C-O bond scission of *4*-IBPE proceeds via the dehydration-hydrogenation route. Thus, it is of importance to understand the exact pathway of transformation of *4*-IBPE to *4*-IBEB.

Conclusive evidence of the reaction pathway can be obtained with deuteration studies by determining the positions at which deuterium is incorporated in the resulting *4*-IBEB by means of ^1H, ^2H and ^{13}C NMR spectroscopy. The power of deuteration experiments in elucidating hydrogenation mechanisms was underlined by the work of Burwell [11]. Within the scope of this topic, Ranade and Prins [12] applied deuteration to conclude that C-O bond scission in 1-indanol hydrogenation over Rh/C took place only by direct hydrogenolysis on the support. The aim of this work is to identify the pathway of transformation of 4-IBPE to 4-IBEB over Pd catalysts such as Pd/SiO_2, Pd black and Pd/C using multinuclear NMR spectroscopy.

2.1. Experimental

2.1.1. Materials

4-IBAP was purchased from Alfa Aesar, 4-IBPE was 'home made' at the Organic Chemistry Department of the Delft University of Technology, cyclohexane (undeuterated), 5% Pd/C and Pd black were purchased from Aldrich. The isotopic purity of deuterium gas (Aldrich) was 99.8%. All chemicals were used as received without further purification. The 'in-house' prepared Pd black was obtained by calcining Pd (II) nitrate precursor (Aldrich) in air at 673 K followed by reduction in flowing H_2 at 373 K. The preparation of the Pd/SiO_2 has been described elsewhere [9].

2.1.2. Deuteration

The deuteration experiments were performed in a stainless steel autoclave of 500 ml (Scheme 3). In a typical deuteration experiment, the desired amount of reactant (4-IBAP) and solvent (cyclohexane) were charged to the reactor along with the pre-reduced catalyst. The contents (~200 ml) were flushed with nitrogen three times at room temperature. After the desired reaction temperature was attained, the system was pressurized with deuterium (^2H) to the required pressure and the stirrer was switched on. The semi-batch experiments were carried out at standard conditions of 373 K, 0.15 mol/L of 4-IBAP in cyclohexane and 2.0 MPa ^2H pressure using 0.3 g of catalyst and a stirring speed of 1500 rpm. After the completion of the reaction, the reactor was cooled to room temperature and depressurized prudently. Off-line GC analysis was performed by a Chrompack gas chromatograph (CP9001 autosampler), equipped with a CP Sil 8 CB column (50 m × 0.25 mm). The conditions were: FID temperature, 523 K; injector temperature, 523 K; the column temperature was ramped uniformly from 323 K to 523 K at 6.7 K/min. After the reaction, the catalyst was filtered from the reaction mixture

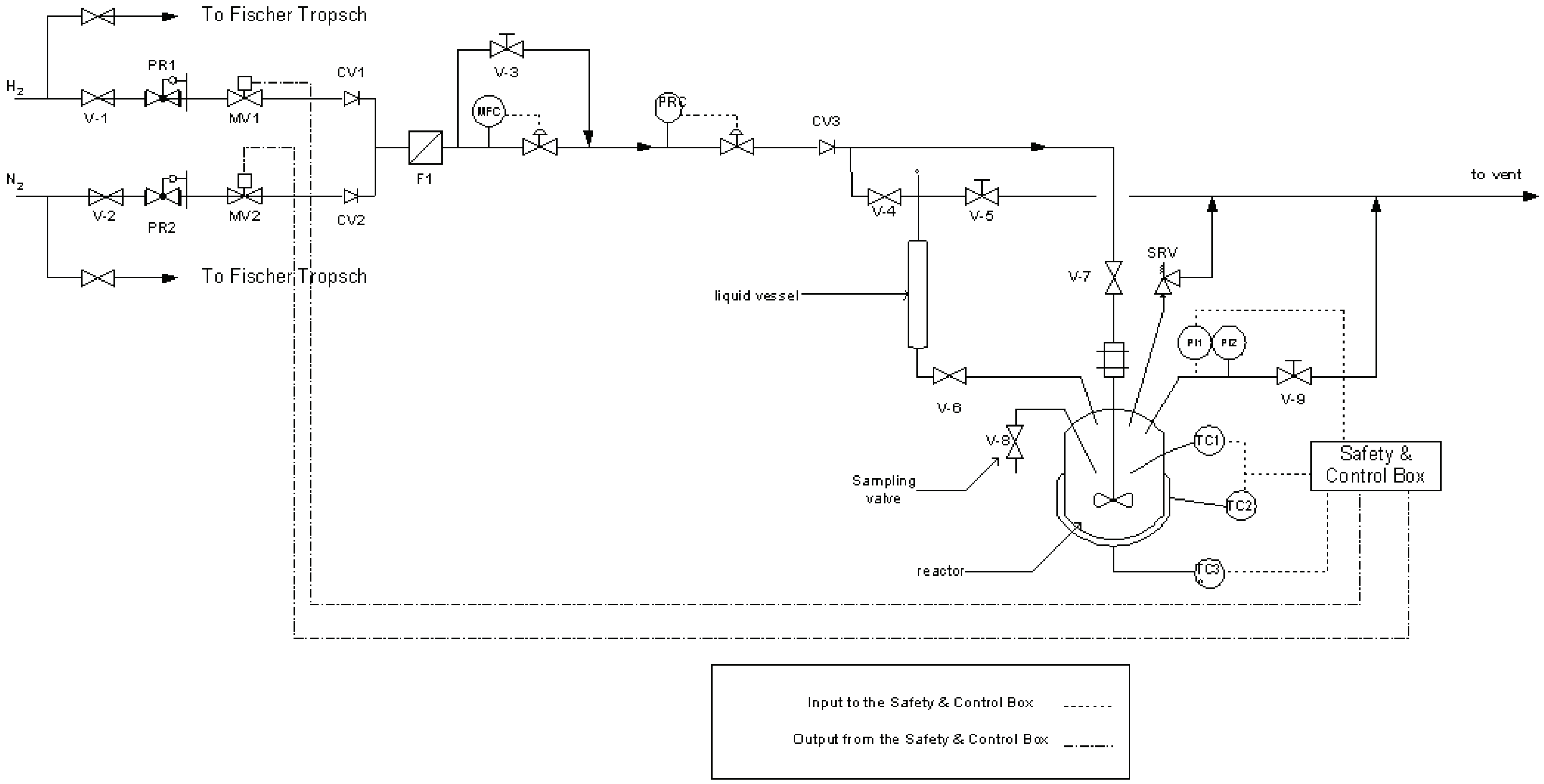

Scheme 3: Reactor set-up for deuteration/hydrogenation of 4-isobutylacetophenone

and the product 4-IBEB was obtained from cyclohexane under reduced pressure. The NMR spectra were recorded on a Varian Inova-300 spectrometer operating at 25 °C at 300 MHz, 75 MHz and 46 MHz for ^{1}H, ^{13}C and ^{2}H, respectively. Samples were prepared in 5 mm tubes using $CDCl_3$ and TMS as an internal standard.

2.1.3. Surface Chemistry

Temperature Programmed Decomposition- Mass Spectroscopy (TPD-MS) measurements were performed in a conventional flow apparatus using a quartz microreactor and He as carrier gas flowing at 50 STP cm^3/min. About 200 mg of sample (5% Pd/C) was heated with a rate of 10 K/min up to 1173 K. The desorption of gaseous species from the sample were monitored by a quadrupole mass spectrometer (Balzers) connected on-line with the reactor. Mass spectra were recorded in multiple ion detection (MID) mode using a channeltron detector. The evolved CO_2 and CO were calibrated by a method described by Wang and McEnaney [13] using thermal decompositions of calcium carbonate and calcium oxalate.

Titration curves were used to determine the surface acidity of the commercial 5% Pd/C sample [14]. Weighed amounts of material (~280 mg) were mixed with a KCl solution (7 ml 0.1 M). Increasing amounts (50 – 500 µl) of aqueous NaOH (0.5 M) solution were added. After sealing and equilibrating with gentle agitation for 72 h at room temperature, the pH values of the solutions were determined using a Metrohm Ion-Activity-Meter 580. In order to quantify the various types of acidic surface groups, the Boehm titration method was followed [15]. The results are expressed as mmol OH^- equivalent/g_{carbon}.

NH_3-TPD to determine the surface acidity of the SiO_2 sample (50 mg) was carried out in a Micromeritics TPR/TPD 2900 in the temperature range 473 – 723 K after three consecutive saturation steps with pure NH_3 at 473 K.

3. Results and Discussion

Deuteration experiments offer a possibility to distinguish between the pathways of transformation of 4-IBPE to 4-IBEB (Scheme 2). If the transformation proceeds through the dehydration-hydrogenation route, then deuterium incorporation should be observed at carbon 6, whereas no deuterium incorporation on this carbon would be expected if the transformation proceeded by direct hydrogenolysis of the C-O bond. Under the chosen experimental conditions, saturation of the aromatic ring did not occur for all the catalysts studied. In the absence of proton-deuterium exchange, three deuterium atoms (two on carbon 5 and one on carbon 6) should be theoretically incorporated into the product 4-IBEB if dehydration-hydrogenation is the main pathway, and two deuterium atoms (on carbon 5) if hydrogenolysis is the predominant route. As seen from the ^1H NMR spectrum (Figure 1), extensive deuterium incorporation is observed on carbon 5 and carbon 7 when Pd/SiO_2 is used as a catalyst, indicating H/D exchange at the benzylic positions. As the integral for a single proton (assumed to be not subjected to exchange) on carbon 8 (1.8 ppm) is 6.94, an integral of 13.88

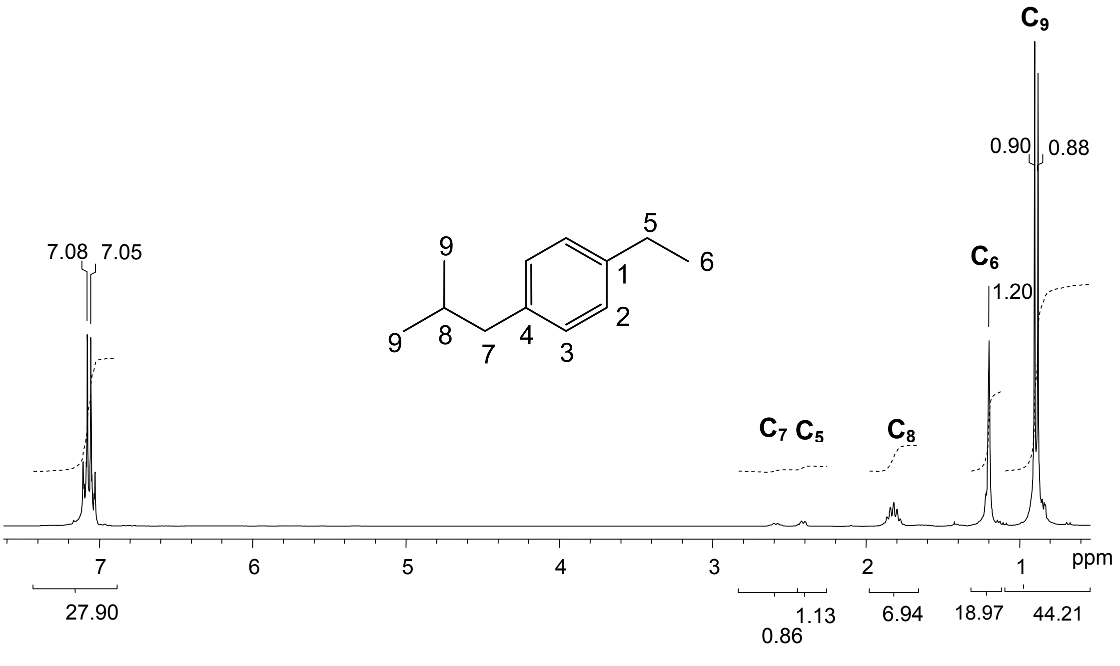

Figure 1: ^1H NMR spectrum of 4-IBEB obtained by 4 -IBAP deuteration over Pd/SiO_2

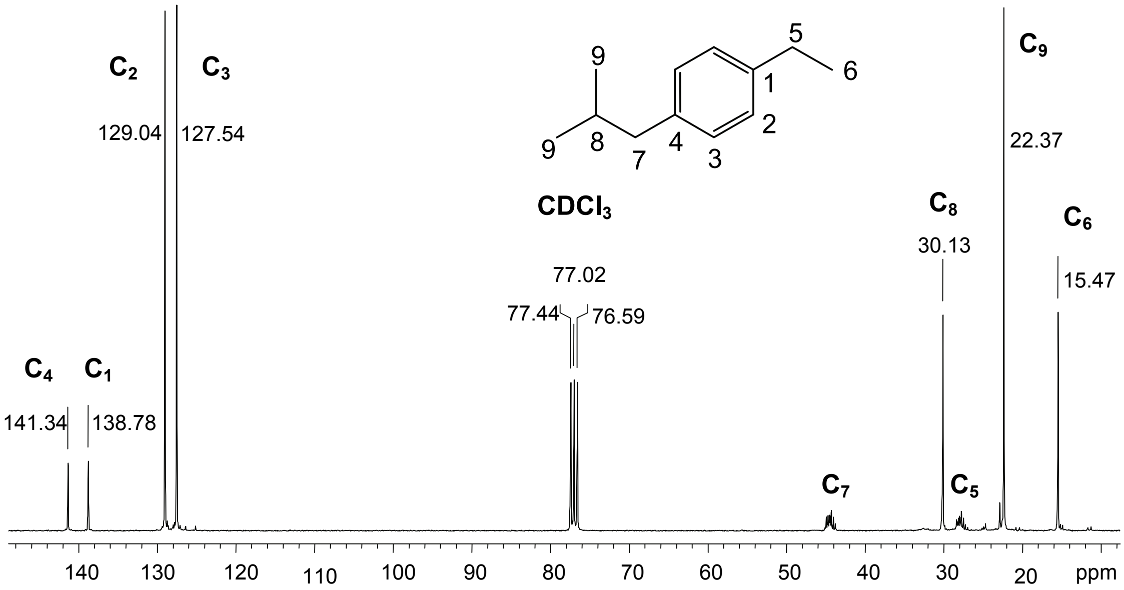

Figure 2: ^{13}C NMR spectrum of 4-IBEB obtained by 4-IBAP deuteration over Pd/SiO$_2$

would be expected theoretically for the two hydrogens on carbon 5 (2.4 ppm, 2H) and on carbon 7 (2.6 ppm, 2H) in the absence of any addition/exchange of deuterium. The observed integrals of 0.86 on carbon 7 and of 1.13 on carbon 5 imply 94% incorporation of deuterium on carbon 7 and 92 % on carbon 5.

In the normal ^{13}C NMR spectrum, carbon atoms with no deuterium bonded to them appear as singlets, because the carbon nucleus is decoupled from the hydrogen nucleus. Multiplicity arises because of the coupling of a carbon nucleus with a deuterium atom [12]. From the ^{13}C NMR spectrum (Figure. 2), it is clear that no significant deuterium incorporation occurs on the aromatic carbons 1-4 or on carbons 6, 8, and 9, as they would otherwise show multiplicity. The extensive deuterium exchange on carbon 7 can be explained by the fact that the benzylic C-H bond is weaker than the others and leads to the formation of a conjugated adsorbed system after the C-H dissociation (Scheme 4). Repeated C-H dissociation and D — * addition can account for essentially complete exchange at carbon 7.

Besides CD$_2$ type carbon atoms, the presence of some CH$_2$ and CHD type carbon atoms on carbon 5 is also seen from the detailed ^{13}C NMR spectrum (Fig 3). The triplet (28.38, 28.121, 27.862 ppm) and the quintet (28.28, 28.02, 27.77, 27.52, 27.26 ppm) both with coupling constant (*J*) about 19 Hz are

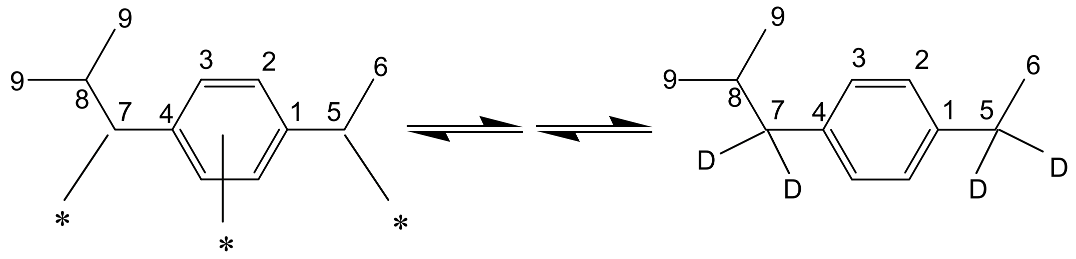

Scheme 4: H/D exchange/addition occurring on carbon 5 and carbon 7 of *4*-IBEB

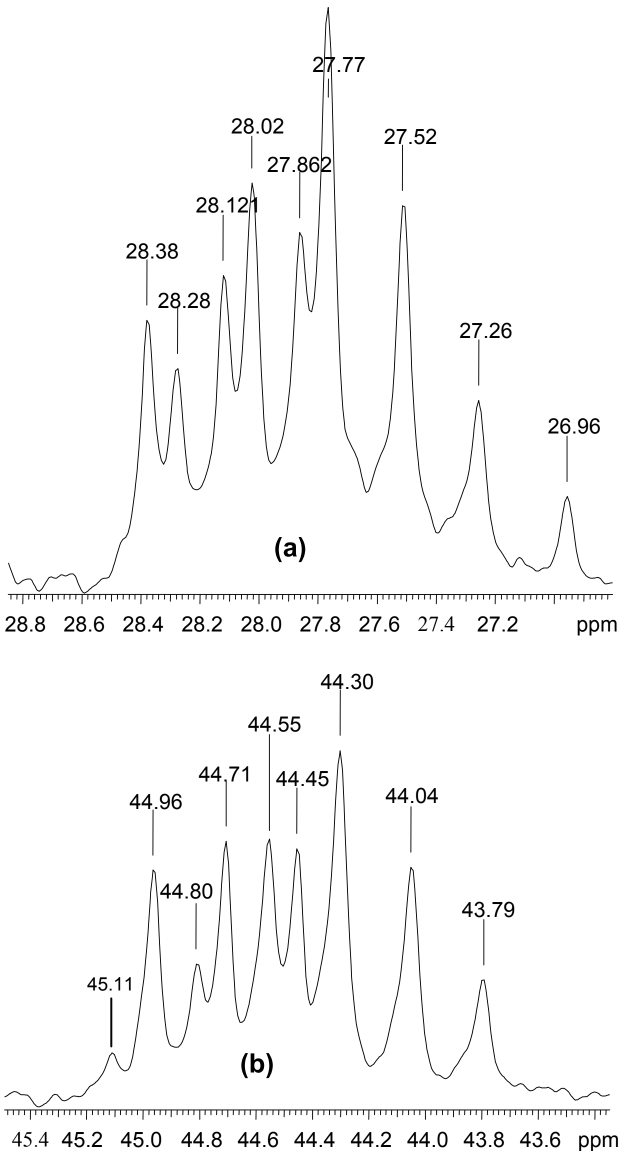

Figure 3: ^{13}C NMR spectra of *4*-IBEB indicating (a) multiplicity on carbon 5 and (b) multiplicity on carbon 7

attributed to the mono- and bi-deuterated carbon 5 (Figure. 3 a). The peak at 26.96 in Figure. 3 a, is assigned to the CH_2 type carbon. Similarly, the presence of mono- and bi-deuterated carbon was also seen on carbon 7 as a triplet (44.45, 44.71, 44.96 ppm) and a quintet (43.79, 44.04, 44.30, 44.55, 44.80 ppm) with the same coupling constant (Figure. 3 b). Additionally, some residual CH_2 type carbon 7 was found at 45.11 ppm. The source of the hydrogen could either be the substrate or the solvent as also suggested by Ranade and Prins [12]. An experiment in which the catalyst was reduced with hydrogen instead of deuterium also gave

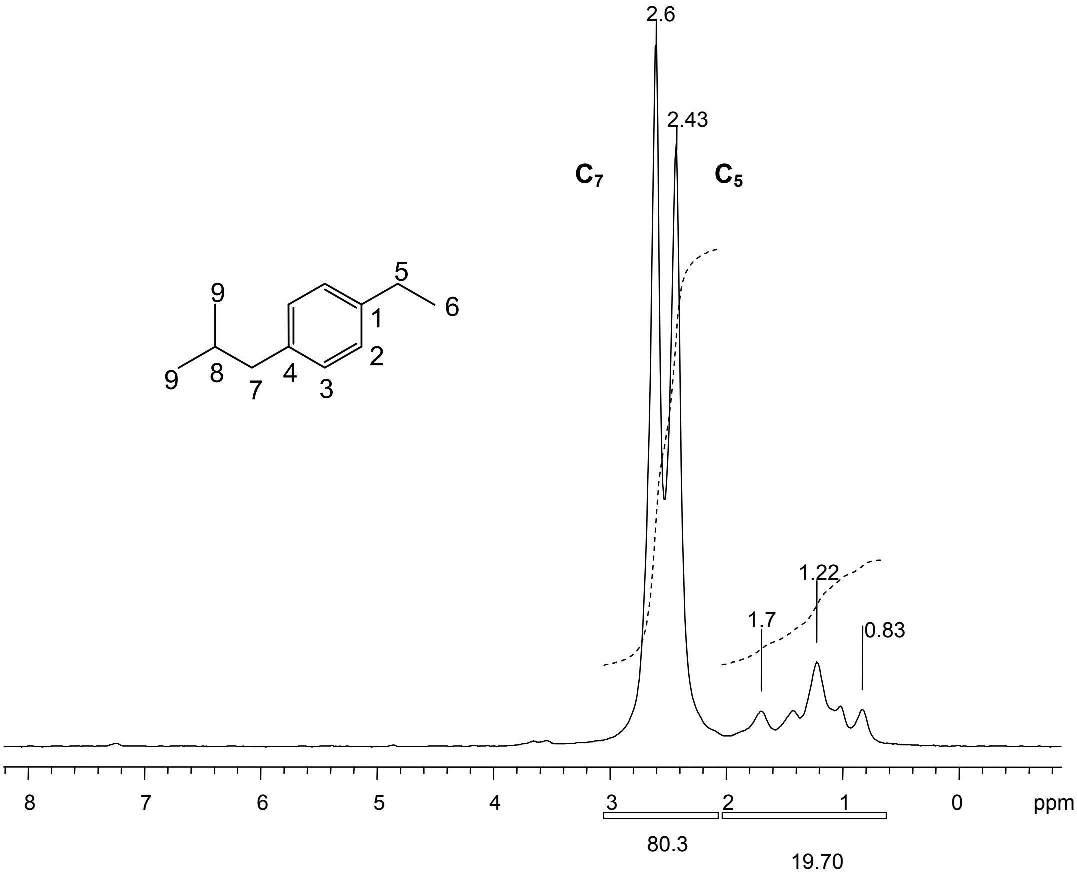

Figure 4: Proton decoupled ^2H NMR spectrum of *4*-IBEB product of the deuteration of *4*-IBAP over Pd/SiO_2

similar results as those shown in Figure. 3, although the degree of deuteration was obviously lower (by 7%).

Two peaks at 2.4 and 2.6 ppm in the proton-decoupled ^2H NMR spectrum provide us with conclusive evidence of deuterium incorporation on carbon atoms 5 and 7, respectively (Figure. 4). Furthermore, the presence of minor peaks is observed in the ^2H NMR spectrum in the range from 0 to 2 ppm, which could be attributed to an artefact.

The essential absence of deuterium on carbon 6 (Figure. 4) demonstrates that the transformation of *4*-IBPE to *4*-IBEB over a Pd/SiO_2 occurs exclusively by direct hydrogenolysis of the C-O bond. The elimination of H_2O from *4*-IBPE leading to *4*-IBSty can be excluded. There are two possible mechanisms to explain the hydrogenolysis of *4*-IBPE (*i*) an S_N2 type mechanism in which the surface hydrogen displaces the hydroxyl group from its attachment to the carbon atom [10] or (*ii*) a more stepwise mechanism starting with the

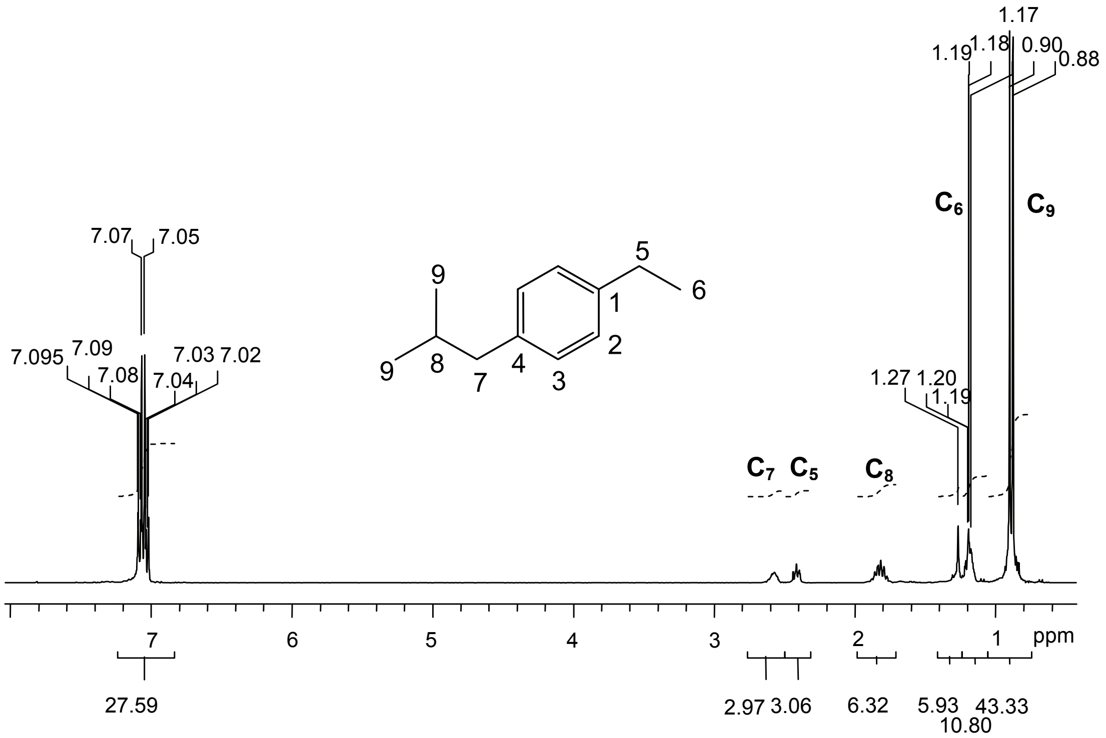

Figure 5: ^{1}H NMR spectrum of 4-IBEB obtained by 4-IBAP deuteration over Pd/C

dissociation of the C-O bond and temporary bonding of the OH group and of the hydrocarbon residue on the Pd surface.

The ^{1}H, ^{2}H and ^{13}C NMR spectra of 4-IBEB obtained by 4-IBAP deuteration over 5% Pd/C differed considerably from those obtained using the 5% Pd/SiO_2 catalyst. Apart from 78% and 74% deuterium incorporation on carbons 7 (2.6 ppm, 2H) and 5 (2.4 ppm, 2H) respectively, as seen from the ^{1}H NMR spectrum of the product 4-IBEB (Figure. 5), significant deuterium incorporation was also observed on carbon 6 (1.19 ppm). This was further confirmed by the multiplicity of the peak corresponding to carbon 6 in the ^{13}C NMR spectrum (Figure. 6). The proton decoupled ^{2}H NMR spectrum (Figure. 7) indicates the presence of deuterium on carbon 6 (1.24 ppm) in addition to that on carbon 5 (2.4 ppm) and carbon 7 (2.6 ppm). This indicates that the transformation of 4-IBPE to 4-IBEB occurs via a combination of the dehydration-hydrogenation pathway and the direct hydrogenolysis pathway over a Pd/C catalyst. Based on the ^{1}H NMR spectrum, an integral of 18.96 would be expected for the hydrogens on carbon 6 (1.2 ppm, 3H), as the integral for a single proton on carbon 8 (1.8 ppm) is 6.32. The integral of 10.8

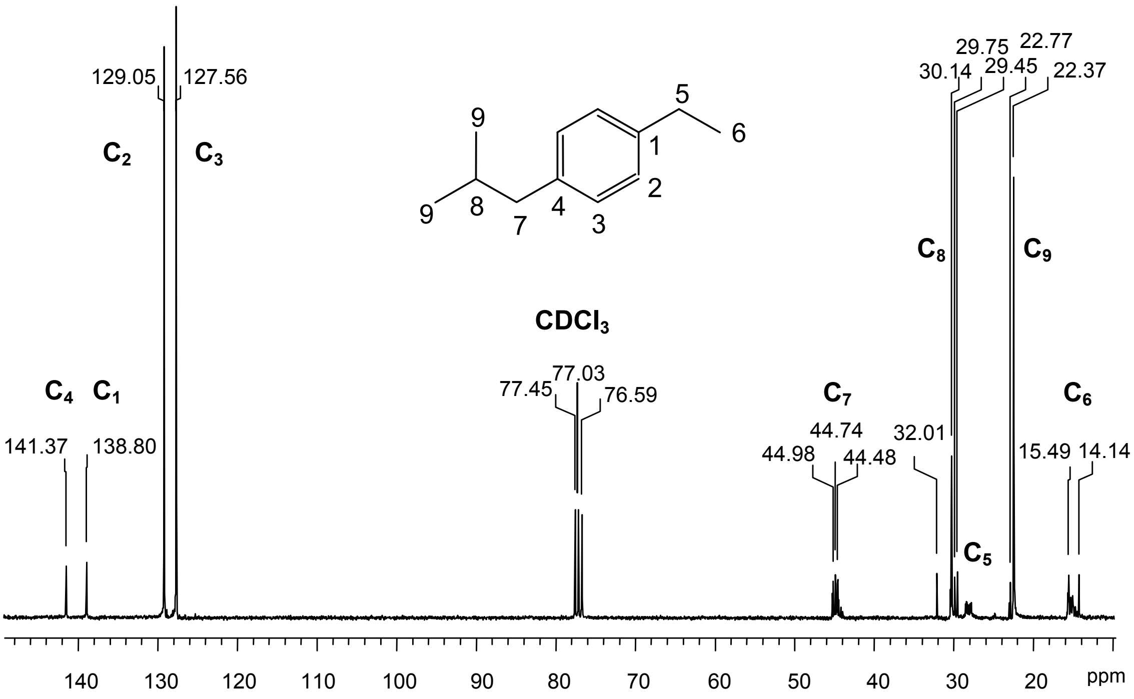

Figure 6: ^{13}C NMR spectrum of 4-IBEB obtained by 4-IBAP deuteration over Pd/C

on carbon 6 suggests 43 % deuterium incorporation as compared to a theoretically expected 33 % deuterium incorporation. However, it was not possible to distinguish between the presence of CH_2D type carbons or CHD_2 and CD_3 type carbons on carbon 6. This result is in contrast to that presented by Ranade and Prins [12], who concluded that the C-O bond scission of 1-indanol over a Rh/C catalyst occurred solely by direct hydrogenolysis. This

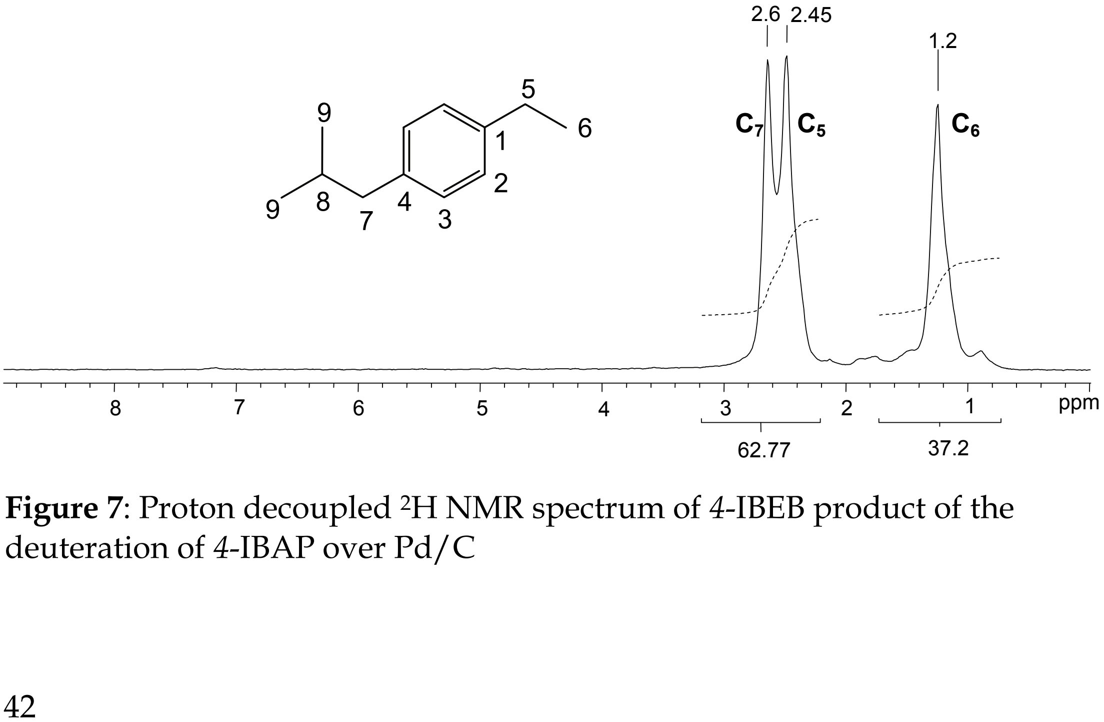

Figure 7: Proton decoupled ^{2}H NMR spectrum of 4-IBEB product of the deuteration of 4-IBAP over Pd/C

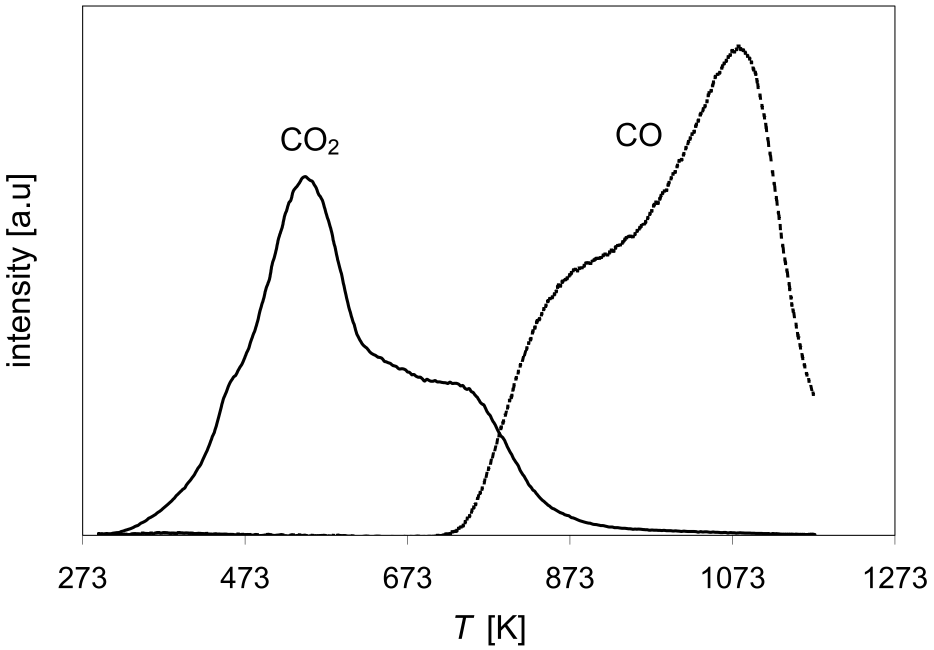

Figure 8: TPD profiles of 5% Pd/C catalyst

can be explained by the fact that carbon supports are frequently activated prior to deposition of the active metal by treatment with mineral acids that oxidize the surface. This oxidative treatment leads to the creation of surface acidic sites [16,17], which might impart acidity to the Pd/C catalyst, thereby promoting the dehydration of the 4-IBPE in our case. This assumption suggests that the C-O bond scission pathway is dependent on the acidity of the support used.

TPD-MS measurements are useful to characterize the type of surface oxygen groups present on the carbon [18]. In an inert atmosphere, the surface oxygen complexes desorb primarily as CO and CO_2. CO_2 appears at relatively low temperatures and is attributed to the decomposition of carboxylic acid and/or anhydride groups: acidic groups where C is bonded to two oxygen atoms. On the other hand, CO desorption occurs at higher temperatures from the decomposition of different types of surface oxygen complexes, i.e. phenolic, carbonyl, quinone, ether and pyrone groups: weakly acidic, neutral and basic groups, where C is bonded to one oxygen atom. The TPD profile of the 5% Pd/C (Figure. 8) shows the presence of CO_2 and CO peaks. The CO_2 evolution ranges from 300 K to around 1050 K, with a large maximum at 550 K and shoulders around 750 K. The former peak can be assigned to carboxylic acid

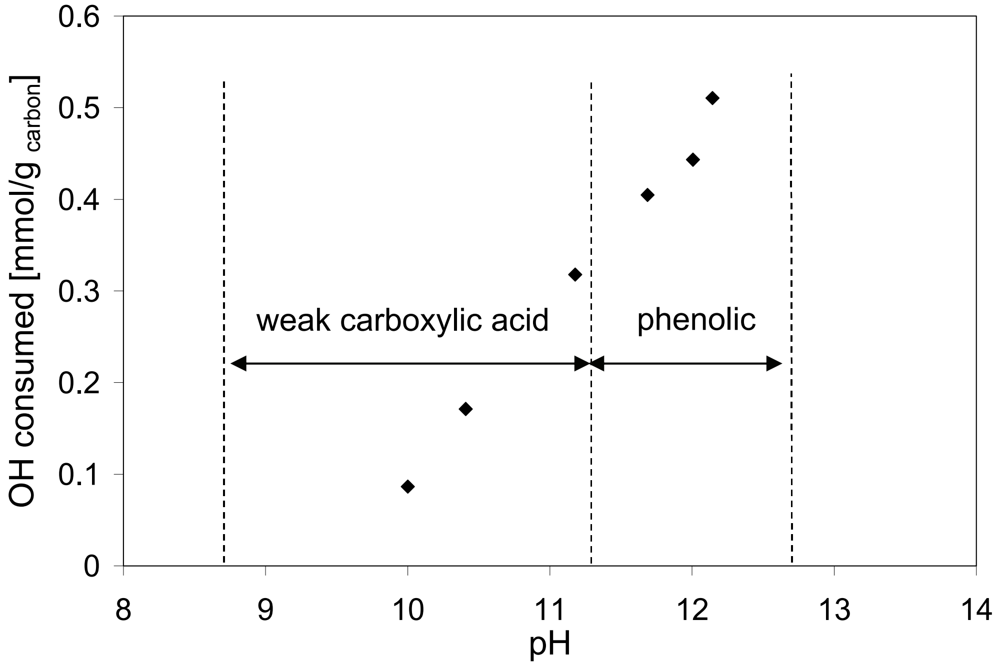

Figure 9: Base adsorption capacity of 5% Pd/C as a function of pH

groups and the latter peak to lactonic groups [18]. The groups that are decomposed above 810 K produce mainly CO and CO_2 and are attributed to the anhydride groups. The CO_2 desorption peak shows the presence of acidic sites on the 5% Pd/C catalyst used.

The titration method gives additional information on the character of the oxygen surface functionalities. The titration curve for 5% Pd/C is shown in Figure. 9, which indicates the presence of weak carboxylic acid groups as well as phenolic groups on the carbon surface. The presence of these groups might impart sufficient acidity to the carbon support to account for the observed dehydration of 4-IBPE to 4-IBSty over 5% Pd/C. The NH_3-TPD spectrum of the SiO_2 support (not shown here) did not show any desorption of NH_3, indicating that the SiO_2 support did not possess sufficiently strong acidic sites. This might explain the reason for not observing the dehydration-hydrogenation pathway on using Pd/SiO_2.

To elucidate whether the hydrogen dissociated on the Pd or the hydrogen that spilt over onto the support after dissociation on Pd was responsible for the hydrogenolysis of the C-O bond, a hydrogenation run was performed over a Pd black catalyst. The formation of 4-IBEB (Figure. 10) implied that the hydrogenation occurs on the Pd surface without the involvement of the

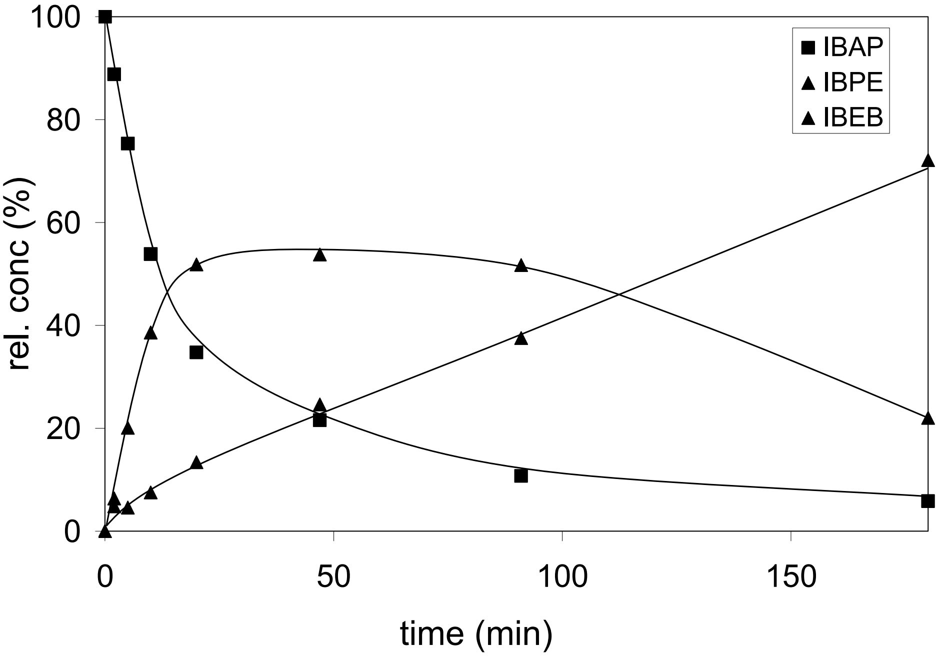

Figure 10: Relative concentration versus time profile for the hydrogenation of 4-IBAP over a commercial Pd black catalyst
Reaction Conditions: w_{cat} = 0.1g, T = 373 K, P_{H2} = 2.0 MPa, C_{IBAP} = 0.27 mol/L

hydrogen that is spilt over on the support. Furthermore, the initial reaction rate (mmol/m^2_{Pd}/s) for the hydrogenation run over Pd black was in the same order of magnitude as compared to that over a Pd/SiO_2 catalyst. Clearly spill-over hydrogen is not involved in the direct hydrogenolysis of the C-O bond of 4-IBPE over Pd.

4. Conclusions

Deuteration in combination with multinuclear NMR spectroscopy resulted in the elucidation of the pathway of the C-O bond scission of 1-(4-isobutylphenyl)ethanol (4-IBPE) to 4-isobutylethylbenzene (4-IBEB) over Pd/SiO_2, Pd/C and unsupported Pd black. The C-O bond scission of 4-IBPE occurred exclusively by the direct hydrogenolysis route over Pd/SiO_2 and Pd black, whereas the dehydration-hydrogenation route also plays an important role when Pd/C was used. This is attributed to the relatively higher acidity of the carbon support as compared to the SiO_2 support. Experiments performed with unsupported Pd black suggest that the hydrogen dissociated on the metal surface plays the major role in the direct hydrogenolysis on Pd without any involvement of the support.

Acknowledgements

Kristina Djanashvili is acknowledged for performing the multinuclear NMR analyses. Nadine F. Polder is acknowledged for performing part of the deuteration experiments as a requirement of the graduate curriculum. Prof. dr. Herman van Bekkum and dr. Guido Mul are also thanked for fruitful discussions.

Reference List

1. E. Breitner, E. Roginski, and P. N. Rylander, 'Low Pressure Hydrogenation of Ketones With Platinum Metal Catalysts', *Journal of Organic Chemistry*, 24 (**1959**) 1855.

2. H. U. Blaser, A. Indolese, A. Schnyder, H. Steiner, and M. Studer, 'Supported Palladium Catalysts for Fine Chemical Synthesis', *Journal of Molecular Catalysis A: Chemical*, 173 (**2001**) 3.

3. V. Elango, 'Method for Producing Ibuprofen', EP 0400 892 A2 (**1990**) to Hoechst Celanese Corp.

4. R. A. Sheldon, 'Chirotechnology: Industrial Synthesis of Optically Active Compounds', (**1993**) 56, Dekker, New York.

5. D. A. Ryan, 'Method of Producing 1-(4-Isobutylphenyl) Ethanol', EP 0358 420 A2 (**1990**) to Hoechst Celanese Corp.

6. K. Saeki and K. Shima, 'Preparation of Aromatic Carbinols From Aromatic Ketones', JP 0262 837 (**1990**) to Daicel Chem. Ind. Ltd.

7. S. P. Mathew, M. V. Rajashekharam, and R. V. Chaudhari, 'Hydrogenation of *p*-Isobutyl Acetophenone Using a Ru/Al_2O_3 Catalyst: Reaction Kinetics and Modeling of a Semi-Batch Slurry Reactor', *Catalysis Today*, 49 (**1999**) 49.

8. M. V. Rajashekharam and R. V. Chaudhari, 'Kinetics of Hydrogenation of *p*-Isobutyl Acetophenone Using a Supported Ni Catalyst in a Slurry Reactor', *Chemical Engineering Science*, 51 (**1996**) 1663.

9. N. Thakar, R. J. Berger, F. Kapteijn, and J. A. Moulijn, 'Modelling Kinetics and Deactivation for the Selective Hydrogenation of an Aromatic Ketone', *Chemical Engineering Science*, (**2007**) *in press*.

10. A. P. G. Kieboom, J. F. De Kreuk, and H. van Bekkum, 'Substituent Effects in the Hydrogenolysis of Benzyl Alcohol Derivatives Over Palladium', *Journal of Catalysis*, 20 (**1971**) 58.

11. R. L. Burwell Jr., 'Deuterium As a Tracer in Reactions of Hydrocarbons on Metallic Catalysts', *Accounts of Chemical Research*, 2 (**1969**) 289.

12. V. S. Ranade and R. Prins, 'Hydrogenolysis of Benzylic Alcohols on Rhodium Catalysts', *Chemistry: A European Journal*, 6 (**2000**) 313.

13. J. Wang and B. McEnaney, 'Quantitative Calibration of a TPD-MS System for Carbon Monoxide and Carbon Dioxide Using Calcium Carbonate and Calcium Oxalate', *Thermochemica Acta*, 190 (**1991**) 143.

14. H. E. van Dam and H. van Bekkum, 'Preparation of Platinum on Activated Carbon', *Journal of Catalysis*, 131 (**1991**) 335.

15. H. P. Boehm, 'Some Aspects of the Surface Chemistry of Carbon Black and Other Carbons', *Carbon*, 32 (**1994**) 759.

16. M. A. Fraga, E. Jordao, M. J. Mendes, M. M. A. Freitas, J. L. Faria, and J. L. Figueiredo, 'Properties of Carbon-Supported Platinum Catalysts: Role of Carbon Surface Sites', *Journal of Catalysis*, 209 (**2002**) 355.

17. F. Rodriguez-Reinoso, 'The Role of Carbon Materials in Heterogeneous Catalysis', *Carbon*, 36 (**1998**) 159.

18. J. L. Figueiredo, M. F. R. Pereira, M. M. A. Freitas, and J. J. M. Orfao, 'Modification of the Surface Chemistry of Activated Carbons', *Carbon*, 37 (**1999**) 1379.

3

Evaluation of deactivation mechanisms of Pd catalyzed hydrogenation of *4*-isobutylacetophenone

Pd catalysts were investigated for the hydrogenation of *4*-isobutylacetophenone (*4*-IBAP) and for Pd/SiO_2 an improved (compared to the non-patented literature) yield of nearly 80 % of the desired product *1*-(*4*-isobutylphenyl)ethanol (*4*-IBPE) was obtained. However, severe catalyst deactivation was observed. The spent catalyst was characterized using a wide variety of thermal (TGA, TPO-MS), microscopic (TEM) and spectroscopic (DRIFT, LEIS) characterization techniques. Pd leaching did not occur. Oligomerization of *4*-IBAP by condensation reactions due to the acidity imparted by the presence of isolated silanol groups on SiO_2 is proposed as one of the causes of catalyst deactivation. Pd crystallite growth and strong chemisorption of the H_2O liberated by *4*-IBPE hydrogenolysis also contributed to the loss of catalytic activity. The conclusions are supported by the high stability of Pd black in catalyzing the reaction.

This chapter is published in the *Journal of Catalysis*, 248 (**2007**) 249-257.

1. Introduction

The liquid phase hydrogenation of *4*-isobutylacetophenone (*4*-IBAP) (Scheme 1) using supported noble metal catalysts is a step in the new catalytic route developed by Hoechst-Celanese [1] for the synthesis of Ibuprofen, a non-steroidal anti-inflammatory drug. The secondary alcohol derivative, *1*-(*4*-isobutylphenyl)ethanol (*4*-IBPE) is the product of interest in this case. The *4*-IBPE is further carbonylated to yield Ibuprofen. Most of the earlier work on *4*-IBAP hydrogenation is patented and only a few publications deal with the reaction mechanism and selectivity issues. The existing literature on the hydrogenation of *4*-IBAP is presented in Table 1 [2]. The Hoechst-Celanese patent [1] focuses on the carbonylation step for the synthesis of Ibuprofen and the hydrogenation step is only mentioned in one example; for this step, a large quantity of Pd/C catalyst is used (*4*- IBAP: 5% Pd/C in a weight ratio of 7:1). The knowledge provided by the patents is very limited and general in nature. The hydrogenation of *4*-IBAP using Ru/Al_2O_3 and Ni/HY has been investigated in detail [2, 3] and the kinetics has been determined for these catalysts. In general, it is observed that the use of high hydrogen partial pressures and a co-catalyst system are desirable to obtain a high selectivity to the desired *4*-IBPE. The use of a supported Pd catalyst is preferred, as Pd is well known to selectively hydrogenate the carbonyl functional group of an aromatic ketone at relatively mild conditions to the hydroxyl group [4]. With the aim of maximizing the yield of the desired product *4*-IBPE, Pd was

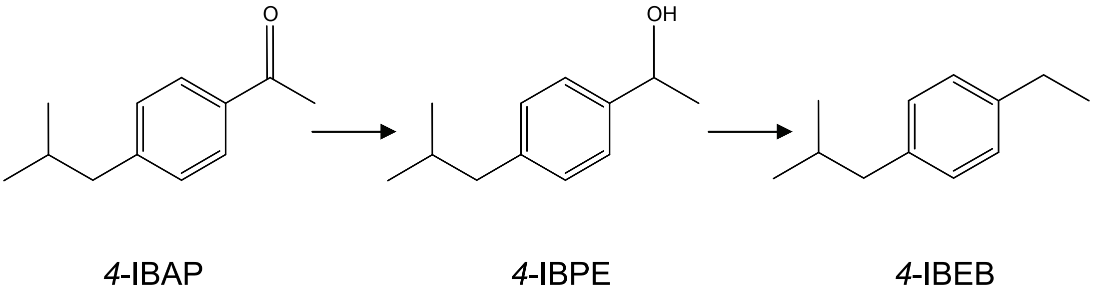

Scheme 1: Reaction scheme for the hydrogenation of *4*-isobutylacetophenone over supported Pd catalysts

Table 1: Literature review on *4*-IBAP hydrogenation

Catalyst	**Promoter**	**Solvent**	***T* (K)**	**P_{H2} (MPa)**	**Conversion 4-IBAP (%)**	**Selectivity 4-IBPE (%)**	**Ref**
Pd/C	-	MeOH	303	6.8	99	97	[1]
Pd/C	Triethyl amine	MeOH	333	8.2	97	100	[6]
Pd/C	Aq. NaOH	n-hexane	373	10.5	99	97	[1]
10% Ni/HY	NaOH	MeOH	373-393	3.0	75	75	[3]
2% Ru/Al_2O_3	-	MeOH	373-398	3.4-6.2	76	60	[2]
10% Ni-1% Pt/HY	NaOH	MeOH	373	3.0	95	65	[5]

therefore tested over a variety of supports such as SiO_2, C and $CaCO_3$.

Deactivation of noble metal catalysts is quite common in the bulk chemicals industry and has been well documented [7,8]. Loss of catalytic activity due to coke formation is well known for Fluidized Catalytic Cracking (FCC), oxidative dehydrogenations and reforming processes [9]. Albers *et al.* [10] reviewed the poisoning and deactivation of supported palladium catalysts and concluded that the nature of the carbonaceous deposits and the strength of their interactions with surface sites of palladium catalysts are crucial with respect to a detrimental impact on activity. Only a few reports exist on catalyst deactivation in the much more complex fine chemical industry [11]. Although no mention has been made of catalyst deactivation problems in the existing patents on 4-IBAP hydrogenation [1,6,12], Rajashekharam *et al.* [5] observed a significant decrease of the activity on catalyst reuse for the hydrogenation of 4-IBAP using Ni/HY catalyst. These authors proposed the use of a bimetallic Ni-Pt/HY catalyst that gave a slightly improved stability on reuse, but did not evaluate the cause of catalyst deactivation. Although we achieved a relatively high yield (~80%) of the desired product 4-IBPE using a Pd/SiO_2 catalyst in a non-polar solvent as compared to that existing in literature [2,3], the catalyst system was not satisfactory due to the severe catalyst deactivation observed. Since there is not much insight into the catalyst deactivation features for this important reaction (and other members of the class of aromatic ketones), this prompted us to investigate the catalyst deactivation for 4-IBAP hydrogenation over Pd/SiO_2. Five theoretically possible reasons for catalyst deactivation suggest themselves (*i*) presence of strongly adsorbing impurities in the commercially available SiO_2 support or reactants (*ii*) polymerization of the 4-isobutylstyrene intermediate possibly formed during the transformation of 4-IBPE to 4-IBEB (*iii*) Strong adsorption of H_2O liberated during the transformation of 4-IBPE to 4-IBEB (*iv*) Pd crystallite growth and (*v*) oligomerization of 4-IBAP or 4-IBPE by condensation type of reactions. In this work, we analyze the possible contribution of each of the above-mentioned phenomena towards catalyst deactivation.

2. Experimental

2.1. Materials and catalyst preparation

4-IBAP was purchased from Alfa Aesar. *n*-decane and *n*-hexadecane were purchased from Aldrich, USA. All the chemicals were used as delivered without further purification. *n*-decane and cyclohexane were used as non-polar solvents, methanol was used as a polar solvent and *n*-hexadecane was used as internal standard. 5 wt.% Pd/C, 5 wt.% Pd/$CaCO_3$ and Pd black are commercially available catalysts.

A series of Pd/SiO_2 catalysts were prepared by the wet-impregnation technique. Palladium acetate trimer purchased from Alfa Aesar was used as the palladium precursor and Davisil 643 (35-74 μm) was used as SiO_2 support. In a typical procedure to prepare the Pd/SiO_2 catalyst, the required amount of precursor was dissolved in excess of toluene and added dropwise to the required amount of SiO_2 support suspended in toluene with continuous mixing. The mixing was carried out overnight. The catalyst was filtered from toluene under vacuum and dried in an oven at 373 K for 16 h. It was subsequently heated to 673 K at 0.5 K/min and calcined in air at 673 K for 5 h.

2.2. Catalyst Characterization

2.2.1. Volumetric N_2 physisorption

N_2 physisorption experiments were performed at 77 K on a Quantachrome Autosorb 6B apparatus after degassing in vacuum at 423 K for 16 h. The amount of sample used was 0.1 g for the fresh catalyst and 0.05 g for the spent catalyst. The specific surface area of the samples was determined from the adsorption isotherms by the BET theory.

2.2.2. CO chemisorption

The catalyst samples (0.1 g for fresh samples and 0.05 g for spent samples) were first dried in vacuum at 403 K (this dry sample weight was used in the calculations). Subsequently, the samples were reduced (100% H_2, 50 cm^3/min, 2

h) at 373 K, followed by evacuation (2 h) at 403 K. The adsorption measurements were performed at 313 K using CO as adsorbate and assuming a CO:Pd = 1:1 stoichiometric ratio. Both the in-situ pre-treatment and the analysis were performed on the Quantachrome Autosorb-1C.

2.2.3. Inductively Coupled Plasma-Optical Emission Spectroscopy (ICP-OES)

ICP-OES of the 'in-house' prepared Pd/SiO_2 catalysts was performed in a PerkinElmer Plasma 2000 apparatus to determine the Pd loading. For the analysis, the samples were dried at 413 K for 5 h and then dissolved in a 1% HF and 1.3 % H_2SO_4 solution.

2.2.4. Transmission Electron Microscopy

Transmission Electron Microscopy (TEM) was performed using a Philips CM30T electron microscope with a LaB_6 filament as the source of electrons operated at 300 kV. The reduced samples were mounted on Quantifoil microgrid carbon polymer supported on a copper grid by placing a few droplets of a suspension of the ground sample in hexane on the grid, followed by drying at ambient conditions.

2.2.5. Thermogravimetric analysis

Thermal analysis was performed on a TGA/SDTA851^e thermobalance from Mettler Toledo using approximately 20 mg sample. In the presence of flowing air (100 cm^3/min), the thermogravimetric (TG) and differential thermogravimetric (DTG) burn-off profiles of the spent catalyst sample were measured with a heating rate of 10 K/min from 298 K to 1073 K.

2.2.6. Temperature Programmed Oxidation-Mass Spectrometry (TPO-MS)

TPO-MS measurements were performed in a conventional flow apparatus using a quartz microreactor and He as a carrier gas flowing at 50 cc/min. About 50 mg of the sample was heated with a rate of 10 K/min from 298 K to 1173 K. The gaseous species from the sample were monitored by a prisma quadrupole mass spectrometer (Balzers) connected on-line with the reactor. Mass spectra were recorded in multiple ion detection (MID) mode using a channeltron detector. The evolved CO_2 and CO were calibrated by a method described by Wang and McEnaney [13] using thermal decompositions of calcium carbonate and calcium oxalate. A 10% correction for the fragmentation of CO_2 to CO was determined by this method, which was close to the 11% correction claimed by the manufacturers.

2.2.7. Diffuse Reflectance Infrared Fourier Transform (DRIFT)

DRIFT spectra for the fresh and spent Pd/SiO_2 samples were recorded on a single beam Nicolet Magna 550 FT-IR spectrometer in a Spectratech DRIFT accessory, against a background spectrum recorded for a sample cup filled with KBr. The spectra were obtained by collection of 256 scans at 8 cm^{-1} resolution and are displayed in absorption reflectance units.

2.2.8. Low Energy Ion Scattering (LEIS)

LEIS experiments were performed in the ultra-high vacuum LEIS instrument, which had a base pressure in the low 10^{-10} mbar range. The pressure increased to 10^{-9} – 10^{-8} mbar during LEIS experiments due to noble gas influx from the ion source. The primary ions were mass selected, focussed and directed perpendicularly to the target. Ions scattered through 145° are accepted by the analyzer. The analyzer is a double toroidal electrostatic analyzer, which makes very efficient use of the backscattered particles by measuring simultaneously a continuous part of the energy spectrum of the backscattered particles and 320° of the azimuthal range. The ion-beam was rastered over an area of 2×2 mm^2 during the measurements, thus reducing the ion-induced damage even more. The catalyst samples were mildly compacted by manually pressing a pestle on a sample holder filled with powder. $^4He^+$ and Ne^+ measurements were performed on 2×2 mm^2 areas of the fresh Pd/SiO_2 sample and of the SiO_2 support itself. Two spent catalyst samples were also analyzed (*i*) Pd/SiO_2 held at reaction temperature for 12 h in a mixture of reactant and solvent under a N_2

atmosphere under stirring (*spent Pd/SiO$_2$, N$_2$*) and (*ii*) Pd/SiO$_2$ held at reaction temperature for 12 h in reactant and solvent followed by a hydrogenation run for 5 h (*spent Pd/SiO$_2$, H$_2$*). Since it is not possible to differentiate between carbon present in the product/solvent and that present in the oligomers by the LEIS technique, the catalyst samples *spent Pd/SiO$_2$, H$_2$* and *spent Pd/SiO$_2$, N$_2$* were calcined in static air at 503 K in order to burn off any traces of product or solvent prior to LEIS measurements.

3. Hydrogenations

Catalytic hydrogenation of *4*-IBAP was carried out in a 500 ml capacity stainless steel stirred reactor (Premex, Switzerland). In a typical hydrogenation experiment, the catalyst was reduced *in-situ* at 373 K under a hydrogen pressure of 10 bar. After cooling, depressurizing and flushing the reactor with N$_2$, the desired amounts of reactant (*4*-IBAP), solvent (*n*-decane) and internal standard (*n*-hexadecane) were charged to the reactor from the liquid holding vessel. The contents (~ 200 ml) were flushed with nitrogen three times at room temperature. After the desired reaction temperature was attained, the system was pressurized with hydrogen to the required pressure. The reaction was started by switching on the stirrer and this was taken as time t = 0. The progress of the reaction was determined by monitoring the hydrogen supply rate (keeping reactor pressure constant) as a function of time. Most semi-batch experiments were carried out at standard conditions of 373 K and 2.0 MPa H$_2$ pressure in *n*-decane using 0.1 g catalyst and a stirring speed of 1500 rpm. After the completion of the reaction as indicated by no further hydrogen consumption, the reactor was cooled to room temperature and depressurized prudently. In all experiments, concentration-time data were generated by intermediate sampling of the liquid phase (~ 250 μl) and analyzing the samples using a gas chromatograph (Chrompack CP9001 equipped with an autosampler), fitted with a CP Sil 8 CB column (50 m × 0.25 mm). The

Table 2: Metal loading of catalysts and corresponding surface areas

Catalyst	Active metal surface area (m^2/g_{cat})	Average Pd crystal size (nm)	Pd dispersion (%)
0.8 % Pd/SiO_2 [a]	1.4	3.6	30
2.4% Pd/SiO_2 [a]	3.4	3.5	32
5% Pd/C [b]	7.4	3.4	33
5% Pd/$CaCO_3$ [b]	1.4	17.5	6
Pd black [b]	6.7	74	1.5

[a] : Pd loading determined by ICP

[b] : Commercial catalyst

conditions were: FID temperature, 523 K; injector temperature, 523 K; and column temperature was increased linearly from 323 K to 523 K at 6.7 K/min.

4. Results

The actual Pd loading as well as the active metal surface area of the various catalysts used is shown in Table 2. Figure 1 compares the initial activity (at 20% conversion) for a 2.4 wt. % Pd/SiO_2 catalyst in polar and non-polar solvents.

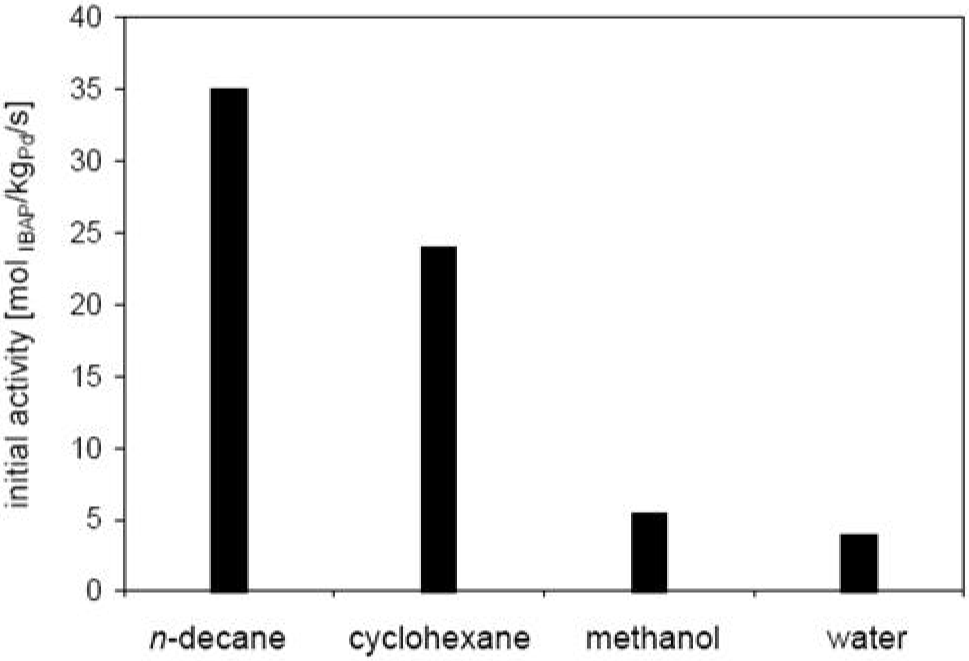

Figure 1: Initial activity of 2.4 % Pd/SiO_2 for 4-IBAP hydrogenation in different solvents at standard conditions
Reaction Conditions: w_{cat} = 0.1 g, C_{IBAP} = 0.27 mol/L, T = 373 K, P_{H2} = 2.0 MPa, stirring rate = 1500 rpm

The highest initial activity ($mol_{IBAP}/kg_{Pd}/s$) was observed for a non-polar solvent (*n*-decane), which was then used as the solvent of choice for all further reactions. The 'in-house' prepared 2.4 wt.% Pd/SiO_2 catalyst performed at least as good as the commercial 5 wt.% Pd/C catalyst (Fig. 2), based on the initial activity, normalized with respect to the active metal surface area ($mmol_{IBAP}/m^2_{Pd}/s$) for a fair comparison between catalysts of different loadings. The 2.4 wt. % Pd/SiO_2 showed a relatively high activity and full conversion in a reasonable time period and hence was used for all further experiments. Reference to Pd/SiO_2 hereafter implies a 2.4 wt.% Pd loading unless specified otherwise.

Only two major products were observed in GC analysis, identified as *1*-(*4*-isobutylphenyl)ethanol (*4*-IBPE) and *4*-isobutylethylbenzene (*4*-IBEB) using GC-MS. A similar reaction profile was observed on using Pd black. This

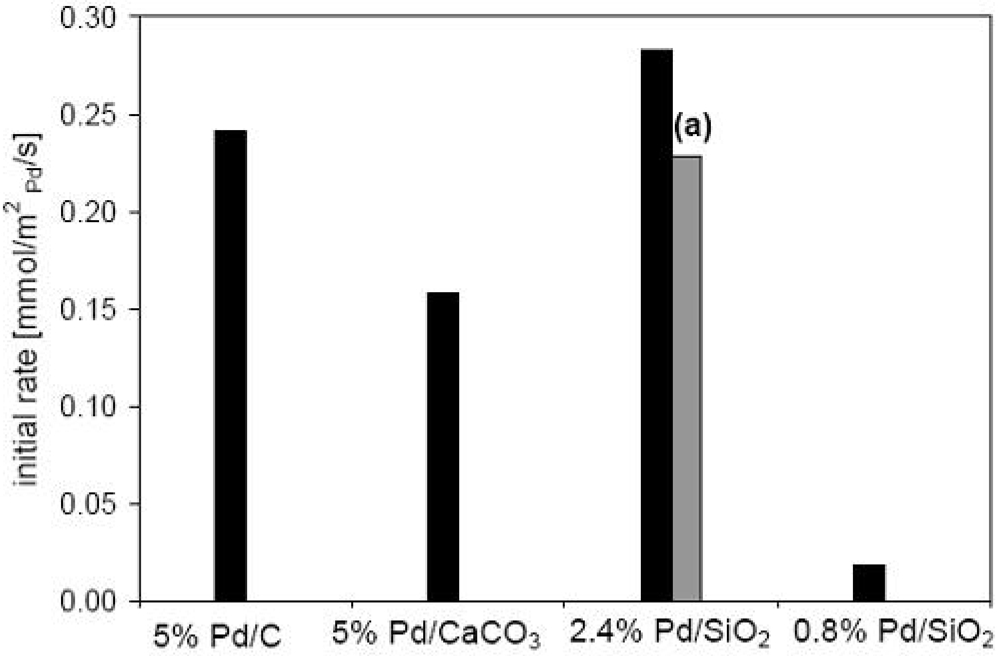

Figure 2: Initial activity of different catalysts for 4-IBAP hydrogenation under standard conditions. **a)** Reaction started after overnight heating under inert atmosphere
Reaction Conditions: w_{cat} = 0.1 g, C_{IBAP} = 0.27 mol/L, T = 373 K, P_{H2} = 2.0 MPa, solvent *n*-decane, stirring rate = 1500 rpm

suggests that the transformation of 4-IBPE to 4-IBEB occurs via direct hydrogenolysis on the metal surface. Conclusive evidence of the hydrogenolysis pathway and the absence of the 4-isobutylstyrene intermediate were obtained by deuteration studies [14]. The reaction scheme for 4-IBAP hydrogenation is shown in Scheme 1. To confirm the absence of Pd leaching into the reaction mixture, the reaction was carried out until 50 % conversion (Figure 3 a) followed by hot-filtration. The filtered reaction mixture was reheated to the reaction temperature (T = 373 K), pressurized with hydrogen and stirred for 50 min. No further reaction occurred as indicated by the absence of H_2 consumption. When fresh catalyst was added (Figure 3 b), the reaction proceeded further to completion, which confirmed the absence of significant Pd leaching into solution. This result was also supported by ICP analysis of the spent reaction mixture, which did not show any significant presence of Pd in the liquid reaction mixture (< 0.5 $mg_{Pd}/kg_{soln.}$)

The H_2O liberated during the transformation of 4-IBPE to 4-IBEB has an inhibiting effect. The activity reduced 5-6 times upon addition of 15 wt.% H_2O (with respect to the reactant 4-IBAP) [15]. Figure 4 (a) shows the performance of

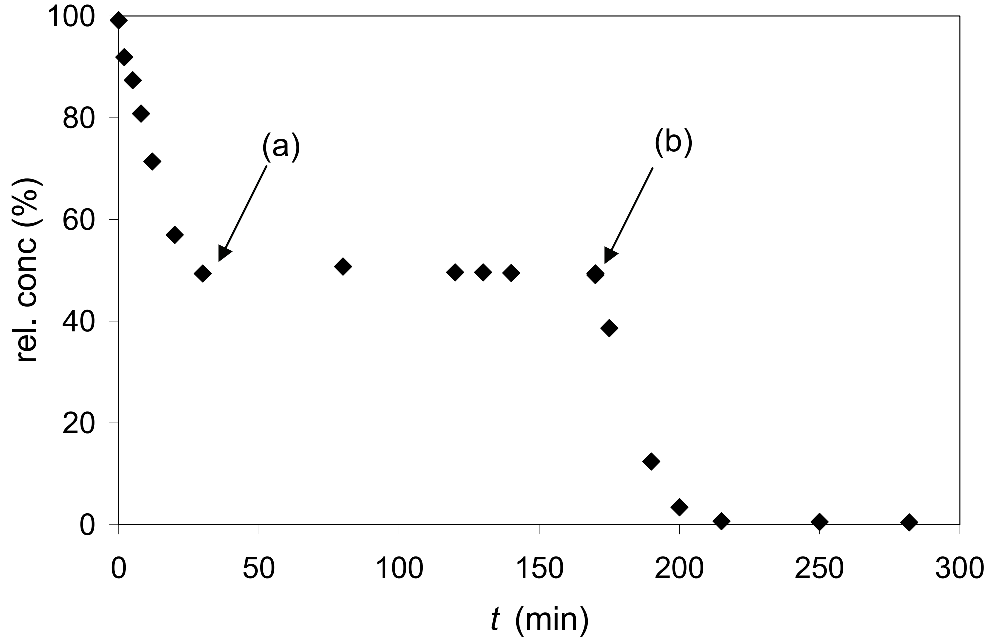

Figure 3: Relative 4-IBAP concentration versus time in a hydrogenation experiment

Reaction Conditions: w_{cat} = 0.1 g, C_{IBAP} = 0.27 mol/L, solvent *n*-decane, T = 373 K, P_{H2} = 2.0 MPa, stirring rate = 1500 rpm

a) H_2 supply stopped and catalyst filtered off; **b)** addition of 0.1 g fresh catalyst

Pd/SiO_2 for the hydrogenation of 4-IBAP using 0.1 g of catalyst. A yield (= selectivity × conversion) of nearly 80 % to 4-IBPE was observed, while only about 50% is reported in literature [2,3]. The 4-IBPE yield however passed through a maximum and appeared to be dependent on the amount of catalyst used (Figure 4 b). A drop in activity was observed when the reaction mixture along with the catalyst was held at the reaction temperature (T = 373 K) for an extended period of time (~12 h) and subsequently pressurized with H_2 (Figure 2 a), as compared to when the reactor was immediately pressurized with H_2 on attaining the reaction temperature. The drop in initial activity on successive hydrogenation runs without catalyst treatment is shown in Figure 5 for Pd/SiO_2 and Pd/C.

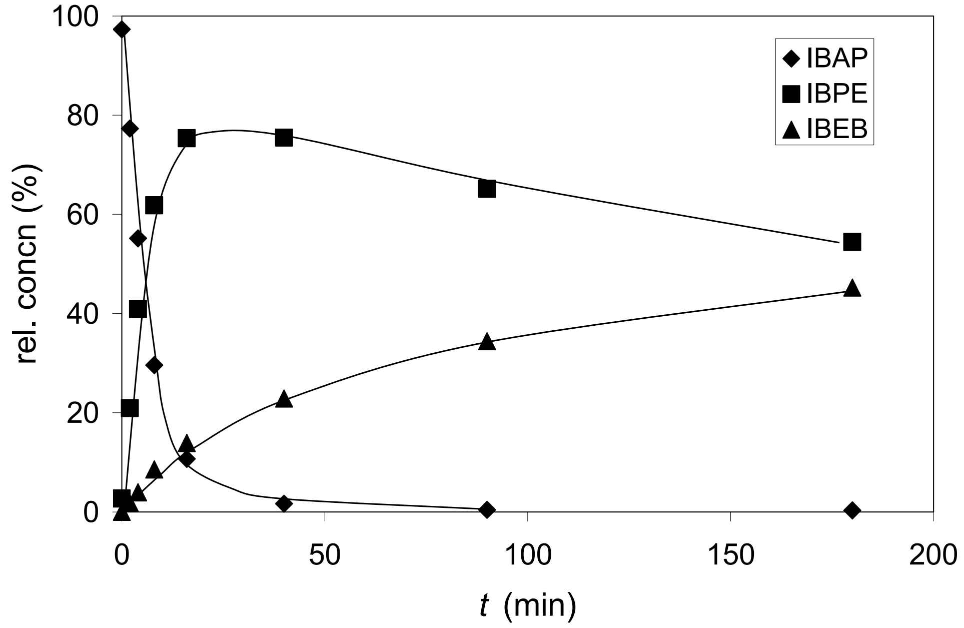

Figure 4 (a): Relative concentration profiles during 4-IBAP hydrogenation with Pd/SiO_2 as a function of reaction time under standard reaction conditions **Reaction Conditions:** w_{cat} = 0.1g, T = 373 K, P_{H2} =2.0 MPa, C_{IBAP} = 0.27 mol/L, solvent *n*-decane

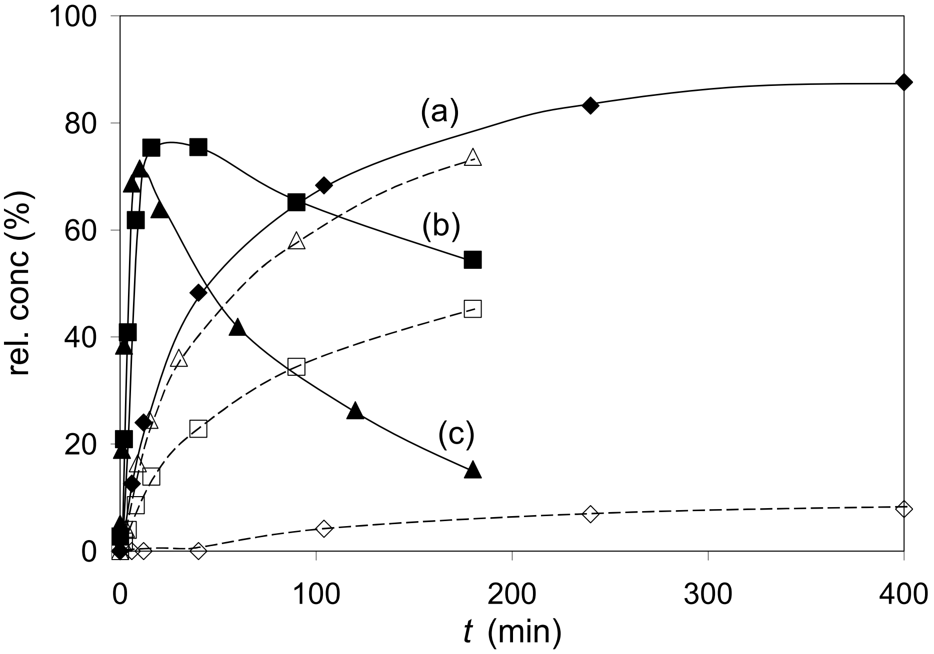

Figure 4 (b): Relative 4-IBPE (solid symbols) and 4-IBEB (open symbols) concentration as a function of time for different catalyst amounts
Reaction Conditions: T = 373 K, P_{H2} =2.0 MPa, C_{IBAP} = 0.27 mol/L, solvent *n*-decane
a) 0.05 g of catalyst **b)** 0.1 g of catalyst **c)** 0.15 g of catalyst

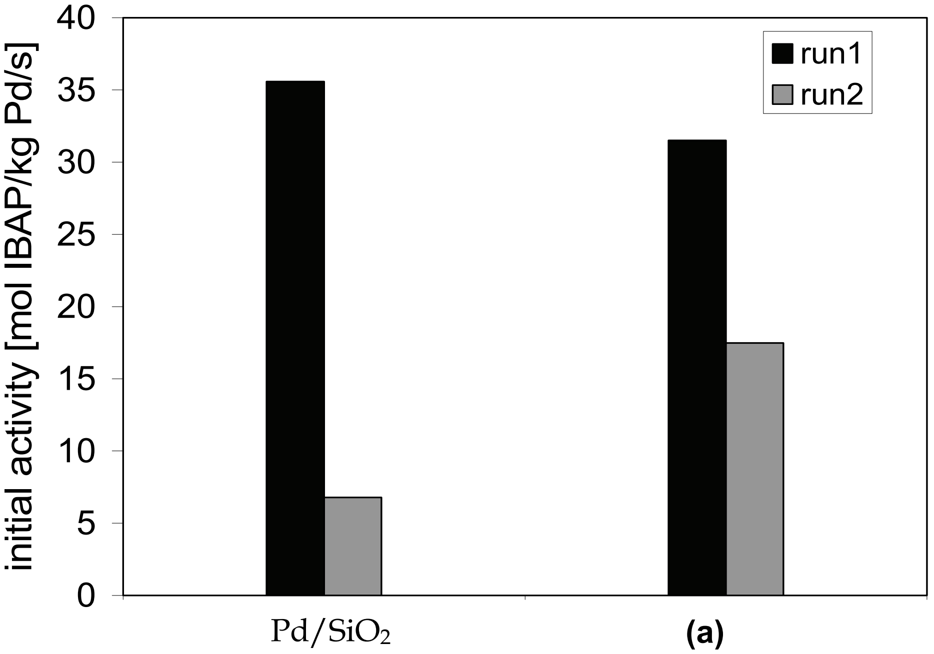

Figure 5: Activity drop on successive runs during 4-IBAP hydrogenation
Reaction Conditions: T = 373 K, P_{H2} = 2.0 MPa, w_{cat} = 0.1g, C_{IBAP} = 0.27 mol/L, solvent *n*-decane

4.1. Catalyst characterization

The fresh and spent Pd/SiO_2 catalysts were characterized using transmission electron microscopy (TEM), N_2 physisorption and CO chemisorption. TEM studies on fresh Pd/SiO_2 revealed Pd particle sizes in the range of 0.5-3 nm (Figure 6 a). CO chemisorption studies on Pd/SiO_2 indicate an average Pd crystallite size of 3.5 nm (based on hemispherical geometry), confirming the TEM results. The Pd crystallite size slightly increases to 4-5 nm for the spent catalyst (Figure 6 b) as compared to the fresh catalysts (ref. Figure 6 (a)). CO chemisorption was also performed on a spent Pd/SiO_2 calcined at similar conditions (T = 503 K) as that of the samples studied by LEIS, and also on a spent Pd/SiO_2 calcined at T = 873 K. The sample calcined at T = 503 K showed an apparent drop of 80 % in the Pd chemisorption capacity, which can be attributed to the presence of deposits on the Pd surface that block access of the CO probe molecules during chemisorption. The sample calcined at T = 873 K showed a drop of only 30 % in the Pd chemisorption capacity. Calcining the sample at 873 K should be sufficient to oxidize all deposits on the catalyst surface and the 30% drop in the chemisorption capacity can be attributed to Pd

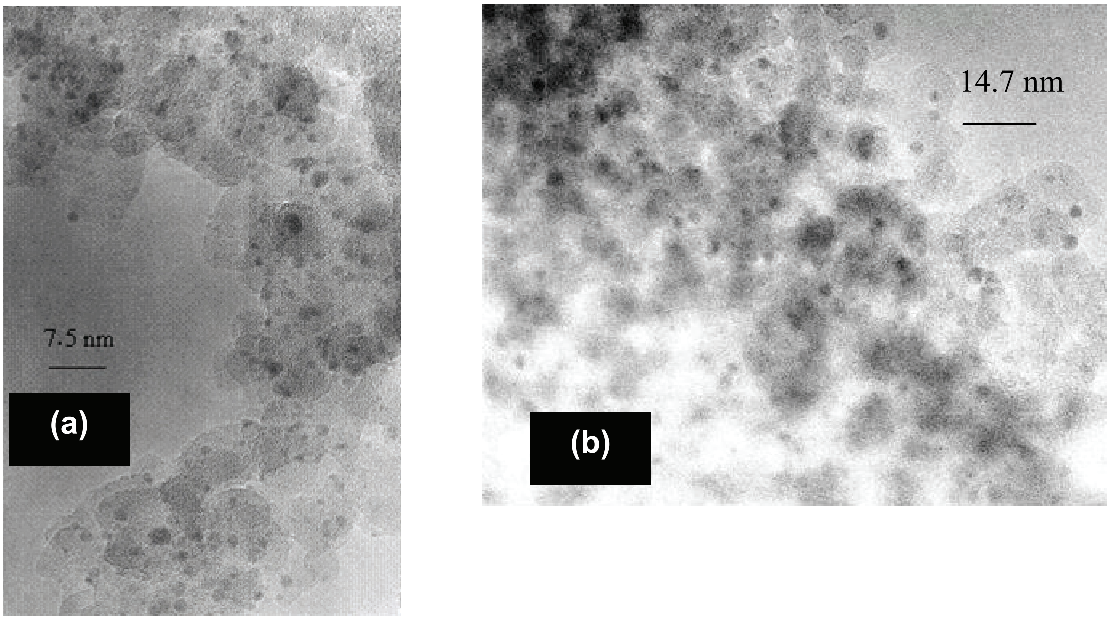

Figure 6: TEM images of **a)** fresh Pd/SiO_2 **b)** spent Pd/SiO_2

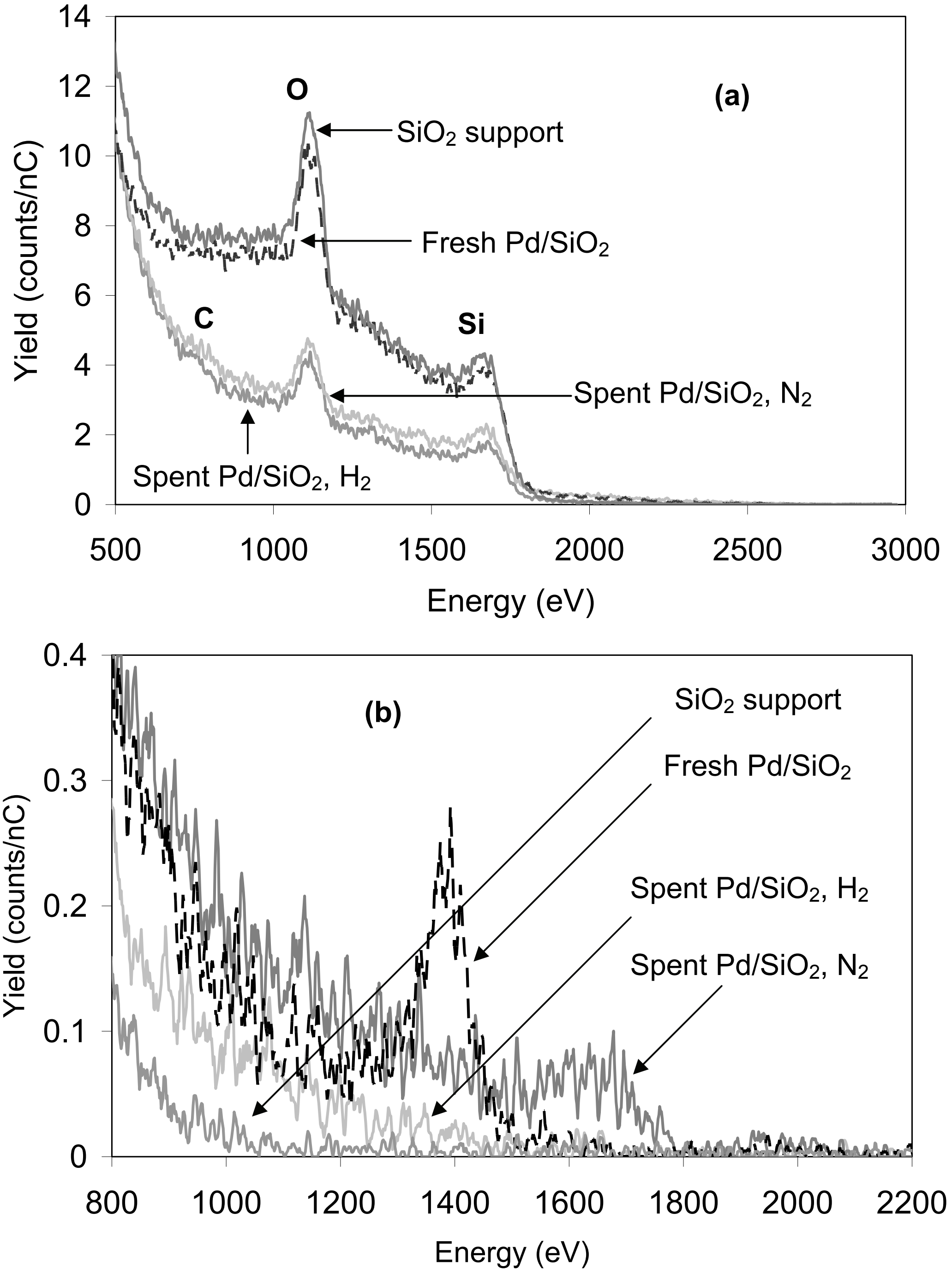

Figure 7 (a) $^4He^+$ and **Figure 7(b)** Ne^+ LEIS spectra for the 'as received' samples. Sample numbers indicated in the figure

sintering occurring due to high temperature calcination. N_2 physisorption also indicated an apparent drop of 12% in the specific SiO_2 surface area of the spent Pd/SiO_2.

Figures 7 (a, b) show the analysis of all the samples studied with the LEIS technique. Sample *Pd/SiO_2, H_2* and sample *Pd/SiO_2, N_2* contain organic carbonaceous deposits as seen from the small carbon peak corresponding to ~750 eV and also from the lower intensities of O and Si as compared to the fresh Pd/SiO_2 and the SiO_2 support respectively (Figure 7 a). The Pd is also completely covered by deposits as seen in Figure 7 b. The sample *Pd/SiO_2, N_2* shows the presence of an additional compound with atomic mass 141 with energy ~1600 eV (Figure 7 b).

The thermogravimetric analysis in air of the spent Pd/SiO_2 is shown in Figure 8. The spent catalyst was first calcined at 473 K for 1 h in order to desorb/burn the solvent and products adsorbed on it. The Single point Differential Thermal Analysis (SDTA) along with the DTG indicates whether the component desorbs from the sample or is burnt off. A peak on the SDTA profile corresponding to a trough on the DTG profile indicates the combustion of the component from the sample. An important weight loss is observed around 550 K, with another around 700 K. Two DTG peaks are also observed in this range of temperature.

The temperature-programmed oxidation coupled with mass spectrometry (TPO-MS) is a useful technique to characterize the nature of species deposited

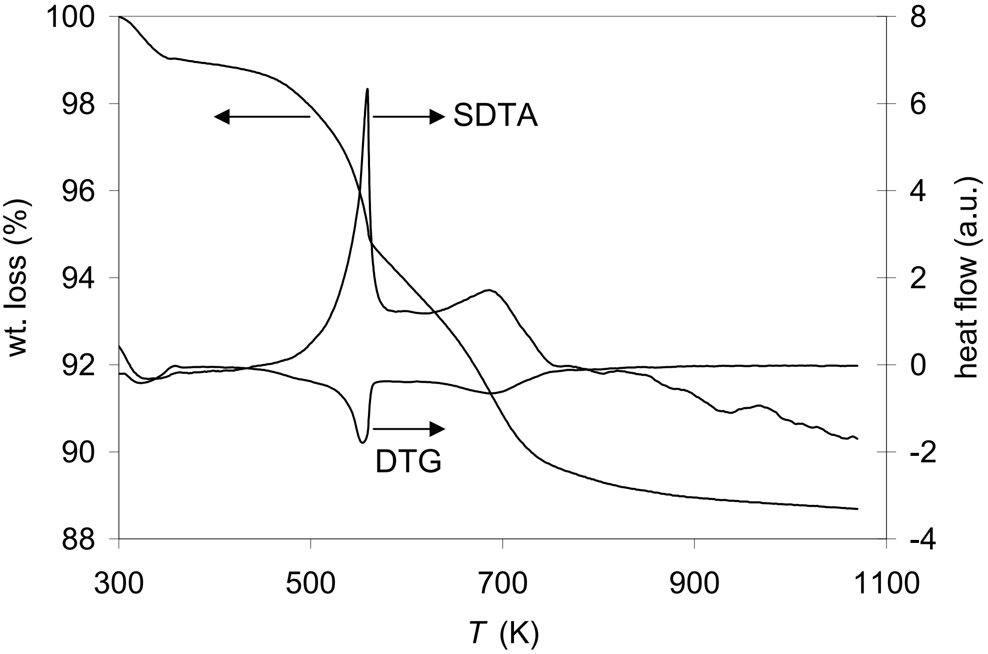

Figure 8: TGA in air of spent Pd/SiO_2

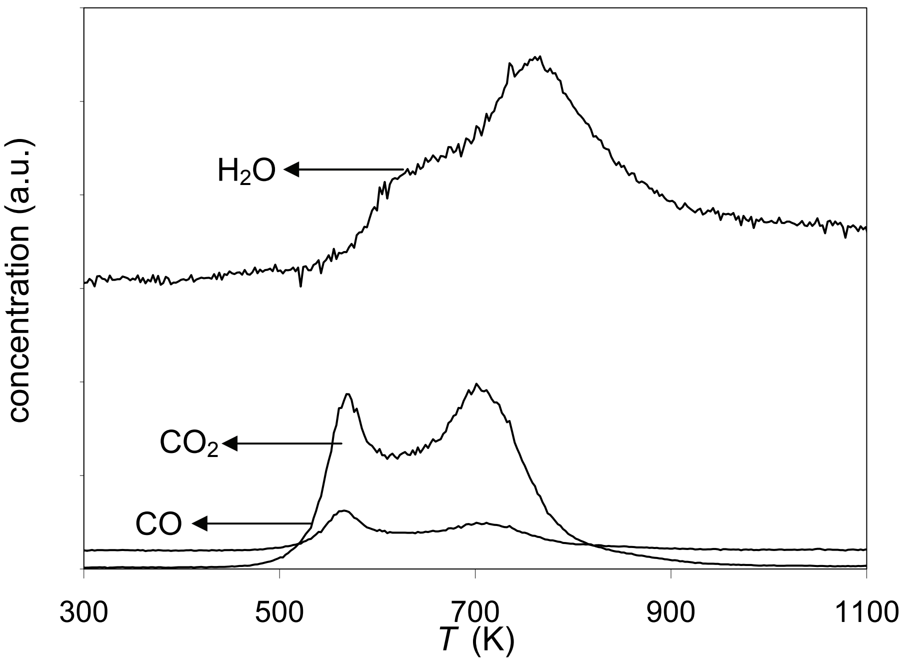

Figure 9: TPO-MS of spent Pd/SiO_2

on the catalyst surface. The TPO-MS profile of the spent Pd/SiO_2 is shown in Figure 9. The catalyst sample was from the same batch of spent catalyst that was used for the TGA test. Three distinct profiles are observed in Figure 9, which correspond to the evolution of CO, CO_2 and H_2O. The H_2O evolution

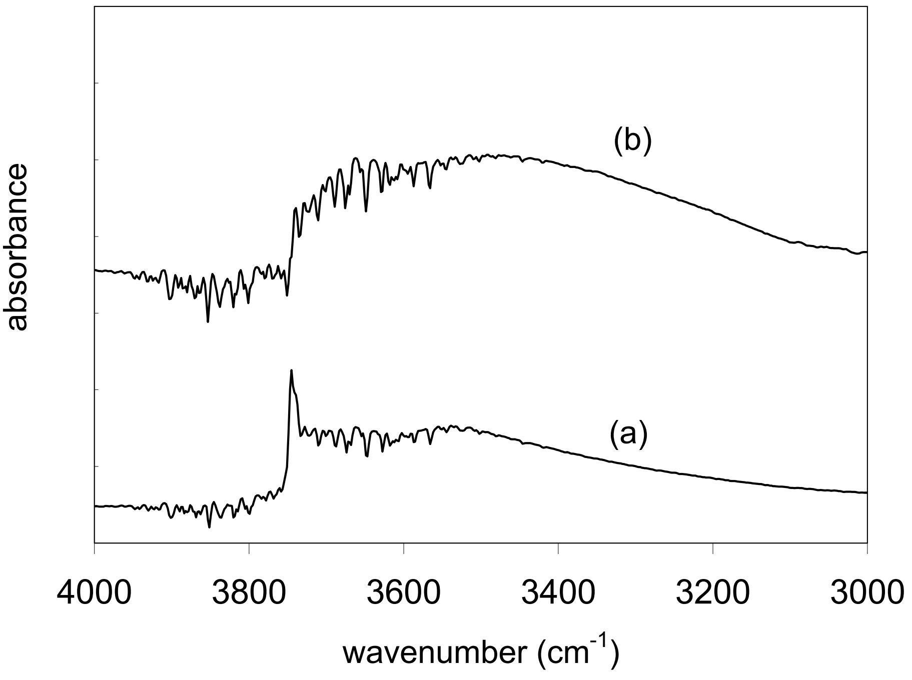

Figure 10: FTIR spectra of **(a)** fresh Pd/SiO_2 and **(b)** spent Pd/SiO_2

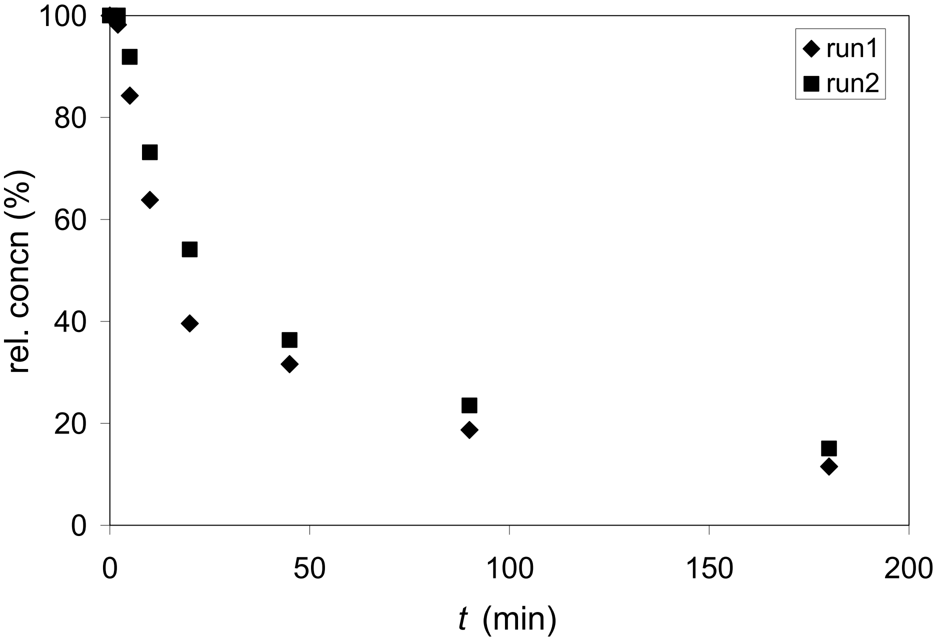

Figure 11: Relative concentration versus time profile as a function of successive semi-batch runs using Pd black
Reaction Conditions: w_{cat} (run 1) = 0.1 g, wcat (run 2) = 0.075 g, T = 373 K, P_{H2} = 2.0 MPa, C_{IBAP} = 0.27 mol/L

peak is corrected for the H_2O evolved due to dehydroxylation of SiO_2 at elevated temperatures. The FTIR spectra of the fresh and of the spent Pd/SiO_2 are shown in Figure 10. A sharp band observed at 3745 cm^{-1} indicates the presence of isolated silanol groups in the SiO_2 support [16]. The performance of Pd black during successive hydrogenation runs is shown in Figure 11. The catalyst was dried at 373 K after the first run and charged to the reactor along with a fresh reaction mixture. Comparable conversion levels were observed in both runs, so significant deactivation does not take place. Figure 12 shows the performance of a commercial 5% Pd/$CaCO_3$ catalyst for the hydrogenation of 4-IBAP. The formation of the undesired 4-IBEB can be attributed to the hydrogenolysis capabilities of Pd [17].

5. Discussion

5.1. Solvent and support effects

Since methanol is the most commonly employed solvent for this reaction as reported in literature it was included in this study too, for which a very low activity was observed. Although only a low activity was observed when H_2O

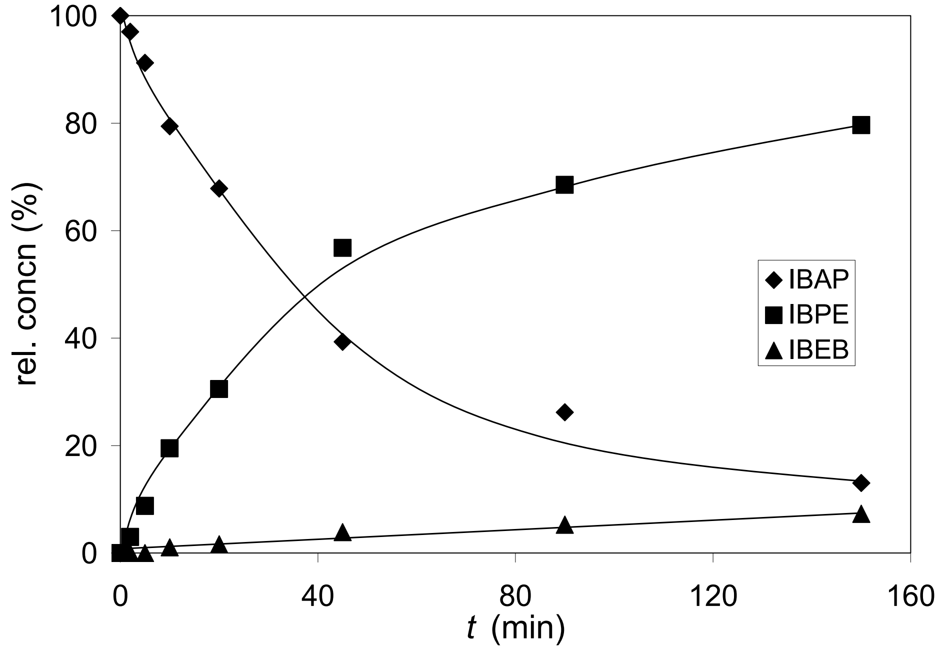

Figure 12: Relative concentration profiles during 4-IBAP hydrogenation with Pd/$CaCO_3$ as a function of reaction time under standard reaction conditions **Reaction Conditions:** w_{cat} = 0.1g, T = 373 K, P_{H2} =2.0 MPa, C_{IBAP} = 0.27 mol/L, solvent *n*-decane

was used as a solvent (< 5% conversion), a moderate catalytic activity was still observed when H_2O was present (~15 wt.% with respect to 4-IBAP) with *n*-decane as solvent. Jaganathan *et al.* [18] observed a similar H_2O inhibitive effect (also for H_2O concentrations > 15 wt.%) for the catalytic hydrogenation of *p*-nitrocumene over Pd/Al_2O_3 and Araya *et al.* [19] observed this effect during methane combustion over Pd/SiO_2 .On replacing H_2O with a non-polar solvent (*n*-decane), the hydrogenation of 4-IBAP proceeded to full conversion. The low activity observed on using excess H_2O (> 15 wt. %) might be explained due to the hydrophobicity of the organic substrates in a non-polar reaction environment. At lower H_2O concentrations, it is possible that H_2O forms a thin film around the SiO_2 due to the cohesive interaction of H_2O with hydrophilic surface silanol groups, leading to agglomeration of the catalyst particles and, as a consequence, to an increased mass transfer resistance for the reactants [20]. Although no experiments were performed under controlled conditions to prove film formation, clusters of the catalyst particles in H_2O droplets were nevertheless observed on opening the reactor after the reaction. The formation of 4-iBuAr$C(OH)_2CH_3$ by hydration of the ketone, which strongly binds to the Pd surface preventing the attack of the hydride could also explain the inhibitive effect of H_2O. Another advantage of using a non-polar solvent is that the ether derivative of 4-IBPE, an unwanted side-product, which is usually formed in presence of methanol as a solvent [5], is eliminated by the use of *n*-decane. A slightly lower activity was achieved using cyclohexane as a solvent (Figure 1), which is explained by the fact that the solubility of hydrogen in *n*-decane is higher than in cyclohexane (Table 3). The lower activity of Pd/$CaCO_3$ as compared to the 2.4 % Pd/SiO_2 catalyst (Figure 2) could be attributed to the lower surface area of the $CaCO_3$ support (~40 m^2/g), which has a negative impact on the Pd dispersion and possibly on the crystal structure. The improved 4-IBPE selectivity on using Pd/SiO_2 could be attributed to the small Pd crystallite size (0.5 – 3 nm), as a drop in 4-IBPE selectivity to 50% was observed on using Pd black, which had an average crystallite size of 74 nm.

5.2. Catalyst Deactivation

The reaction profiles for 4-IBAP hydrogenation (Fig. 4 b) showed a strong dependence on the catalyst loading, indicating that the catalyst probably deactivated during the course of reaction. Although this trend seems obvious for an intermediate product in a consecutive reaction, the levelling off of the 4-IBEB profile on using a low catalyst concentration (w_{cat} = 0.05 g) suggests that this behaviour could also be partly attributed to catalyst deactivation. The possibility of the presence of feed poisons was excluded based on GC-MS and

Table 3: Solubility of hydrogen in solvents at reaction conditions

Solvent	Conditions	Solubility (mole fraction)	Reference
n-Decane	T= 373 K P_{H2} = 2.04 MPa	2.04×10^{-2}	[21]
Cyclohexane	T= 373 K P_{H2} = 2.04 MPa	1.12×10^{-2}	[22]

the LEIS analysis. LEIS appeared to be a very informative technique in this respect, since it convincingly showed that neither the SiO_2 support nor the spent catalysts (*Pd/*SiO_2*,* H_2 and *Pd/*SiO_2*,* N_2) contained any traces of strongly adsorbing impurities. The impurity of atomic mass 141 (energy ~ 1600 eV) as seen in Figure 7 (b) is attributed to Ce and can be explained by the contamination of the spent catalyst (*sample Pd/*SiO_2*,* N_2) during calcination (prior to the LEIS analysis) as the same crucible had been used earlier for CeO_2 calcination. However, a severe loss of greater than 80 % in the hydrogenation activity was observed after the first run (Figure 5). Rajashekharam *et al.* [5] also observed severe deactivation for the hydrogenation of 4-IBAP with Ni/HY catalyst. Polymerization of the 4-isobutylstyrene formed as intermediate leading to catalyst deactivation can be excluded, as the C-O bond scission of 4-IBPE occurred by direct hydrogenolysis i.e. the 4-isobutylstyrene intermediate was never formed during the transformation of 4-IBPE to 4-IBEB. Chang *et al.* [23] reported water poisoning for selective hydrogenation of isoprene using Pd/δ-Al_2O_3. In our studies, the water formed by the hydrogenolysis of 4-IBPE could possibly deactivate the catalyst. Calcining the spent Pd/SiO_2 at 373 K in air restored only ~ 50% of the original catalyst activity and therefore strong H_2O chemisorption was not the only reason for catalyst deactivation.

A common reason for catalyst deactivation is the formation of strongly adsorbing oligomeric/carbonaceous deposits from reactants or products due to undesired side reactions, which lead to loss of activity by blocking the active sites [10]. For high temperature gas-phase reactions in oil refineries, deactivation is usually associated with the formation of coke by a high degree of dehydrogenation. However for liquid phase reactions at much lower reaction temperatures, deactivation due to oligomerization reactions is more probable [24-26]. The activity can sometimes be recovered by removing the deposits with a suitable solvent. However, washing the catalyst with pentane or acetone did not significantly improve the activity in our studies.

CO chemisorption studies on the spent Pd/SiO_2 indicated an apparent drop in Pd surface area from 3.4 m^2/g_{SiO2} to only 0.3 m^2/g_{SiO2}. In principle, the apparent loss of Pd surface area as measured by CO chemisorption could be attributed to oligomeric deposits covering the Pd surface but also to Pd crystallite growth. TEM analyses also reveal a slight increase in the Pd crystallite size (Figure 6 a, b), but a statistically representative TEM analysis is not easy to obtain.

Two significant weight losses due to exothermic processes (SDTA) were observed in TGA of the spent catalyst (Figure 8). A similar profile has been observed for Pt reforming catalysts [27,28]. The first peak could be attributed to the combustion of organic deposits on the metal and the second peak to the deposits on the support [29,30], as deduced from the exothermic peak in the SDTA profile. The TPO-MS profiles (Figure 9) exhibit CO and CO_2 evolution at two distinct temperatures (~ 550 K and 700 K), in accordance with the TGA results. A 10% correction is made for the fragmentation of CO_2 to CO in the mass spectra. It is also interesting to note that H_2O is evolved from 550 – 800 K, which indicates that the deposits on the catalyst surface also contain hydrogen. From the TGA and TPO-MS analyses (Figures 8 and 9), it is concluded that oligomeric deposits on the catalyst are at least partly responsible for the deactivation. These oligomers block the access of CO probe molecules on the Pd crystallites during the CO chemisorption, which contributes to the apparent drop in calculated dispersion. The presence of C and the low intensity of Si on *sample Pd/SiO*$_2$*, N*$_2$ and *sample Pd/SiO*$_2$*, H*$_2$ (compared to the Si intensity of the SiO_2 support) as studied by LEIS (Figure 7 a) confirm the formation of oligomers, which also partly cover the SiO_2 support. This is also supported by reduction in the BET surface area of SiO_2. The low sensitivity of the LEIS instrument to C results in a very small peak for C (Figure 7 a), but is still significant [31].

The presence of isolated silanol groups that can impart local acidity to the SiO_2 support is seen from Figure 10. Based on this observation, we propose that 4-IBAP, an aromatic ketone, undergoes oligomerization by condensation type reactions, thereby leading to the formation of higher molecular weight species and subsequently deactivating the catalyst mainly by fouling. This could also explain the drop in catalyst activity when the catalyst and the reaction mixture were heated for 12 h in a N_2 atmosphere, as shown in Figure 2 (a). TGA of the spent SiO_2 sample subjected to a hydrogenation run under standard conditions (w_{SiO2} = 0.1 g, T = 373 K, C_{IBAP} = 0.27 mol/L) showed a single exothermic peak (SDTA) ~ 700 K, confirming the role of the SiO_2 support in oligomerization. The contribution of 4-IBPE to oligomerization seems unlikely since theoretically, a maximum of only two 4-IBPE molecules can condense to form an ether which might be insufficient to form oligomers. Furthermore, it was not possible to perform catalyst stability studies using 4-IBPE, as the 4-IBPE (in the absence of hydrogen atmosphere) was dehydrogenated to 4-IBAP at the reaction temperature (T = 373 K) as observed by ATR-FTIR studies. Pressurizing the reactor with H_2 at room temperature itself would lead to the formation of 4-IBEB at lower temperatures thus leading to erroneous results.

Since the oligomerization is proposed to occur due to the acidic nature of the isolated silanol groups on the Pd/SiO_2, the use of Pd black should not lead to any oligomerization/deactivation. A successive hydrogenation run performed using Pd black led to nearly similar conversion levels in both runs indicating that the deactivation was very modest (Figure 11). This further confirms our proposition that the isolated silanol groups on the SiO_2 support led to oligomer formation. Calcining the spent Pd/SiO_2 at an extreme temperature of 873 K led to a 30% drop in the Pd surface area. Considering that the hydrogenations were performed at only 373 K, the contribution of Pd crystallite growth to catalyst deactivation must be insignificant as compared to the contribution of oligomers. Thus, the catalyst deactivation during 4-IBAP hydrogenation over Pd/SiO_2 is proposed to occur due to combined effects of (*i*) oligomerization (*ii*) strong H_2O inhibition and (*iii*) Pd crystallite growth.

The deactivation phenomenon was not restricted to the Pd/SiO_2 catalysts and was also observed for the commercial 5% Pd/C and 5% Pd/Al_2O_3 catalysts. Elsewhere it is shown that this Pd/C contains relatively strong acid sites, explaining the deactivation by oligomerization [14]. The alumina supported catalyst was not analyzed in detail, but it is reasonable to assume that acid sites are also present here. Deactivation was also observed over a 5% Pd/$CaCO_3$ catalyst, indicating that the deactivation phenomenon was not restricted to acidic supports only. Thus the deactivation due to oligomerization is an inherent feature of supported Pd catalyzed 4-IBAP hydrogenation, irrespective of the type of support (acidic or basic) used.

Since the hydrophilicity of SiO_2 led to loss of catalytic activity due to H_2O adsorption and the isolated silanol groups were proposed to be responsible for the condensation reactions of 4-IBAP, the use of a hydrophobic SiO_2 could provide a solution. Pd was impregnated on a commercially available hydrophobic SiO_2 support (Aerosil R972) in which the silanol groups are methylated. However, poor catalyst stability was observed in this case also. Due to the absence of a large number of hydroxyl groups, a very small amount of Pd incorporation was achieved (0.15 wt.% Pd/SiO_2). Subsequent calcinations of the impregnated catalyst at elevated temperatures (473 - 673 K), necessary to convert the Pd acetate precursor to Pd oxide also resulted in the regeneration of the silanol groups, which could explain the poor observed stability on reuse.

6. Conclusions

Amongst the different supported Pd catalysts studied, Pd/SiO_2 showed the highest initial activity for hydrogenation of 4-IBAP. The 80% yield of 4-IBPE is significantly higher than that reported in the non-patented literature. The catalyst severely deactivated after a semi-batch run. Leaching of Pd into the reaction medium does not occur. Characterization of the spent catalyst by a wide variety of techniques indicated that the formation of oligomers was one of the causes for the loss of catalytic activity. The presence of strongly adsorbing impurities leading to deactivation was excluded by LEIS analysis. Pd crystallite growth was also observed. The H_2O liberated during 4-IBPE hydrogenolysis chemisorbed on the Pd leading to loss of catalytic activity. The presence of isolated silanol groups resulted in an increased acidity of the SiO_2 support, leading to the formation of oligomeric species on the catalyst surface and consequent deactivation.

Acknowledgements

Prof. H. H. Brongersma and A. Knoester (Calipso B.V.) are acknowledged for the LEIS analysis and discussions. Prof. W. Buijs is thanked for his valuable inputs. B. van der Linden is acknowledged for assistance with TGA, TPO-MS and DRIFT set ups.

Reference List

1. E. Varadaraj, 'Method for Producing Ibuprofen', EP 0400 892 A2 (**1990**) to Hoechst Celanese Corp.

2. S. P. Mathew, M. V. Rajashekharam and R. V. Chaudhari, 'Hydrogenation of *p*-Isobutyl Acetophenone Using a Ru/Al_2O_3 Catalyst: Reaction Kinetics and Modeling of a Semi-Batch Slurry Reactor', *Catalysis Today*, 49 (**1999**) 49.

3. M. V. Rajashekharam and R. V. Chaudhari, 'Kinetics of Hydrogenation of *p*-Isobutyl Acetophenone Using a Supported Ni Catalyst in a Slurry Reactor', *Chemical Engineering Science*, 51 (**1996**) 1663.

4. H.U. Blaser, A. Indolese, A. Schnyder, H. Steiner and M. Studer, 'Supported Palladium Catalysts for Fine Chemical Synthesis', *Journal of Molecular Catalysis A: Chemical*, 173 (**2001**) 3.

5. M. V. Rajashekharam and R. V. Chaudhari, 'Improved Stability of a Bimetallic Ni-Pt Catalyst for Hydrogenation of Acetophenone and Substituted Derivatives', *Catalysis Letters*, 41 (**1996**) 171.

6. D. A. Ryan, 'Method of Producing *1*-(*4*-Isobutylphenyl) Ethanol', EP 0358 420 A2 (**1990**) to Hoechst Celanese Corp.

7. J. A. Moulijn, A. E. van Diepen and F. Kapteijn, 'Catalyst Deactivation: Is It Predictable? What to Do?', *Applied Catalysis A: General*, 212 (**2001**) 3.

8. G. F. Froment, 'Coke Formation in Catalytic Processes: Kinetics and Catalyst Deactivation', *Studies in Surface Science and Catalysis*, 111 (**1997**) 53.

9. C. H. Bartholomew, 'Mechanisms of Catalyst Deactivation', *Applied Catalysis A: General*, 212 (**2001**) 17.

10. P. Albers, J. Pietsch and S. F. Parker, 'Poisoning and Deactivation of Palladium Catalysts', *Journal of Molecular Catalysis A: Chemical*, 173 (**2001**) 275.

11. D. Y. Murzin and T. Salmi, 'Deactivation in Liquid Phase Heterogeneous Catalytic Reactions', *Trends in Chemical Engineering*, 8 (**2003**) 137.

12. K. Saeki and K. Shima, 'Preparation of Aromatic Carbinols From Aromatic Ketones', JP 0262 837 (**1990**), to Daicel Chemical Ltd.

13. J. Wang and B. McEnaney, 'Quantitative calibration of a TPD-MS system for carbon monoxide and carbon dioxide using calcium carbonate and calcium oxalate', *Thermochemica Acta* 190 (**1991**) 143.

14. N. Thakar, N. F. Polder, K. Djanashvili, H. van Bekkum, F. Kapteijn and J. A. Moulijn, 'Deuteration Study to Elucidate Hydrogenolysis of Benzylic Alcohols Over Supported Palladium Catalysts', *Journal of Catalysis*, 246 (**2007**) 344.

15. N. Thakar, R. J. Berger, F. Kapteijn and J. A .Moulijn, 'Modelling Kinetics and Deactivation for the Selective Hydrogenation of an Aromatic Ketone Over Pd/SiO_2', *Chemical Engineering Science*, (**2007**) *in press.*

16. J. C. Groen, L. A. A. Peffer, J. A. Moulijn and J. Perez-Ramirez, 'Mechanism of Hierarchial Porosity Development in MFI Zeolites by Desilication: The Role of Aluminum As a Pore-Directing Agent', *Chemistry - A European Journal*, 11 (**2005**) 4983.

17. P. N. Rylander, 'Catalytic Hydrogenation Over Platinum Metals', Academic Press, New York (**1967**).

18. R. Jaganathan, V. G. Ghugikar, R. V. Gholap, R. V. Chaudhari and P. L. Mills, 'Catalytic Hydrogenation of *p*-Nitrocumene in a Slurry Reactor', *Industrial and Engineering Chemistry Research*, 38 (**1999**) 4634.

19. P. Araya, S. Guerrero, J. Robertson and F. J. Gracia, 'Methane Combustion Over Pd/SiO_2 Catalysts With Different Degrees of Hydrophobicity', *Applied Catalysis A: General*, 283 (**2005**) 225.

20. B. M. A. Wolfenbuttel, T. A. Nijhuis, A. Stankiewicz and J. A. Moulijn, 'Influence of water on fast hydrogenation reactions with monolithic and slurry catalysts', *Catalysis Today*, 69 (**2001**) 265.

21. E. Brunner, 'Solubility of Hydrogen in 10 Organic Solvents at 298.15, 323.15 and 373.15 K', *Journal of Chemical Engineering Data*, 30 (**1985**) 269.

22. M. Herskowitz, J. Wisniak and L. Skladman, 'Hydrogen Solubility in Organic Liquids', *Journal of Chemical Engineering Data*, 28 (**1983**) 164.

23. J. R. Chang, T. B. Lin and C. H. Cheng, 'Pd/α-Al_2O_3 Catalysts for Isoprene Selective Hydrogenation: Regeneration of Water Poisoned Catalysts', *Industrial and Engineering Chemistry Research*, 36 (**1997**) 5096.

24. L. P. Tiainen, M. A. Paivi, A. K. Neyestenaki, T. Salmi and D. Y. Murzin, 'Modelling of Catalyst Deactivation in Liquid Phase Reactions: Citral Hydrogenation on Ru/Al_2O_3', *Reaction Kinetics and Catalysis Letters*, 78 (2003) 251.

25. E. Santacesaria, M. Di Serio, R. Velotti and U. Leone, 'Kinetics, Mass Transfer, and Palladium Catalyst Deactivation in The Hydrogenation Step of the Hydrogen Peroxide Synthesis Via Anthraquinone', *Industrial and Engineering Chemistry Research*, 33 (**1994**) 277.

26. M. Burgener, R. Wirz, T. Mallat and A. Baiker, 'Nature of Catalyst Deactivation During Citral Hydrogenation: a Catalytic and ATR-IR Study', *Journal of Catalysis*, 228 (**2004**) 152.

27. C. L. Li, O. Novaro, E. Munoz, J. L. Boldu, X. Bokhimi, J. A. Wang, T. Lopez and R.Gomez, 'Coke Deactivation of Pd/H-Mordenite Catalysts Used for C_5/C_6 Hydroisomerization', *Applied Catalysis A: General*, 199 (**2000**) 211.

28. J. Barbier, 'Deactivation of Reforming Catalysts by Coking - a Review', *Applied Catalysis*, 23 (**1986**) 225.

29. S. K. Sahoo, S. S. Ray and I. D. Singh, 'Structural Characterization of Coke on Spent Hydroprocessing Catalysts Used for Processing of Vaccum Gas Oils', *Applied Catalysis A: General*, 278 (**2004**) 83.

30. W. J. Kim, E. W. Shin, J. H. Kang and S. H. Moon, 'Performance of Si Modified Pd Catalyst in Acetylene Hydrogenation: Catalyst Deactivation Behavior', *Applied Catalysis A: General*, 251 (**2003**) 305.

31. J. M. A. Harmsen, W. P. A. Jansen, J. H. B. J. Hoebink, J. C. Schouten and H. H. Brongersma, 'Coke Deposition on Automotive Three-Way Catalysts Studied With LEIS', *Catalysis Letters*, 74 (**2001**) 133.

4

Modelling kinetics and deactivation for the selective hydrogenation of an aromatic ketone over Pd/SiO_2

The kinetics for the selective hydrogenation of *4*-isobutylacetophenone (*4*-IBAP) to *1*-(*4*-isobutylphenyl) ethanol (*4*-IBPE) over a Pd/SiO_2 catalyst has been studied in a semi-batch reactor over a wide range of operating conditions. The effects of varying temperature, catalyst amount, H_2 partial pressure, substrate concentration and the effect of H_2O on the activity and selectivity have been studied and an adequate kinetic model with Langmuir-Hinshelwood type rate expressions is proposed based on mechanistic insights. The effect of deactivation due to oligomerization on catalyst activity has also been incorporated in the model. The selected model assumes the competitive adsorption of dissociated hydrogen and reactants and products on the same active site. Further, the addition of the second H atom to *4*-IBAP and the hydrogenolysis of *4*-IBPE by an S_N2 mechanism are considered as the rate-determining steps. Optimized operating conditions for maximizing the yield of *4*-IBPE could be obtained using this kinetic model.

This chapter is accepted for publication in *Chemical Engineering Science*, article in press

1. Introduction

The selective hydrogenation of aromatic ketones to aromatic alcohols is an important reaction in the fine chemical industry. The selective hydrogenation in both gas and liquid phases of various aromatic ketones has been reported in literature (Table 1). Although noble metals such as Pt, Rh, Ru have been used, the use of a supported Pd catalyst is preferred, as Pd is well known to selectively hydrogenate the carbonyl functional group of an aromatic ketone at relatively mild conditions to the hydroxyl group [1]. The selective hydrogenation of *4*-IBAP to *4*-IBPE (Scheme 1) is an intermediate reaction step in the multistep synthesis of Ibuprofen [2]. The consecutive hydrogenolysis of *4*-IBPE to *4*-isobutylethylbenzene (*4*-IBEB) is the major cause for a decreased selectivity and is to be avoided. Rajashekaram and Chaudhari [3] have studied the kinetics for the liquid phase hydrogenation of *4*-isobutylacetophenone over a supported Ni catalyst. Mathew *et al*. [4] have also studied the kinetics for the liquid phase hydrogenation of *4*-isobutylacetophenone over a supported Ru catalyst (Table 2). No literature, however, about the kinetics of this hydrogenation over the most preferred catalyst Pd exists. We observed that a Pd/SiO_2 catalyst undergoes deactivation during the hydrogenation of *4*-IBAP, which will be reported in detail elsewhere [5]. Rajashekharam and Chaudhari [6] also observed deactivation of the supported Ni catalyst for *4*-IBAP hydrogenation. However

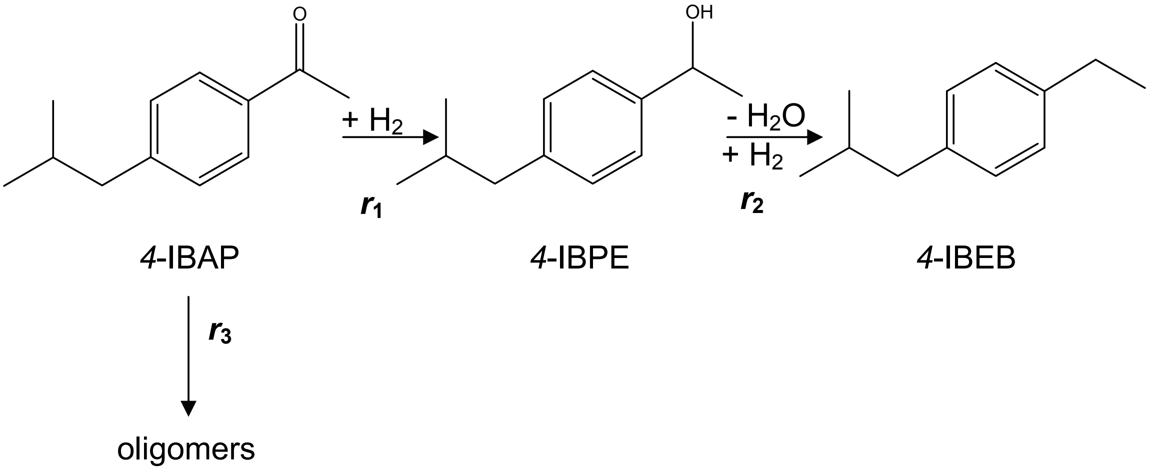

Scheme. 1: Reactions during hydrogenation of *4*-IBAP over Pd/SiO_2

Table 1: Literature survey for the hydrogenation of aromatic ketones

Author	Substrate	Catalyst	Remarks
Santori *et al*.[7]	Acetophenone, benzophenone	Mono- and bi-metallic Pt catalysts	Improved selectivity observed on using bi-metallic catalyst
Malyala *et al*.[8]	Acetophenone and substituted derivatives	Mono- and bi-metallic Pt catalysts	Studied activity, selectivity and stability
Lavaud *et al*.[9]	Acetophenone	Pd/HFAU	Identified a complex reaction scheme
Bergault *et al*.[10]	Acetophenone	Supported Rh	Modeled kinetics and intraparticle diffusion limitations
Masson *et al*.[11]	Acetophenone	Cr promoted Raney Ni	Studied influence of nature of solvent
Lin *et al*.[12]	Acetophenone	Supported Pt	Studied SMSI effects

no mention about catalyst stability was made in their work on kinetic modelling. This work was undertaken with a view to model the kinetics and deactivation of 4-IBAP over a Pd/SiO_2 catalyst and to explore the optimum operating conditions to maximize the yield of the desired product 4-IBPE.

2. Experimental

2.1. Materials

4-IBAP was purchased from Lancaster, U.K. *n*-decane was purchased from Aldrich, USA. All the chemicals were used as delivered without further purification. The Pd/SiO_2 catalyst was prepared by wet impregnation technique using Pd acetate trimer as the precursor and toluene as a solvent with continuous stirring. The catalyst was then filtered, dried at 373 K for 12 h followed by calcination at 673 K for 4 h [13]. The catalyst was reduced in-situ prior to use at 373 K in H_2. Characterization of the Pd/SiO_2 catalyst by CO chemisorption resulted in a Pd surface area of 3.4 m^2/g_{SiO2}, a Pd crystallite size of 3.5 nm and a Pd dispersion of 32%. The SiO_2 support used was commercially available (Davisil 643) and had an average particle size of 35-74 μm as measured by N_2 physisorption.

2.2. Hydrogenations

Catalytic hydrogenation of 4-IBAP was carried out in a 500 cm^3 capacity stainless steel reactor equipped with a gas-induced stirrer (Premex, Switzerland) and an external injection vessel situated above the reactor. In a typical hydrogenation experiment, after in-situ reduction of the catalyst, the desired amounts of reactant and solvent (~200 cm^3) were charged to the reactor from an external injection vessel at room temperature. The reactor volume was flushed three times with nitrogen at room temperature. After the desired reaction temperature was reached, the system was pressurized with hydrogen to the desired level. The reaction was started by switching on the stirrer (1500 rpm) and this was taken as time t = 0 min. The progress of the reaction was determined by monitoring the hydrogen supply rate (keeping

Table 2: Kinetic models for 4-IBAP hydrogenation proposed in literature

Catalyst [ref]	Mechanism	Model Equation	Remarks
Ni/HY [Rajashekharam *et al.*, [3]]	Reaction of molecularly adsorbed H_2 and liquid phase reactants	$r = \frac{C_{\mathrm{cat}}\, k_1\, C_{\mathrm{H_2}}\, C_{\mathrm{IBAP}}}{(1 + K_{\mathrm{H2}}\, C_{\mathrm{H2}})}$	Catalyst stability and effect of H_2O not addressed
Ru/Al_2O_3 [Mathew *et al.*, [4]]	Reaction of molecularly adsorbed H_2 and liquid reactants	$r = \frac{C_{\mathrm{cat}}\, K_H C_{\mathrm{H_2}} k_j C_{\mathrm{j}}}{(1 + K_{\mathrm{H_2}}\, C_{\mathrm{H_2}} + \sum_{j=1,3} K_j\, C_j)^2}$	Effect of H_2O not addressed. Catalyst did not deactivate

reactor pressure constant) as a function of time. These semi-batch experiments (21 experiments) were performed at varying catalyst concentrations (0.26 – 0.78 g/L), initial 4-IBAP concentrations (0.14 – 1.0 mol/L), H_2 partial pressure (1.0 – 4.0 MPa), initial H_2O concentrations (0.14 – 0.45 mol/L) and temperatures (333, 353 and 373 K). After the completion of the reaction process as indicated by no further observable hydrogen consumption, the reactor was cooled to room temperature and depressurized prudently. In all experiments, concentration-time data were generated by intermediate sampling of the liquid phase (~ 250 μl) and analyzing the samples using a Chrompack gas chromatograph (CP9001 with an autosampler), which was equipped with a CP Sil 8 CB column. The dimensions of the column were 50 m × 0.25 mm. The conditions were: FID temperature, 523 K; injector temperature, 523 K; and column temperature was increased linearly from 323 K to 523 K at 6.7 K/min.

3. Results

3.1. Mass Transport Effects

In order to obtain intrinsic kinetic data, care has to be taken that mass transport to or from the catalytically active sites does not interfere with the intrinsic rate measurements. The Carberry number to exclude gas-liquid mass transfer limitations and the Wheeler-Weisz parameter were estimated for both the reactants (H_2 and 4-IBAP) to indicate the absence of internal diffusion limitations. The Wheeler-Weisz parameter ($\Phi \leq 0.15$) was satisfied for all experiments, except for one experiment performed at the highest H_2 partial pressure, where Φ was 0.16 (T=373 K, w_{cat} = 0.1g, C_{IBAP} = 0.27 mol/L, P_{H2} = 40 bar). However, since the catalyst effectiveness factor η_{IBAP} for this particular experiment was still 92%, mass transfer limitations were neglected in all experiments. All these calculations are based on initial reaction rates and, therefore, represent worst-case scenarios.

3.2. Reaction Models

The consecutive transformation of 4-IBPE to 4-IBEB occurs on the Pd sites by direct hydrogenolysis of the C-O bond of 4-IBPE, as opposed to the dehydration-hydrogenation route in which the support also participates. This conclusion is based on deuteration studies performed by us [14]. Ranade and Prins [15] have drawn similar conclusions for hydrogenolysis of benzylic alcohols over an Rh catalyst. The hydrogenolysis of 4-IBPE to 4-IBEB leads to the production of an H_2O molecule and as hydrophilic SiO_2 is used as a support, it is important to study the effect of H_2O on the reaction rate. Since increasing the H_2O concentration lowered the initial reaction rate, the adsorption of H_2O should be considered in the rate expression. Similarly, higher 4-IBAP concentrations (> 0.5mol/L) also lowered the initial reaction rate. It was difficult, however, to attribute this behaviour either solely to kinetics or to deactivation, since the use of a batch reactor makes it difficult to distinguish the kinetics from the deactivation behaviour. Three phenomena are proposed to cause catalyst deactivation, (*i*) oligomerization of the reactant 4-IBAP by condensation reactions, (*ii*) strong adsorption of H_2O and (i*ii*) Pd crystallite growth [5]. Although not very common, deactivation modelling has been performed earlier in semi-batch reactors especially for hydrogenations related to fine chemistry [16], [17]. The influence of different 4-IBPE concentrations on the reaction performance was not studied for reasons discussed later (section 4). To describe the influence of the reaction parameters, four different kinetic models for 4-IBAP hydrogenation (Scheme 1) were considered assuming that the surface reaction is rate determining and the other steps are in quasi equilibrium, while hydrogen adsorbs dissociatively. The different models are described below.

Model 1: Competitive adsorption of dissociated hydrogen and organic compounds takes place, assuming addition of the second H atom to adsorbed 4-IBAP as the rate-determining step (*r.d.s*) for the first reaction. The hydrogenolysis of 4-IBPE is proposed to occur via an S_N2 mechanism, in which a hydrogen atom displaces the hydroxyl group attached to the carbon atom [18]. The addition of the first H atom resulting in the protonation of the OH group of 4-IBPE is reversible, whereas the simultaneous loss of the resulting leaving group (OH_2^+) and the addition of the second hydrogen atom to the protonated 4-IBPE is assumed to be the *r.d.s*. The deactivation (r_3) is proposed to occur by condensation reaction of two 4-IBAP molecules adsorbed adjacent to each other, leading to the formation of oligomeric species covering the Pd catalyst in a kind of fouling process.

Model 2 differs from *model 1* in that the deactivation (r_3) occurs due to a single adsorbed 4-IBAP molecule.

Model 3 is similar to *model 1*, but assumes the addition of the first H to adsorbed 4-IBAP as the *r.d.s* of the first reaction.

Model 4 is also similar to *model 1*, but deactivation (r_3) occurs by a side reaction of two adjacently adsorbed 4-IBPE molecules.

3.3. Elementary Processes in Langmuir Hinshelwood Model 1

The elementary steps in *model 1* occurring during the hydrogenation are as mentioned in the scheme on the following page.

$$\mathrm{IBAP} + {*} \longleftrightarrow \mathrm{IBAP}^*$$

$$\mathrm{H_2} + 2{*} \longleftrightarrow 2\mathrm{H}^*$$

$$\mathrm{IBAP}^* + \mathrm{H}^* \longleftrightarrow \mathrm{IBAP{+}H}^* + {*}$$

$$\mathrm{IBAP{+}H}^* + \mathrm{H}^* \xrightarrow{r_1} \mathrm{IBPE}^* + {*} \quad \text{(r.d.s)}$$

$$\mathrm{IBPE}^* \longleftrightarrow \mathrm{IBPE} + {*}$$

$$\mathrm{IBPE}^* + \mathrm{H}^* \longleftrightarrow \mathrm{IBPE{+}H}^* + {*}$$

$$\mathrm{IBPE{+}H}^* + \mathrm{H}^* \xrightarrow{r_2} \mathrm{IBEB} + \mathrm{H_2O}^* + {*} \quad \text{(r.d.s)}$$

$$\mathrm{H_2O}^* \longleftrightarrow \mathrm{H_2O} + {*}$$

The following rate expressions were obtained for the individual reaction steps in scheme for *model 1*.

$$r_1 = \frac{C_{\mathrm{cat}}\, a\, k_1\, C_{\mathrm{IBAP}}\, P_{\mathrm{H_2}}}{\left(1 + K_{\mathrm{IBAP}} C_{\mathrm{IBAP}} + \sqrt{K_{\mathrm{H}} P_{\mathrm{H_2}}} + K_{\mathrm{H_2O}} C_{\mathrm{H_2O}}\right)^2} \tag{1}$$

$$r_2 = \frac{C_{\mathrm{cat}}\, a k_2\, C_{\mathrm{IBPE}}\, P_{\mathrm{H_2}}}{\left(1 + K_{\mathrm{IBAP}} C_{\mathrm{IBAP}} + \sqrt{K_{\mathrm{H}} P_{\mathrm{H_2}}} + K_{\mathrm{H_2O}} C_{\mathrm{H_2O}}\right)^2} \tag{2}$$

$$r_3 = \frac{C_{\mathrm{cat}}\, a\, k_3\, C_{\mathrm{IBAP}}{}^2}{\left(1 + K_{\mathrm{IBAP}} C_{\mathrm{IBAP}} + \sqrt{K_{\mathrm{H}} P_{\mathrm{H_2}}} + K_{\mathrm{H_2O}} C_{\mathrm{H_2O}}\right)^2} \tag{3}$$

$$a = \exp\left(-\alpha \frac{C_{\mathrm{olig}}}{C_{\mathrm{cat}}}\right) \tag{4}$$

The experimental data did not allow us to distinguish between deactivation due to oligomerization and that due to Pd crystallite growth. As a result, the deactivation attributed to Pd crystallite growth was lumped in a single deactivation rate constant k_3 (equation 3). The loss of catalytic activity due to oligomerization is described by an exponential function (equation 4), which is often used to empirically describe catalyst deactivation [19]. Here α is defined as the inverse of the moles of C in the oligomers theoretically required to cover all Pd sites exposed per gram of catalyst. For the 2.4 % Pd/SiO_2 catalyst, this value was estimated to be 4416 g/mol Pd. The rate constants (k_1, k_2, k_3) are obtained by lumping the actual rate constants together with the adsorption constants ($k_1 = k_1'\cdot K_{IBAP}\cdot K_H$, $k_2 = k_2'\cdot K_H$, $k_3 = k_3'\cdot K_{IBAP}^2$). Based on the optimal estimates of the parameters to be discussed below, the value of the normalized activity *a* decreased during the standard experiment (Figure 1) from 1.0 at *t* =0 to 0.508 at *t* =11000 s. The mass balances for the various components in the batch reactor are given by equations (5)-(9) below. Note that the catalyst concentration C_{cat} is included in the rate expression.

$$\frac{dC_{\mathrm{IBAP}}}{dt} = -r_1 \qquad (5)$$

$$\frac{dC_{\mathrm{IBPE}}}{dt} = r_1 - r_2 \qquad (6)$$

$$\frac{dC_{\mathrm{IBEB}}}{dt} = r_2 \qquad (7)$$

$$\frac{dC_{\mathrm{H_2O}}}{dt} = r_2 \qquad (8)$$

$$\frac{dC_{\mathrm{olig}}}{dt} = r_3 \qquad (9)$$

3. 4. Modelling and Parameter Estimation

The package Athena Visual Studio (version 10.0, Stewart and Associates, 2006[20]) was used for the model discrimination and the non-linear parameter estimation procedure by solving the set of mass balance equations. For all results shown, Bayesian estimation for multiple responses was applied. In total, 205 data points were used over the range of conditions indicated in the experimental section. Tables 3 and 5 summarize the statistical evaluations of the models obtained using all experimental data. The estimated parameter values are given with their approximate 95 % confidence intervals. The rate constants presented in Table 3 contain the adsorption constants. The experiments performed at 373 K were used to obtain the rate and adsorption constants at this temperature. To improve convergence, the rate and equilibrium constants were reparameterized at 353 K and 333 K for their temperature dependency [21] according to equation (10):

$$k_{(T)} = k_{(T_0)} \exp\left(-\frac{E_{act}}{R}\left(\frac{1}{T} - \frac{1}{T_0} \right)\right) \tag{10}$$

T_0 is the reference temperature chosen in the experimental range studied, here 373 K. The activation energies using the lumped rate constants were obtained from the temperature dependencies. The actual activation energies shown in Table 5 were calculated from the activation energies (E_1, E_2, E_3) and the adsorption enthalpies obtained from the optimizations as indicated in Table 4. Dual-site models with different adsorption sites for hydrogen and organic species have also been considered but could only describe the data very poorly and are not discussed further. Figure 1 shows the concentration-time profile for the hydrogenation of 4-IBAP performed at standard reaction conditions. The curves shown in this figure and also in the figures that follow represent the predicted values obtained from *model 1* that gave the best fit and can be explained chemically and which will be discussed later. The relative 4-IBAP concentration versus time profile for different initial 4-IBAP concentrations is shown in Figure 2. The slower reaction rate at 4-IBAP concentrations (> 0.5 mol/L) could be attributed to either substrate inhibition effects or to deactivation. Figure 3 shows the 4-IBAP and 4-IBPE concentration versus time at different hydrogen partial pressures. The experimental results indicate that the reactions are first order in hydrogen pressure. The lower

Table 3: Estimated values of rate and adsorption constants with their 95% confidence intervals for the considered models at T= 373 K and their SS_{res} values

	Model 1	Model 2	Model 3	Model 4
k_1 (L/g_{cat}.atm.s)	1.14 ± 0.25	2.67 ± 0.42	6.11 ± 1.43	3.51 ± 0.98
k_2 (L/g_{cat}.atm.s)	0.095 ± 0.02	0.23 ± 0.04	0.108 ± 0.028	0.537 ± 0.15
k_3 (L^2/mol.g_{cat}.s)	0.024 ± 0.004	0.037 ± 0.006	0.029 ± 0.004	0.227 ± 0.07
K_{IBAP} (L/mol)	76.4 ± 23.7	186 ± 29	91 ± 34	353 ± 72
K_H $(atm)^{-1}$ *	141	141	141	141
K_{H2O} (L/mol)	529 ± 106	589± 101	614 ± 153	589.71 ± 101.3
SS_{res}	0.272	0.175	0.352	0.262

Table 4: Calculation of actual activation energies from lumped values

E_{act1}	=	E_1 - ΔH_{ads_IBAP} -ΔH_{ads_H2}
E_{act2}	=	E_2 -ΔH_{ads_H2}
E_{act3}	=	E_3 - $2 \cdot \Delta H_{ads\_IBAP}$

Table 5: Estimated activation energies and enthalpies of adsorption of the rate and adsorption parameters for model 1 and their 95% confidence intervals

E_{act1} (kJ/mol)	102 ± 15
E_{act2} (kJ/mol)	105 ± 14
E_{act3} (kJ/mol)	117 ± 15
ΔH_{ads_IBAP}(kJ/mol)	-63 ± 12
ΔH_{ads_H2} (kJ/mol)	-68.3 *
ΔH_{ads_H2O} (kJ/mol)	-110 ± 15
SS_{res}	0.211

*: fixed value

pressure results in slower decrease of the desired intermediate product 4-IBPE, this is due to the simultaneously occurring deactivation, as outlined in the discussion.

Figure 4 shows the 4-IBAP concentration as a function of the H_2O concentration. Water clearly has a strong inhibiting influence on the conversion rate. The concentration-time plots of 4-IBAP at the highest substrate concentration (1.0 mol/L) at different temperatures (Figure 5) confirm the expected temperature dependency of the reaction.

Using *model* 1 with the optimal parameter estimates, the desired product yield versus reaction time at different catalyst loadings was calculated for pure 4-IBAP (5.4 mol/L) and at a H_2 partial pressure of 8 MPa (Figure 6). The optimal batch time strongly depends on the catalyst concentration. The lower the catalyst concentration, the slower the maximum yield is approached and the wider the time window to stop the reaction. For high concentrations, this window becomes small and the maximum yield decreases.

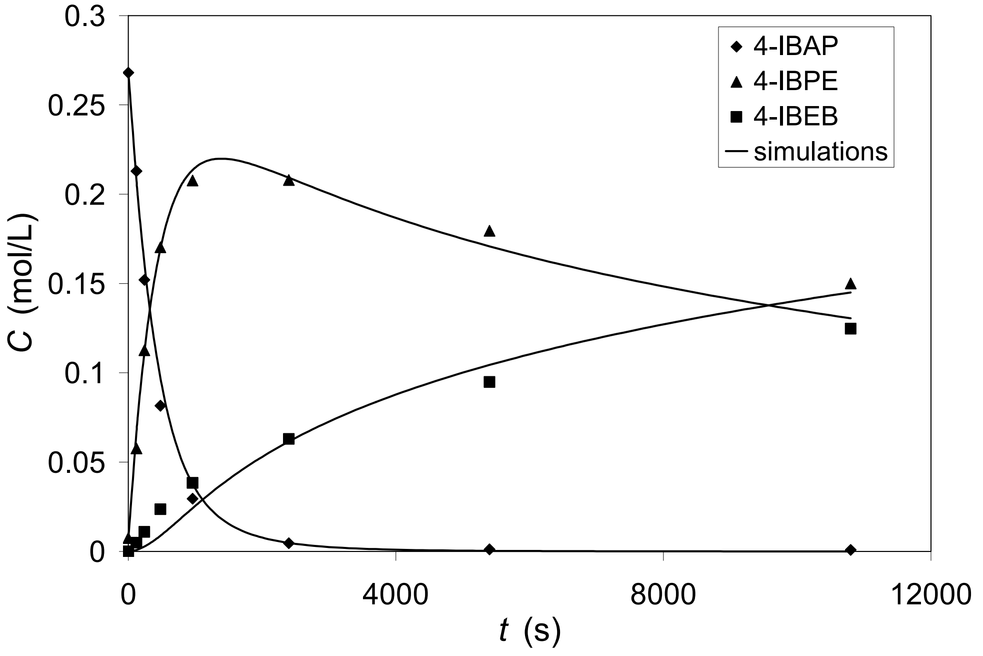

Figure 1: Concentration-time profiles during 4-IBAP hydrogenation in a semi-batch reactor at standard reaction conditions (symbols represent the experimental data, the curves are model 1 predictions with the parameters in Tables 3 and 5)
Reaction Conditions: w_{cat} = 0.1g, C_{IBAP} = 0.27 mol/L, P_{H2} = 20 bar, T = 373 K

4. Discussion

Prior to discussing the modelling results it is important to address the various model assumptions made. Dissociative hydrogen adsorption on noble metals is well established. Since no ring-hydrogenated products were observed in GC analysis, these components did not have to be included in the modelling. The aromatic compound is not expected to hinder the adsorption of the small hydrogen molecule and a single site mechanism involving the competitive adsorption of the adsorbed reactants is plausible. The addition of the second H atom as the rate-determining step for 4-IBAP hydrogenation allows first-order dependence on hydrogen pressure, as observed experimentally, in contrast to a half-order dependency that would be predicted if addition of the first H atom is assumed to be the rate-determining step. Sen and Vannice [22] used a similar argumentation utilizing the bond-order conservation method for a ketone hydrogenation. The intermediate (IBAP+H*) formed by the addition of the first hydrogen atom to 4-IBAP is assumed to have a

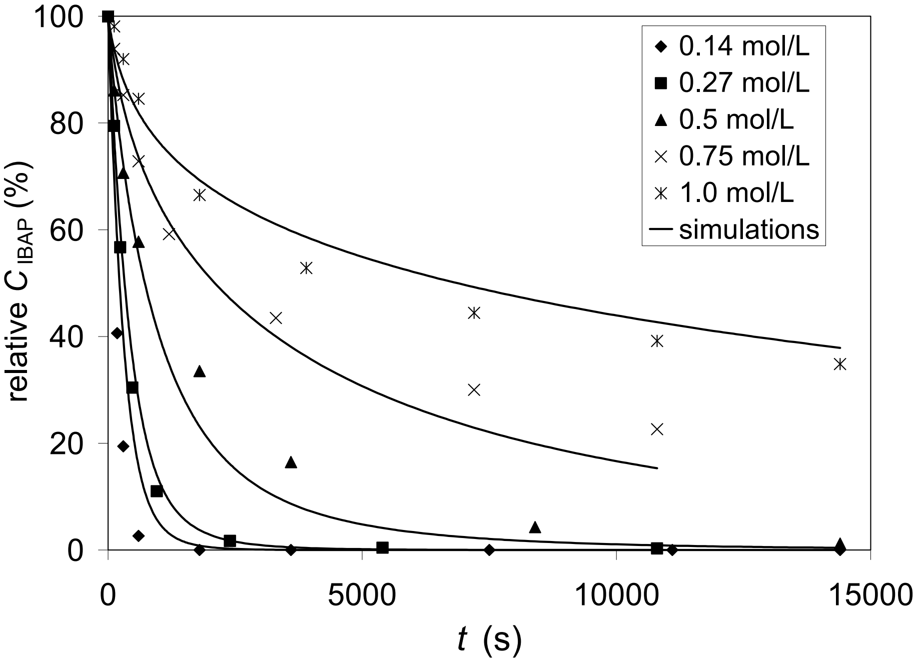

Figure 2: Relative 4-IBAP concentration versus time at different C_{IBAP}. Symbols experimental data, curves model 1 simulation.
Reaction Conditions: w_{cat} = 0.1g, P_{H2} = 20 bar, T = 373 K

negligible surface coverage compared to that of 4-IBAP and H_2O, as a result of which it does not feature in the denominator of the rate expression. The dehydrogenation of 4-IBPE to 4-IBAP at temperatures lower than 373 K was observed in the absence of H_2 using in-situ ATR-FTIR. Figure 7 shows the in-situ IR profile of 4-IBPE in the presence of Pd/SiO_2 heated from room temperature to 373 K. The simultaneous emergence of the asymmetric C=O stretching frequency of 4-IBAP at 1690 cm^{-1} and the disappearance of the C-O asymmetric stretching frequency of 4-IBPE at 1080 cm^{-1} confirm the dehydrogenation. (The peak ~1300 cm^{-1} is attributed to the CH_3 vibration of the CH_3 group adjacent to the carbonyl functional group). Consequently, it was not possible to study the effect of 4-IBPE on the catalyst performance, since the 4-IBPE charged to the reactor (at room temperature) would be dehydrogenated to 4-IBAP at the reaction temperature. If the reactor were pressurized with H_2 at room temperature itself to suppress the dehydrogenation, it would react with the 4-IBAP already present leading to erroneous results. Adding the desired amount of 4-IBPE to the reactor at reaction temperature was also not feasible, since the addition of cold 4-IBPE

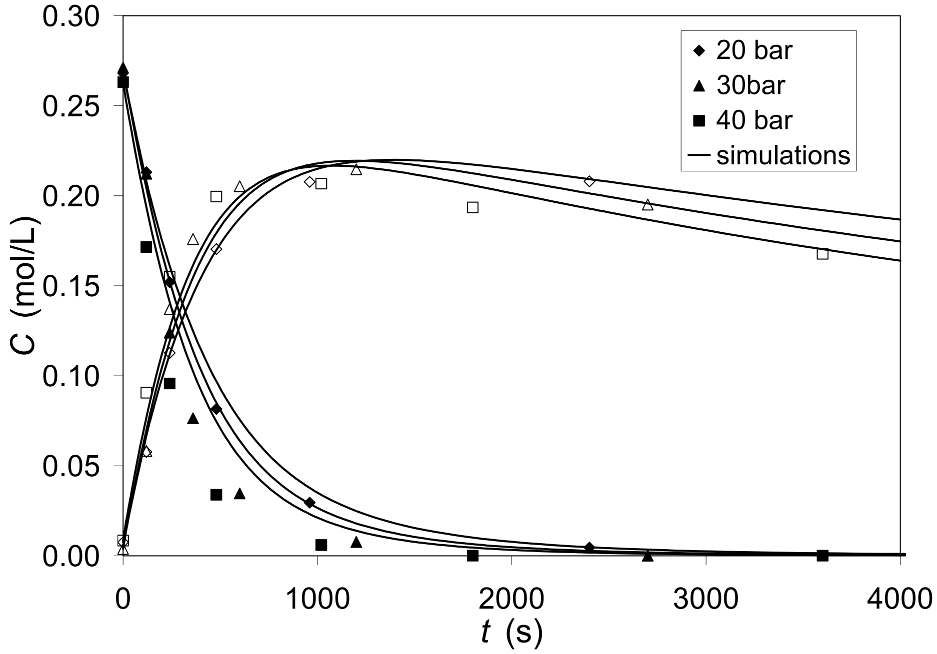

Figure 3: 4-IBAP (solid symbols) and 4-IBPE (open symbols) concentration profiles versus time at different P_{H2}. Symbols experimental data, curves model 1 simulation.
Reaction Conditions: w_{cat} = 0.1g, C_{IBAP} = 0.27 mol/L, T = 373 K

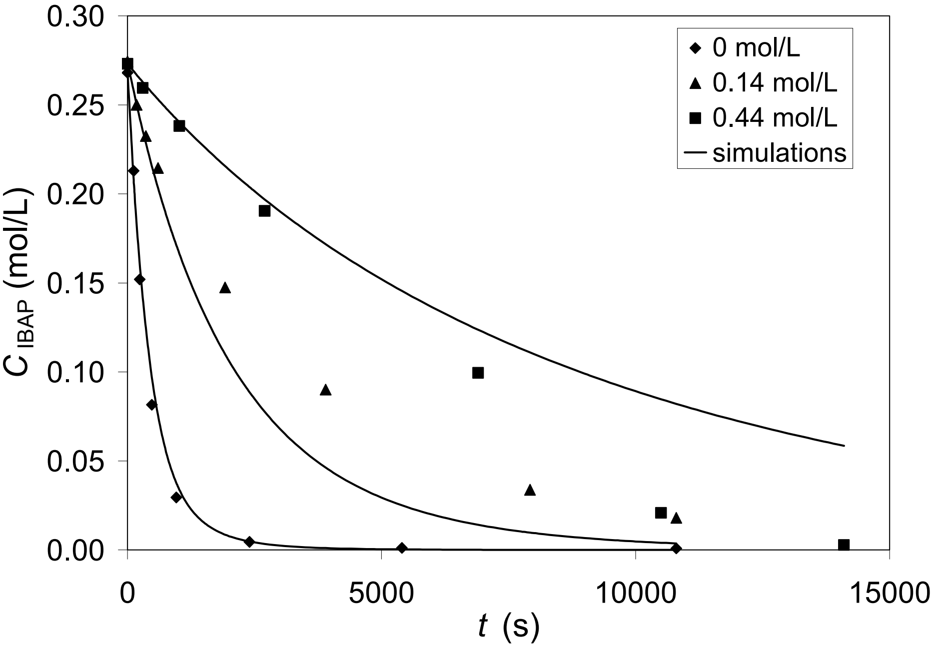

Figure 4: 4-IBAP conversion rate versus time at different C_{H2O}. Symbols experimental data, curves model 1 simulation.
Reaction Conditions: w_{cat} = 0.1g, C_{IBAP} = 0.27 mol/L, P_{H2} = 2.0 MPa, T = 373 K

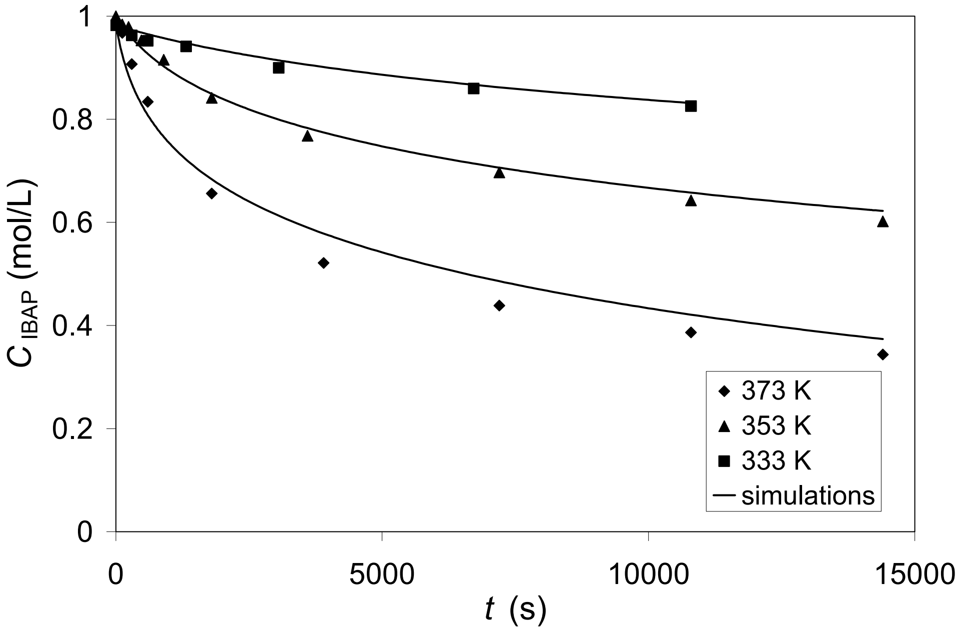

Figure 5: *4*-IBAP conversion rate versus time at different *T*. Symbols experimental data, curves model 1 simulation.
Reaction Conditions: w_{cat} = 0.1g, C_{IBAP} = 0.27 mol/L, P_{H2} = 2.0 MPa

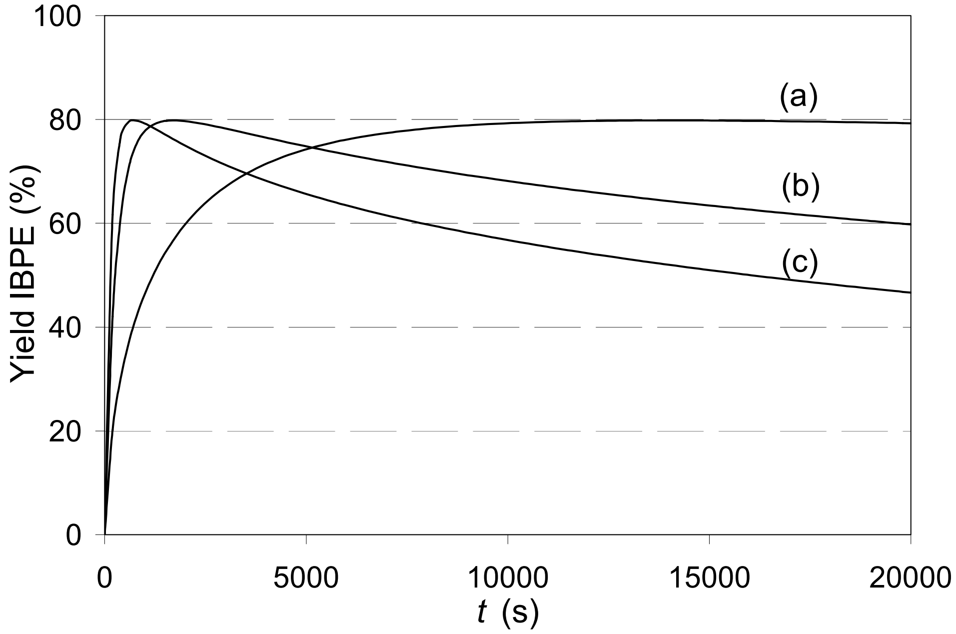

Figure 6: Influence of different catalyst amounts on the yield of *4*-IBPE in the hydrogenation of pure *4*-IBAP (C_{IBAP} = 5.4 mol/L) at P_{H2} = 8.0 MPa and *T* = 373 K. (a) w_{cat} = 1.0 g; (b) w_{cat} = 2.0 g; (c) w_{cat} = 3.0 g

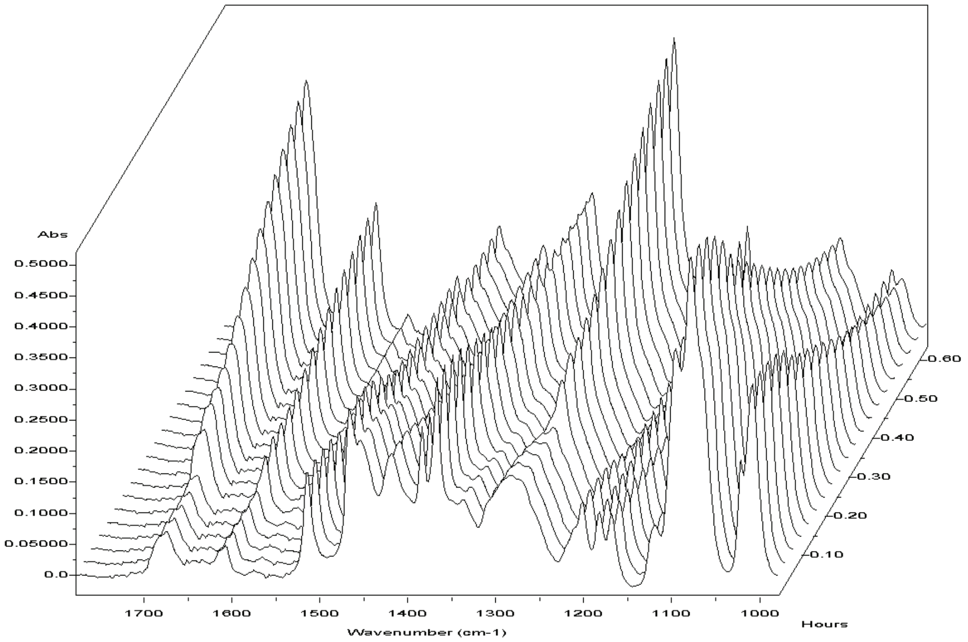

Figure 7: In-situ ATR-FTIR plot indicating the dehydrogenation of 4-IBPE to 4-IBAP over Pd/C in the absence of hydrogen. The asymmetric C-O stretching frequency (~1080 cm^{-1}) of 4-IBPE is seen to decrease with a corresponding increase in the asymmetric C=O stretching frequency (~1690 cm^{-1}) of 4-IBAP.

would lead to temperature fluctuations (~ 6- 8 K) leading to unreliable kinetic data. As a result, the adsorption of 4-IBPE was also assumed to be negligible as compared to the adsorption of 4-IBAP and H_2O since attempts to estimate the adsorption constant for 4-IBPE resulted in a very small value and a 95% confidence range larger than the value itself.

Due to correlation between the kinetic parameters, it was not possible to estimate all parameters reliably. To reduce this correlation, the adsorption constant for hydrogen was estimated from thermodynamic data and the other parameters were estimated using this value. The adsorption entropy for hydrogen gas (-122.09 J/mol/K) on Pd was obtained from literature [23] whereas the hydrogen adsorption constant was obtained from estimates of the adsorption enthalpy for hydrogen gas at room temperature (-82.8 kJ/mol, [24]) and at T= 420 K (-55 kJ/mol, [25]). The enthalpy of adsorption at T=373 K (-68.3 kJ/mol) was approximated by interpolation.

The sum of squared residuals values in Table 3 for the parameter estimations indicate that comparable fits of the data sets was obtained for all the considered models. Nevertheless, *model 3* was eliminated as it had the highest value of the sum of squared residuals. Although *model 2* and *model 4* showed slightly better fits with their lowest values of the sum of squared residuals, these models cannot withstand scrutiny from a chemical point of view. Oligomerization due to a single adsorbed 4-IBAP molecule is very unlikely, which excludes *model 2*. *Model 4* can be excluded since the deactivation due to oligomerization cannot be attributed to 4-IBPE, because only a maximum of two 4-IBPE molecules can condense, which is insufficient to form oligomers. *Model 1* was therefore chosen as the most representative model as it describes the experimental data fairly well over the whole range of operating conditions and is in agreement with chemical principles, a requirement for an acceptable kinetic model.

The activation energies of the individual reaction steps and the heats of adsorption of 4-IBAP, H_2 and H_2O estimated using *model 1* are given in Table 5.

The continuous curve in Figure 1, which results from simulation (*model 1*) using the optimal parameter estimates, excellently describes the experimental data over the entire reaction period. *Model 1* is also able to predict the 4-IBAP consumption profiles for a wide range of initial 4-IBAP concentrations (Figure 2) and hydrogen partial pressures (Figure 3) reasonably well. In Figure 3, the fastest reaction rate is observed at the highest pressure. The deviation observed at higher conversion levels could be due to a combined effect of deactivation and strong H_2O chemisorption, which the model is unable to predict accurately. This could also be the reason for the poor fit observed on increasing the H_2O concentration (Figure 4). However, Figure 5 shows that *model 1* can accurately describe the influence of different temperatures on the 4-IBAP consumption profile for the highest 4-IBAP concentration (1.0 mol/L) studied.

Model 1 was also used to determine the optimum operating conditions for maximum 4-IBPE yield (~80%) with pure 4-IBAP (Figure 6) at 373 K, the highest temperature applied. Since the rate showed a linear dependency on the H_2 partial pressure, the operating pressure was extrapolated to 8.0 MPa although it was outside the range of the measured kinetics. Simulations (not shown) indicate that the yield increases with increasing P_{H2} up to 8.0 MPa and then decreases. This increase is due to the more favourable hydrogenation versus deactivation by 4-IBAP, until the point at which the consecutive hydrogenolysis of 4-IBPE to the undesired 4-IBEB is favoured. Figure 6 reveals that a similar dependence is observed with increasing catalyst amount. This behaviour can be attributed to catalyst deactivation, which helps to slow down the undesired consecutive reaction, although a too small amount of catalyst will already be deactivated before the maximum yield is obtained. This study thus illustrates the importance of a combined analysis of reaction kinetics and catalyst deactivation to maximize the yield of a desired product in batch operation, produced within a reasonable time.

5. Conclusions

The kinetics for the selective hydrogenation of 4-IBAP over a Pd/SiO_2 catalyst has been investigated in a semi-batch slurry reactor over the temperature range of 333 K – 373 K. Catalyst deactivation, occurring as a side reaction of the reactant leading to fouling and an exponentially decaying activity, has been incorporated in the model. A Langmuir-Hinshelwood type rate expression, which assumes competitive adsorption of adsorbed hydrogen and organic species, is proposed. In this model, the addition of the second H atom to the adsorbed 4-IBAP is assumed to be the rate-determining step for the desired first reaction of 4-IBAP to 4-IBPE, while the hydrogenolysis of 4-IBPE on the metal via an S_N2 mechanism is assumed to be the rate-determining step for the undesired consecutive transformation of 4-IBPE to 4-IBEB. The activation energies for individual reactions and the heat of adsorption for 4-IBAP were also estimated from the temperature dependency. The maximum yield of 4-IBPE from pure 4-IBAP at optimized conditions (8.0 MPa and 373 K) is predicted to be about 80%.

Acknowledgements

R. J. Berger is thanked for assistance with the kinetic modelling. M. Stojanovic is also acknowledged for his contributions to this work.

Nomenclature:

$*$: Active site on catalyst surface

a : relative catalyst activity (-)

C_{IBAP} : concentration of 4-IBAP (mol/L)

C_{IBPE} : concentration of 4-IBPE (mol/L)

C_{H2O} : concentration of H_2O (mol/L)

C_{olig} : concentration of oligomers (mol/L)

C_{cat} : catalyst concentration (g/L)

E_1, E_2, E_3 : Activation energies obtained from values of lumped rate constants

$E_{\mathrm{act1}}, E_{\mathrm{act2}}, E_{\mathrm{act3}}$: Actual activation energies of individual reaction steps (kJ/mol)

IBAP+H : Intermediate formed after addition of 1st H atom to 4-IBAP

IBPE+H : Intermediate formed during hydrogenolysis of 4-IBPE

k_1', k_2', k_3' : reaction rate constants

k_1, k_2, k_3 : lumped reaction rate constants (see table 3)

$K_{\mathrm{IBAP}}, K_{\mathrm{H}}, K_{\mathrm{H2O}}$: adsorption constants (see table 3)

P_{H2} : H_2 partial pressure (bar)

r_1, r_2, r_3 : reaction rates (mol/L/s)

R : universal gas constant (8.314 J/mol/K)

T : reaction temperature (K)

T_0 : reference temperature (373 K)

w_{cat} : catalyst amount (g)

Greek Symbols

α : deactivation parameter (g_{cat}/mol)

ΔH_{IBAP}: : enthalpy of adsorption of 4-IBAP (kJ/mol)

ΔH_{H2} : enthalpy of adsorption of H_2 (kJ/mol)

Reference List

1. H. U. Blaser, A. Indolese, A. Schnyder, H. Steiner and M. Studer, 'Supported Palladium Catalysts for Fine Chemical Synthesis', *Journal of Molecular Catalysis A: Chemical*, 173 (**2001**) 3.

2. V. Elango, 'Method for Producing Ibuprofen', EP 0400 892 A2 (**1990**) to Hoechst Celanese Corp.

3. M. V. Rajashekharam and R. V. Chaudhari, 'Kinetics of Hydrogenation of *p*-Isobutyl Acetophenone Using a Supported Ni Catalyst in a Slurry Reactor', *Chemical Engineering Science*, 51 (**1996**) 1663.

4. S. P. Mathew, M. V. Rajashekharam and R. V. Chaudhari, 'Hydrogenation of *p*-Isobutyl Acetophenone Using a Ru/Al_2O_3 Catalyst: Reaction Kinetics and Modeling of a Semi-Batch Slurry Reactor', *Catalysis Today*, 49 (**1999**) 49.

5. N. Thakar, T. J. Schildhauer, W. Buijs, F. Kapteijn and J. A. Moulijn, 'Evaluation of Deactivation Mechanisms of Pd Catalyzed Hydrogenation of 4-Isobutylacetophenone', *Journal of Catalysis*, 248 (**2007**) 249.

6. M. V. Rajashekharam and R. V. Chaudhari, 'Improved Stability of a Bimetallic Ni-Pt Catalyst for Hydrogenation of Acetophenone and Substituted Derivatives', *Catalysis Letters*, 41 (**1996**) 171.

7. G. F. Santori, A. G. Moglioni, V. Vetere, G. Y. M. Iglesias, M. L. Casella and O. A. Ferretti, 'Hydrogenation of Aromatic Ketones With Pt- and Sn-Modified Pt Catalysts', *Applied Catalysis A: General*, 269 (**2004**) 215.

8. R. V. Malyala, C. V. Rode, M. Arai, S. G. Hegde and R. V. Chaudhari, 'Activity, Selectivity and Stability of Ni and Bimetallic Ni-Pt Supported on Zeolite Y Catalysts for Hydrogenation of Acetophenone and Its Substituted Derivatives', *Applied Catalysis A: General*, 193 (**2000**) 71.

9. N. Lavaud, P. Magnoux, F. Alvarez, L. Melo, G. Giannetto and M. Guisnet, 'Transformation of Acetophenone Over Pd HFAU Catalysts – Reaction Scheme', *Journal of Molecular Catalysis A: Chemical*, 142 (**1999**) 223.

10. I. Bergault, P. Fouilloux, C. Joly-Vuillemin and H. Delmas, 'Kinetics and Intraparticle Diffusion Modelling of a Complex Multistep Reaction: Hydrogenation of Acetophenone Over a Rhodium Catalyst', *Journal of Catalysis*, 175 (**1998**) 328.

11. J. Masson, P. Cividino and J. Court, 'Selective Hydrogenation of Acetophenone on Chromium Promoted Raney Nickel Catalysts. III. The Influence of the Nature of Solvent', *Applied Catalysis A: General*, 161 (**1997**) 191.

12. S. D. Lin, D. K. Sanders and M. A. Vannice, 'Influence of Metal-Support Effects on Acetophenone Hydrogenation Over Platinum', *Applied Catalysis A: General*, 113 (**1994**) 59.

13. I. Hoek, T. A. Nijhuis, A. I. Stankiewicz and J. A. Moulijn, 'Performance of the Monolithic Stirrer Reactor: Applicability in Multi-Phase Processes', *Chemical Engineering Science*, 59 (**2004**) 4975.

14. N. Thakar, N. F. Polder, K. Djanashvili, H. van Bekkum, F. Kapteijn and J. A. Moulijn, 'Deuteration Study to Elucidate Hydrogenolysis of Benzylic Alcohols Over Supported Palladium Catalysts', *Journal of Catalysis*, 246 (**2007**) 344.

15. V. S. Ranade and R. Prins, 'Hydrogenolysis of Benzylic Alcohols on Rhodium Catalysts', *Chemistry European Journal*, 6 (**2000**) 313.

16. L. P. Tiainen, M. A. Paivi, A. K. Neyestenaki, T. Salmi and D. Y. Murzin, 'Modelling of Catalyst Deactivation in Liquid Phase Reactions: Citral Hydrogenation on Ru/Al_2O_3', *Reaction Kinetics and Catalysis Letters*, 78 (**2003**) 251.

17. G. D. Yadav and S. P. Nalavade, 'Selectivity Engineering of 4-Phenoxyacetophenone by Acylation of Diphenyl Ether With Ion-Exchange Resins: Modelling of Catalyst Deactivation and Remedies', *Chemical Engineering Science*, 58 (**2003**) 2573.

18. A. P. G. Kieboom, J. F. De Kreuk and H. van Bekkum, 'Substituent Effects in the Hydrogenolysis of Benzyl Alcohol Derivatives Over Palladium', *Journal of Catalysis*, 20 (**1971**) 58.

19. G. F. Froment, 'Modeling of Catalyst Deactivation', *Applied Catalysis A: General*, 212 (**2001**) 117.

20. I. Stewart and Associates, 'Athena Visual Workbench, Version 10.0', http://www. Athenavisual. com (**2006**).

21. R. J. Berger, E. H. Stitt, G. B. Marin, F. Kapteijn and J. A. Moulijn, 'Chemical Reaction Kinetics in Practice', *CATTECH*, 5 (**2001**) 30.

22. B. Sen and M. A. Vannice, 'Metal-Support Effects on Acetone Hydrogenation Over Platinum Catalysts', *Journal of Catalysis*, 113 (**1988**) 52.

23. J. B. Benziger, 'Thermochemical Methods for Reaction Energetics on Metal Surfaces',(Ed. E. Shustorovich) VCH, New York (**1991**) 53.

24. E. Shustorovich, 'The Bond-Order Conservation Approach to Chemisorption and Heterogeneous Catalysis: Applications and Implications', *Advances in Catalysis*, 37 (**1990**) 101.

25. H. Backman, H. Neyestenaki and D. Y. Murzin, 'Mathematical Modelling of *o*-Xylene Hydrogenation Kinetics Over Pd/Al_2O_3', *Journal of Catalysis*, 233 (**2005**) 109.

5

Diffusion-reaction characteristics in monolithic catalysts

The washcoated catalyst layer in the square microchannels of structured catalyst is often unevenly distributed over the surface of the support structure. Consequently, the diffusion of reactants through these coatings is complex and less effective than one might have expected. The subject of this chapter is the analysis of the effect of the presence of the active metal in the macropores on the catalyst effectiveness, and a solution to this problem by applying primer coatings of a non-porous filler material that allows the subsequent deposition of the active material in an egg-shell of uniform thickness. Various samples were prepared in which the macropores of the bare cordierite support were plugged and the square channels pre-rounded with α-Al_2O_3 before applying the active material. The presence of active metal inside the macropores and the subsequent plugging of the macropores by α-Al_2O_3 is conclusively proven by spatially resolved elemental maps. FEM calculations, based on elemental maps, revealed that the diffusion length decreased from 23 μm for a catalyst without priming layer to 10 μm for a catalyst prepared on top of a primed support. The improved performance of the optimized monoliths was demonstrated for the selective hydrogenation of *3*-methyl-*1*-pentyn-*3*-ol to *3*-methyl-*1*-penten-*3*-ol catalyzed by Pd/SiO_2.

This chapter is submitted for publication in *Industrial & Engineering Chemistry Research*

1. Introduction

The subject of this work is the coating of high-surface-area catalyst support materials, (e.g. SiO_2, γ-Al_2O_3) onto a second support structure. Such a two-step approach to support the catalytically active phase is often attractive, as it allows the combination of beneficial features of both components. In this paper, we consider the application of SiO_2, which provides the high surface area to disperse the active phase onto a cordierite monolithic support, which guides the flow of reactants over the catalyst and which gives strength to the entire structure. The analysis presented here, however, is by no means limited to honeycomb or monolithic supports and is applicable to other ceramic structured packing materials such as corrugated sheets and static mixers. We do focus on two aspects of the bare monolithic support structure that occur commonly: (*i*) the square channel geometry leads to uneven thickness of the support material in the corners as compared to the edges and (*ii*) macropores in the monolith walls tend to form pockets of catalytically active material with limited accessibility.

The most common method of applying support-on-support is to paint (washcoat) a slurry solution of the high surface area support onto the structured support [1]. Invariably, the objective of such 'washcoating' is to create an even layer of support material for the catalyst. The evenness of the applied layer is especially relevant for the liquid phase processes with a slow diffusion rate relative to the reaction rate, as for such systems, it is especially critical to be able to predict and control the distance that the reactants and products have to diffuse across. Obviously, painting over non-flat surfaces results in an uneven application of the material. It is especially difficult to prevent the collection of the material by capillary action during drying in sharp bends and pockets. In the case of monolith supports, the washcoat collects into the corners of the wall of the square channels. Typically, the thickness of the coating of the flat part of the wall of a monolith channel is between three and ten times as thin as in the corner. A second problem is the porosity of the support. The slurry suspension that is applied on the material gets drawn into these pores. In many studies of the diffusion effects in washcoats, these pockets are often overlooked [2,3].

There are two main contributions of this work. First, we demonstrate and emphasize that for a commercially available (cordierite) monolith, a significant amount of catalytically active material builds up deep inside the macropores upon washcoating. Direct evidence of this is provided using electron probe micro analysis (EPMA) of the prepared monolith samples. In an earlier contribution [4], we showed that the active metal can be found deep inside the macropores, and in this work the effects of these phenomena are rigorously analyzed. We present numerical diffusion-reaction calculations using experimentally determined distribution of active material, and interpret these calculations in terms of the diffusion length and catalyst effectiveness. Secondly, we show that by applying one or more layers of a non-porous coating - a primer, a uniformly round channel geometry is obtained and the detrimental effects of the previously described problems can be overcome [5,6]. For these improved coatings, we present a similar numerical analysis of experimental elemental maps (EPMA) to quantify the improvements for reactions. Finally, the effectiveness of this procedure is demonstrated and evaluated using reactive experiments.

In the next section, we concisely describe our experimental method and introduce elemental maps for several honeycomb samples. Next, the performance that can be expected from such materials is determined using finite element (FEM) calculations for the geometries that we extract from the EPMA maps, and presented as effectiveness factors as a function of a Thiele modulus. It is shown to be impossible to identify a single length scale of diffusion for these complex washcoat geometries. Finally, results are

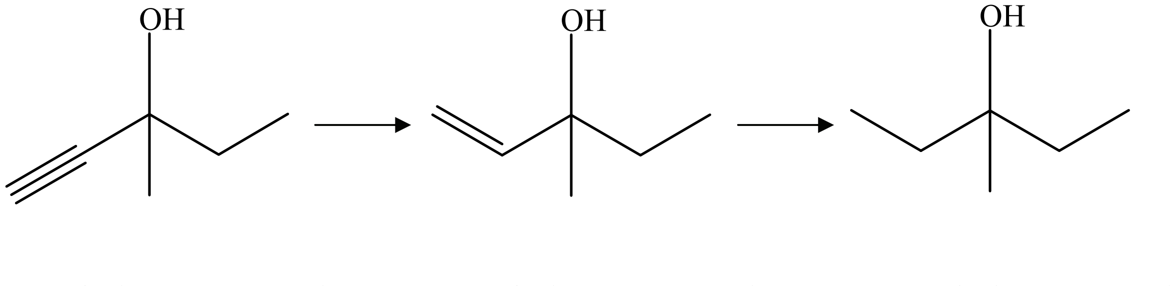

Scheme 1: Schematic representation of the hydrogenation of *3*-methyl-*1*-pentyn-*3*-ol

presented of batch experiments of the consecutive hydrogenation of *3*-methyl-*1*-pentyn-*3*-ol (Scheme 1), operated under moderate diffusion-limited conditions, such that the maximum yield of the intermediate alkene is a good measure for the balance of diffusion and reaction.

2. Experimental

2.1. Materials and Catalyst Preparation

Square channel cordierite monoliths (400 cells per square inch (cpsi), d_c = 1.09 mm, t_w = 0.178 mm, ε_{wall} = 0.74, L_m = 5 cm, d_m = 1 cm) [1] were provided by Corning. α-Al_2O_3 was purchased from Aldrich. High surface area SiO_2 (Grade 633) was purchased from Davisil as catalyst support. *3*-methyl-*1*-pentyn-*3*-ol, *n*-decane (solvent) and *n*-hexadecane (internal standard) were purchased from Aldrich, USA. Palladium acetate trimer, purchased from Alfa Aesar, was used as the palladium precursor. All the chemicals were used as received without further purification.

The bare monoliths were first calcined at 1273 K for 1 h to burn off any organic impurities. These monoliths were immersed in an acidic aqueous suspension of SiO_2 (19 wt. % solids, pH~1), which was ball-milled for 24 h in order to obtain small SiO_2 particles in the range of 5 μm [1]. The excess of this suspension in the channels was blown out using an air gun. The monoliths were then dried at room temperature for 2 h while rotating horizontally in static air, dried in an oven at 373 K for 1 h and calcined at 723 K for 4 h at 1 K/min. The low heating rate was maintained to avoid cracks in the coating. The monoliths prepared by coating SiO_2 onto the bare cordierite are referred to as *single coat layer* monoliths throughout the article.

To round off the square channel geometry, the bare monoliths were first immersed in an acidic α-Al_2O_3/H_2O suspension (58 wt. % solid, pH ~3) for 1 min. A similar procedure as described above for the *single coat layer* monoliths was then followed, except that the calcination temperature was 973 K. This procedure was repeated two more times in order to obtain uniform rounded channels. SiO_2 was coated on these *round channel* monoliths following the technique mentioned above.

The SiO_2 loading on both the *single coat layer* and the *round channel* monoliths varied between 0.12 g and 0.14 g, respectively, for all the samples prepared. Using SiO_2 slurry with a higher pH led to a weak interaction with the α-Al_2O_3 layer resulting in flaking and loss of the SiO_2 coat layer.

Pd was applied to all the monoliths by the following wet-impregnation technique. The required amount of the Pd precursor, corresponding to a 2.5 wt. % loading with respect to the SiO_2 coating, was dissolved in toluene. The impregnation was carried out in a glass set-up specially designed for the treatment of monoliths in liquid phase, where the liquid (~50 ml) is forced through the channels of the monolith by internal recirculation [7]. After 24 h, the solution was drained off and the excess liquid was gently blown out using a controlled airflow. These samples were dried at 388 K for 4 h to remove the solvent and subsequently calcined at 673 K for 4 h.

2.2. Hydrogenations

The selective hydrogenation of *3*-methyl-*1*-pentyn-*3*-ol was performed in a 350 ml turbine autoclave, which is described in detail elsewhere [8]. Briefly, the autoclave was equipped with a vertical cylindrical holder for a maximum of seven monoliths, with maximal length of 5 cm and a diameter of 1 cm, and a turbine with blades, which has a maximum rotation speed of 3000 rpm. In a typical hydrogenation experiment, a single monolith sample (5 cm in length) was reduced in-situ at 373 K using H_2 (P_{H2} = 1.0 MPa) for 1 h. After cooling and depressurizing the hydrogen, the desired amount of reactant, solvent and internal standard (~330 ml) was charged to the reactor from the liquid storage vessel. The contents were flushed with nitrogen three times at room temperature. After the desired reaction temperature was attained, the system was pressurized with hydrogen to the required pressure. The reaction was started by switching on the stirrer and this was taken as time t = 0. The progress of the reaction was determined by monitoring the hydrogen supply rate (keeping reactor pressure constant) as a function of time. The standard conditions were 323 K, 0.5 MPa H_2 pressure, 0.27 mol/L *3*-methyl-*1*-pentyn-*3*-ol in *n*-decane and a stirring speed of 1500 rpm. After the completion of the reaction as indicated by a ceasing hydrogen consumption, the reactor was cooled to room temperature and depressurized. In all experiments, concentration-time data were generated by intermediate sampling of the liquid phase (~ 250 µl) and analyzing the samples using a gas chromatograph (Chrompack CP9001 equipped with an autosampler), which was fitted with a CP Sil 8 CB column (50 m × 0.25 mm). The conditions of the GC analysis were: FID temperature, 523 K; injector temperature, 523 K; and column temperature was increased linearly from 323 K to 523 K at 6.7 K/min.

2.3. Catalyst Characterization

2.3.1. Standard Surface Characterization

The specific surface area of the SiO_2 (~0.14 g) coated on the *round channel* monolith samples was determined by N_2 physisorption at 77 K on a Quantachrome Autosorb 6B after degassing in vacuum at 623 K for 16h.

Scanning Electron Microscopy (SEM) was conducted using a Philips SEM XL 20 equipped with a SED detector for secondary and back-scattered electrons. The magnification range is 10 to 400,000 ×. The samples were first sputtered with gold and mounted on an Al stub to examine the monolith surface coverage by Al_2O_3 and SiO_2. The images were obtained at 15 kV.

Transmission Electron Microscopy (TEM) was performed on the *round channel* monoliths using a Philips CM30T electron microscope with a LaB_6 filament as the source of electrons operated at 300 kV. The samples were mounted on Quantifoil microgrid carbon polymer supported on a copper grid by placing a few droplets of a suspension of the ground sample in hexane on the grid, followed by drying at ambient conditions. To determine the distribution of Pd along the length of the monolith, samples were included from the top and middle section of the monoliths. The Pd crystallites vary from 1.8 – 3.6 nm in diameter. Importantly, no large clustering was observed, except for a few particles of 9 nm in diameter. The average size of the Pd crystallites was ~ 2.4 nm.

CO chemisorption was also performed on the Pd impregnated *single coat layer* and *round channel* monoliths to determine the Pd surface area. The samples were first dried in vacuum at 403 K (this dry sample weight was used in the calculations). Subsequently, the samples were reduced (100% H_2, 50 cm^3/min, 2h) at 373 K, followed by evacuation (2h) at 403 K. The adsorption measurements were performed at 313 K using CO as adsorptive and assuming a CO:Pd = 1:1 stoichiometric ratio. Both the in-situ pre-treatment and the analysis were performed on the Quantachrome Autosorb-1C. CO chemisorption indicated a similar Pd crystallite size as observed by TEM (Table 1).

2.3.2. *Electron Probe Micro-analysis (Spatially reseolved elemental analysis)*

In order to obtain a flat cross-section of the brittle monolithic structure required for executing reliable and quantitative X-ray microanalysis, the sample material was moulded into the electrically conducting methacrylate based resin Technovit 5000. This resin, after hardening, fills the channels of the monolith structure and allows polishing of the sample. The EPMA measurements were performed using a JEOL JXA 8800 M microprobe. Element Mapping was carried out at 20 kV accelerating voltage, 7.5×10^{-8} A, and a dwell time per map-point of 100 ms. Map areas were 100 × 100 points, each located at a distance of 5 micrometers. Mapped elements were Al, Si, and Pd (cordierite is composed of 2MgO: $5SiO_2$: $2Al_2O_3$), at Al Kα, Si Kα, and Pd

Table 1: Surface characterization of monoliths

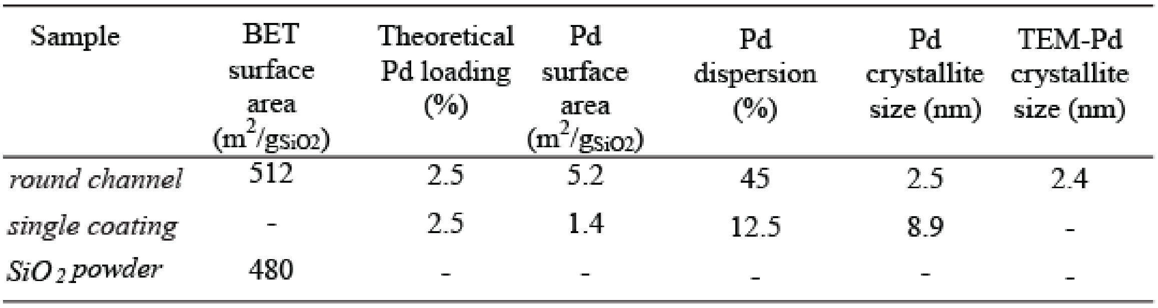

Sample	BET surface area (m^2/g_{SiO2})	Theoretical Pd loading (%)	Pd surface area (m^2/g_{SiO2})	Pd dispersion (%)	Pd crystallite size (nm)	TEM-Pd crystallite size (nm)
round channel	512	2.5	5.2	45	2.5	2.4
single coating	-	2.5	1.4	12.5	8.9	-
SiO_2 powder	480	-	-	-	-	-

Lα wavelengths respectively. After measurement, map-intensities were manually optimized for maximum display of detail.

3. Results and Discussion

3.1. Monolith Characterization

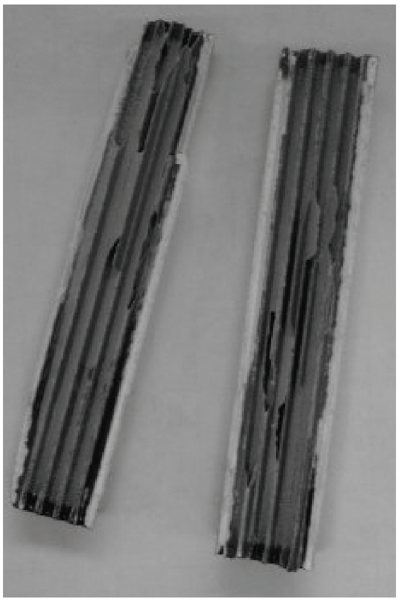

Figure 1: View of the channel interior after cutting a *round channel* monolith sample along its length. The light grey shade indicates α-Al_2O_3 or cordierite and black shade indicates the palladium

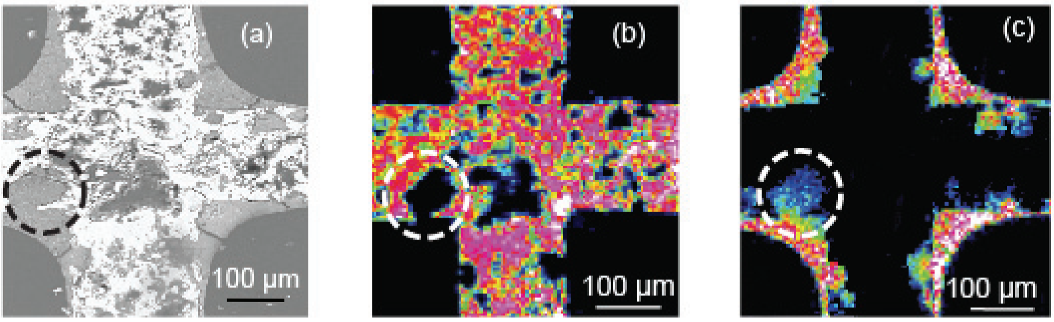

Figure 2: Pictures of cross sections of *single coat layer* monolith sample
(a) SEM image where the light grey patches indicate SiO_2 **(b)** Al elemental map with dark areas corresponding to presence of SiO_2 in macropores **(c)** Pd elemental map obtained by EPMA indicating presence of Pd inside the macropores

The BET surface area of the *round channel* monoliths was 512 m^2/g (corrected for α-Al_2O_3 surface area of 9 m^2/g) as compared to 480 m^2/g of the commercial SiO_2 grade (Table 1). This slight difference in surface area could either be due to inaccuracy during the measurement or details of preparation of the sample. Thus, the acidic SiO_2 slurry (pH~1) used for coating the round-channelled monoliths with SiO_2 did not lead to loss in specific SiO_2 surface area. The uniform distribution of the Pd crystallites on the *round channel* monoliths was confirmed using TEM and CO chemisorption. Further qualitative confirmation of the even distribution of Pd along the entire length of the

Pd content	Subdivision of area		$\int dA$	$\int x_{Pd} dA$
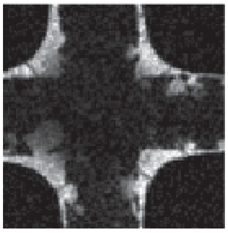		Inner macropores	736 pixels (37%)	213 (%Pd·px) (24%)
		Outer washcoat	1216 pixels (63%)	666 (%Pd·px) (76%)

Figure 3: Pd distribution within and outside macropores based on elemental mapping of a *single coating* monolith

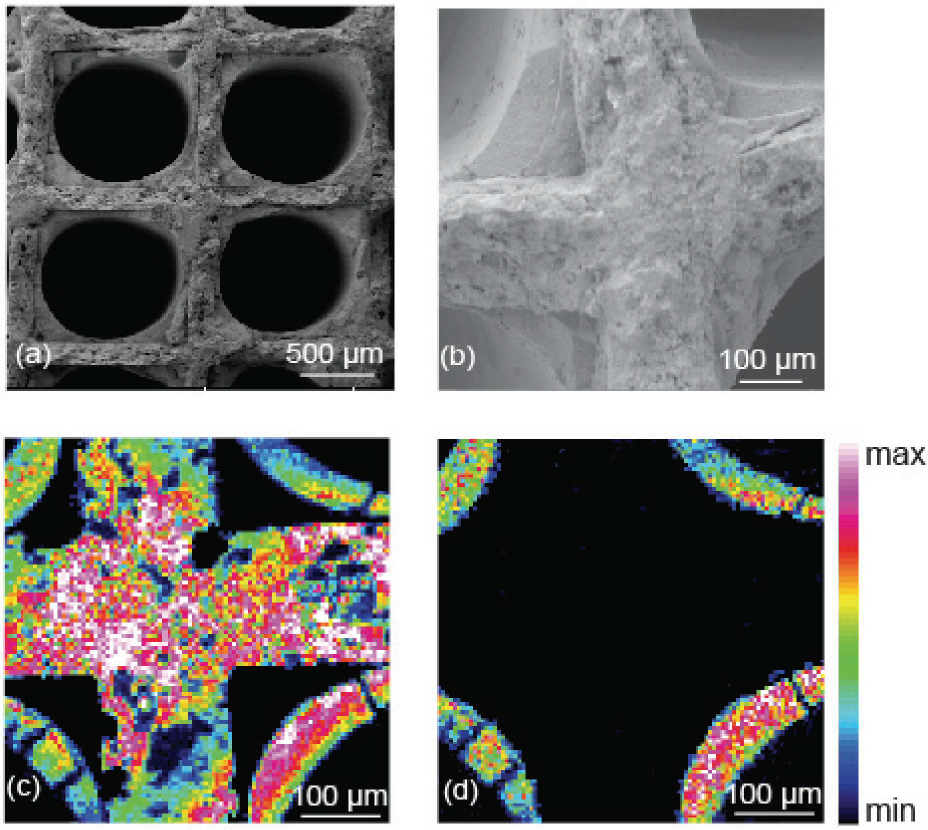

Figure 4: Pictures of cross sections of *round channel* monolith sample
(a) Overview of uniform round channels **(b)** SEM picture of cross section after 3rd dip coating with α-Al_2O_3 **(c)** Si elemental map obtained by EPMA showing the presence of the SiO_2 support layer. The blank region represents the α-Al_2O_3 layers **(d)** Pd elemental map obtained by EPMA indicating presence of Pd only in the SiO_2 coating.

monolith is seen from Figure 1. The lower Pd surface area and dispersion of the *single coat layer* monolith as compared to the *round channel* monolith (Table 1) suggests that the Pd loading on the *single channel* monolith was lower than the targeted 2.5 wt. %, though this was not confirmed by ICP.

3.2. Elemental maps

Figure 2 a shows the SEM picture for the *single coat layer* sample, which was coated only once with SiO_2. The dark areas on the aluminium map (Fig. 2 b) indicate the macropores of the cordierite that can also be identified from the SEM image. The macropores of the cordierite are not strongly interconnected, and some of the macropores that are deep inside the wall are not filled with silica. The most important image is the Pd map (Fig. 2 c), which shows that the outer macropores are filled with the noble metal. We binarized the Pd map from the raw EPMA data and divided the mapped area into a Pd-containing area and a Pd-free area following which the Pd-containing part was subdivided into macropore area and outer washcoat. From the areas of the different zones, we calculated that the applied SiO_2 is distributed between the macropores and outer coating in a ratio of 1:1.65. Upon integrating the Pd content in both areas, we found that the Pd is distributed over both zones in a ratio of 1:3.1 (Fig. 3). It is difficult to accurately determine a washcoat thickness for this material. In the edges, the coating can be as thin as 10 microns, whereas in the corner the average value of the washcoat thickness is 75 microns, averaged over the four corners. The depth of the deposited Pd in the macropores varied evenly between just a few microns to 50 microns.

Figure 4 shows the SEM pictures and the corresponding elemental maps for the *round channel* sample, with three priming coats of α-Al_2O_3. The rounding of the square channel geometry is clearly seen from Fig. 4 a. The different layers corresponding to each dip are clearly visible from the SEM pictures (Fig. 4 b). Although the first priming layer effectively plugs the macropores, three layers are required to obtain uniformly round channel geometry. The dark areas on the silicon map (Fig. 4 c) clearly show how the α-Al_2O_3 collected into the corners and macropores of the cordierite, providing a smooth structure for the SiO_2 coating. From the Pd map (Fig. 4 d), it is evident that no Pd ended up on the α-Al_2O_3 or anywhere else in the cordierite structure. The thickness of the active layer is fairly even: from the map we calculate a

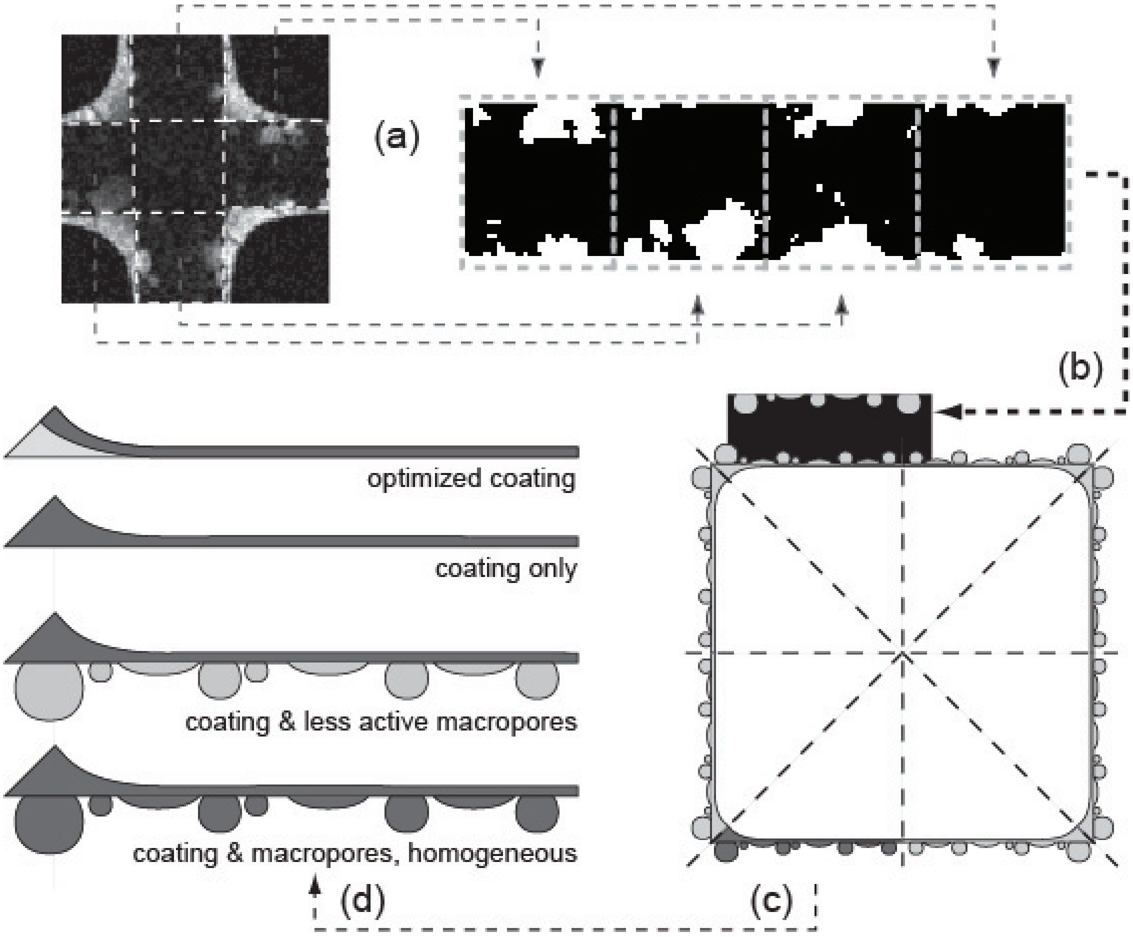

Figure 5: Schematic procedure to define typical catalyst distribution and estimate macropore volume in a *single coating* monolith

minimum thickness of 12 microns, a maximum thickness of 25 microns and an average thickness of 18 microns.

3.3. *Effectiveness Calculations*

Based on the elemental maps and the channel dimensions of the commercially available 400-cpsi monoliths [1], a representative geometry was constructed to calculate effectiveness factors for non-symmetric washcoats, including the contribution of active material in the macropores. Figure 5 shows the schematic procedure to define the irregular washcoat geometry accounting for the presence of active metal in the macropores. This shape was based on the thickness of the washcoat in the edges and the average thickness in the corner of the wall. The macropores were distributed evenly over the wall and the catalyst volume was chosen such that we have the same ratio of 2:1 of internal and external volume as deduced from the elemental map (Fig. 5 a-c). The various models for which the effectiveness and effective diffusion lengths were calculated are shown in Fig. 5 d. In the one-zone model (*coating & macropores, homogeneous)*, the Pd catalyst present in the macropores was assumed to have similar activity as that present in the waschcoat, whereas in the two-zone model (*coating & less active macropores)*, the Pd catalyst present in the macropores was assumed to have half the activity as that present in the washcoat ($k_{macropores} = ½.k_{washcoat}$). Diffusion-reaction calculations (dimensionless) were performed to determine catalyst effectiveness as a function of different Thiele moduli using FEMLAB (a PDE solver tool from COMSOL Inc. that uses the finite element method). A fine mesh was used in all cases to allow reasonable calculation of the internal concentration gradients, assuming a first order reaction in H_2. The concentration gradient in the washcoat for different values of the Thiele modulus ($\phi = 1, 10$) is shown in Figures 6 a-c (for the one-zone and two-zone model), respectively. The catalyst effectiveness plot as a function of different Thiele moduli (Figure 7) for the irregular washcoat geometry considering homogeneously distributed Pd (one-zone model) is compared with that obtained assuming standard slab geometry, the two-zone model and the optimized coating. At higher values of the Thiele modulus, when the reaction is severely diffusion limited, the reaction occurs only in a thin outer layer of the washcoat and the shape of the

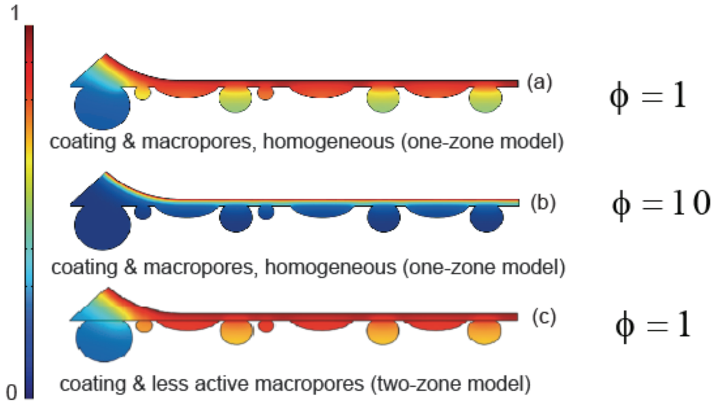

Figure 6: Dimensionless H_2 concentration profiles obtained for the representative irregular washcoat geometry including the contribution of macropores for different Thiele moduli

washcoat does not influence the reaction rate anymore (also seen from Fig. 6 b). Similarly, at very low values of the Thiele modulus, the reaction is kinetically controlled and the catalyst located deep inside the macropores is also available for reaction (Fig. 6 a). Consequently for these asymptotic values, the effectiveness can be defined by an ideal slab geometry for both these extreme cases [2]. However, for Thiele modulus values in the range of unity, the effectiveness factor deviates significantly from that calculated assuming slab geometry. The importance of accounting for the presence of active material inside the macropores (especially for reactions operated in the Thiele modulus region of unity), which would otherwise lead to an overestimation of catalyst effectiveness (up to 15 %), is thus underlined by our work. The effectiveness profiles calculated for the one-zone and the two-zone models overlap, indicating the appropriateness of our approach. The effectiveness profile obtained for the uniform coating matches also that obtained for standard slab geometry confirming the advantage of the priming technique.

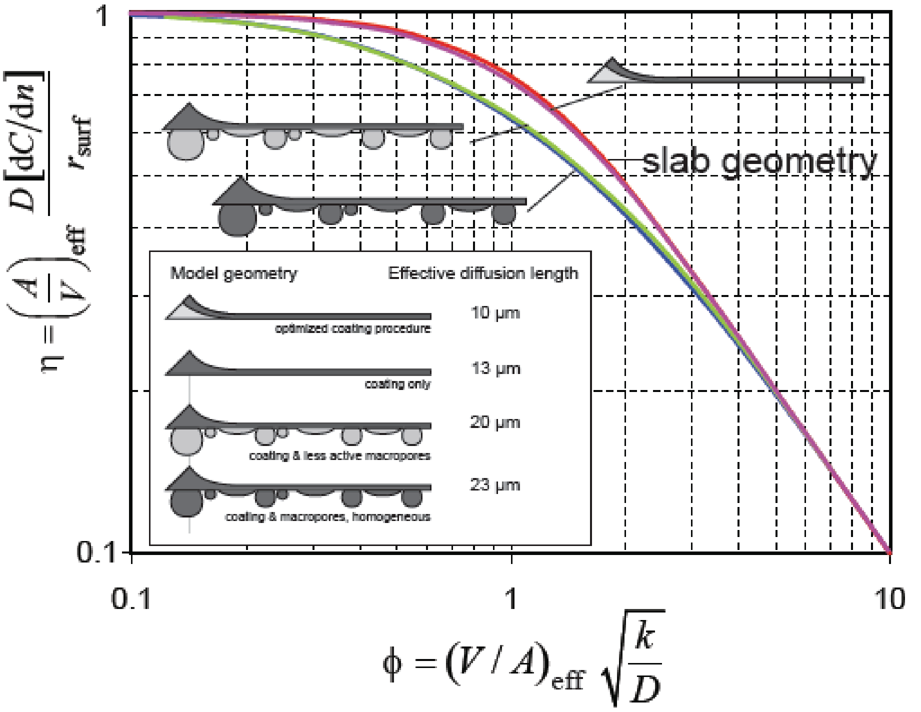

Figure 7: Effectiveness plot for monolith with irregular washcoat geometry compared with a standard slab geometry for 1st order kinetics

3.4. Selective Hydrogenation

The performance of the *single coat layer* and *round channel* monoliths in the selective hydrogenation of *3*-methyl-*1*-pentyn-*3*-ol under internally diffusion-limited conditions is presented in Figures 8 a-b, respectively. An improved maximum yield of the desired intermediate product *3*-methyl-*1*-penten-*3*-ol is observed for the *round channel* monolith as compared to the square channel *single coat layer* sample (87 % versus 80 %). For consecutive reactions, the maximum yield of the intermediate product is lower under internally diffusion-limited conditions and occurs at lower conversion levels. This is observed from Fig. 8 (a-b) indicating less interference of internal diffusion limitations for the *round channel* monolith. Although the *round channel* monolith also shows a higher reaction rate (Table 2), this could be attributed to the higher Pd specific surface area as compared to the *single coat layer* sample (Table 1). The lower magnitude of the internal diffusion limitations (and correspondingly a higher product yield) for the *round channel* sample clearly indicates the effectiveness of plugging the cordierite macropores.

Internal and external transport limitations can be verified from observed reaction rates by the Wheeler-Weisz criterion (Φ) and the Carberry number (Ca), respectively [9,10]. These were evaluated for both hydrogen and the

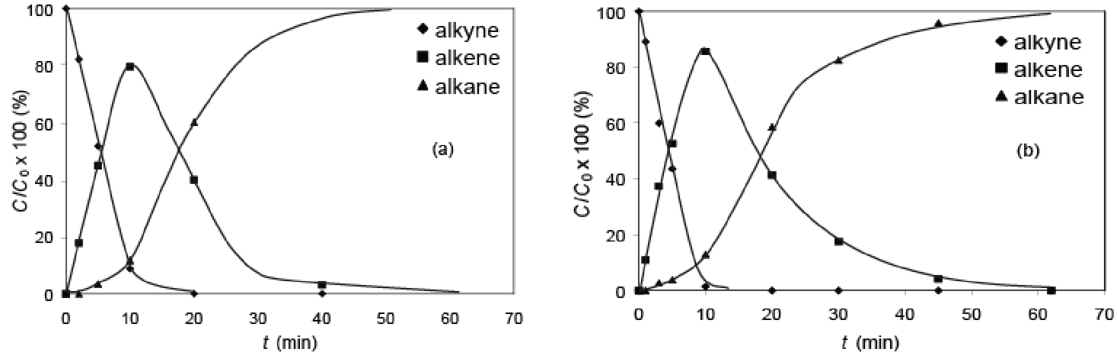

Figure 8: Relative concentration versus time profile for the selective *3*-methyl-*1*-pentyn-*3*-ol hydrogenation

(a): *single coat layer* monolith **(b)**: *round channel* monolith

Reaction Conditions: T = 323 K, C_{alkyne} = 0.27 mol/L, P_{H2} = 0.5 MPa alkyne (Table 2). Although hydrogen is the limiting reactant in terms of the saturated liquid phase concentration and is expected to exhibit the strongest limitations, this could be compensated for by its higher diffusivity (D_{eff}) (Table 3). The effective diffusion length (L) was obtained from the effectiveness plot (Fig. 7) using FEM calculations. Though the external diffusion limitations for hydrogen were insignificant, the reaction was internally diffusion limited for both the reacting components (Table 2). However, the extent of internal diffusion limitations was much lower for the optimized *round channel* monolith due to a shorter and more uniform diffusion length as compared to the *single coat layer* monolith. The lower severity of the diffusion limitations can explain the higher yield of the desired *3*-methyl-*1*-penten-*3*-ol intermediate on using the optimized *round channel*.

It is emphasized that square channel monoliths are less suitable for fast

Table 2: Evaluating mass transport limitations for *single* coating and *round channel* monoliths

	single coat layer	*round channel*
L (μm)	23	10
$r_{v,obs}$ (mol/m$^3_{cat}$/s)*	977.5	1277.6
$Ca_{l-s} = \dfrac{r_{v,obs H_2}}{k_{l-s} \cdot C_{H_2}} < 0.05$	0.057	0.069
$Ca_{g-l} = \dfrac{r_{v,obs H_2}}{k_{g-l} \cdot C_{H_2}} < 0.05$	0.005	0.007
$\Phi_{alkyne} = \dfrac{r_{v,obs} \cdot L^2}{D_{eff} \cdot C_{s\,alkyne}} \left(\dfrac{n+1}{2}\right) < 0.15$	2.5	0.6
$\Phi_{H_2} = \dfrac{r_{v,obs} \cdot L^2}{D_{eff} \cdot C_{s\,H_2}} \left(\dfrac{n+1}{2}\right) < 0.15$	17.6	4.3
Maximum alkene yield (%)	80	87

*: Initial reaction rate at 10% conversion

Table 3: Diffusivity values for alkyne and hydrogen in decane

	3-Methyl-1-pentyn-3-ol	Hydrogen	
C (mol/L)	0.27	0.02	[11]
D (m^2/s)	3.87×10^{-9}	1.47×10^{-8}	[12]
$D_{eff} = 0.1\,D$ (m^2/s)	3.87×10^{-10}	1.47×10^{-9}	

selective hydrogenations or oxidations due to the depicted diffusion issues. Since the suggested channel rounding is commercially a less attractive manufacturing step, the use of hexagonal channel geometries offer a much better starting point in this respect [1]. The impact of the macro porosity however, has still to be considered.

4. Conclusions

Elemental mapping (EPMA), combined with numerical analysis of reaction and diffusion, is an indispensable tool to quantitatively evaluate the quality of coatings of supported catalysts. We found that as much as one-third of the applied washcoat can be present inside the macropores of the cordierite. Expensive noble metals that are subsequently applied by wet-impregnation end up in these macropores to a significant extent. Ignoring these filled up macropores leads to an overestimation of the catalyst effectiveness, in particular when the Thiele modulus is of the range of unity. Priming of the structured catalyst support with a low surface area, non-porous coating, e.g. α-Al_2O_3, overcomes the aforementioned problems, and results in a washcoat with a narrow distribution of coating thickness and consequently an optimum utilization of the catalyst. The positive effect of plugging the macropores on the product yield was demonstrated for the internally diffusion-limited selective hydrogenation of *3*-methyl-*1*-pentyn-*3*-ol.

Acknowledgements

Jack Voncken is thanked for performing EPMA measurements. Michiel Kreutzer is acknowledged for fruitful discussions. Brahim Daouairi is acknowledged for developing the monolith coating procedure as a part of his graduate research.

Notation

A : external surface area catalyst (m^2)
C : concentration (mol/L)
Ca : Carberry number (-)
D : diffusivity (m^2/s)
D_{eff} : effective diffusivity (m^2/s)
d_{c} : channel diameter (mm)
d_{m} : diameter of monolith sample (cm)
k : 1st order rate constant
L : effective diffusion length (μm)
L_{m} : length of monolith sample (cm)
$r_{\mathrm{v,\ obs}}$: observed reaction rate ($mol/m^3_{cat}/s$)
t_{w} : wall thickness (mm)
V : catalyst volume (Pd/SiO_2) (m^3_{cat})

Greek Symbols

$\varepsilon_{\mathrm{wall}}$: wall porosity (-)
Φ : Wheeler-Weisz modulus (-)
ϕ : Thiele modulus (-)

Reference List

1. T. A. Nijhuis, A. E. W. Beers, T. Vergunst, I. Hoek, F. Kapteijn and J. A. Moulijn, 'Preparation of Monolithic Catalysts', *Catalysis Reviews – Science and Engineering*, 42 (**2001**) 345.

2. D. Papadias, L. Edsberg and P. Bjornbom, 'Simplified Method for Effectiveness Factor Calculations in Irregular Geometries of Washcoats', *Chemical Engineering Science*, 55 (**2000**) 1447.

3. R. E. Hayes, B. Liu and M. Votsmeier, 'Calculating Effectiveness Factors in Non-Uniform Washcoat Shapes', *Chemical Engineering Science*, 60 (**2005**) 2037.

4. E. Crezee, P. J. Kooyman, J. Kiersch, W. G. Sloof, G. Mul, F. Kapteijn and J. A. Moulijn, 'Dispersion and Distribution of Ruthenium on Carbon-Coated Ceramic Monolithic Catalysts Prepared by Impregnation', *Catalysis Letters*, 90 (**2003**) 181.

5. A. F. Pérez-Cadenaz, F. Kapteijn and J. A. Moulijn, 'High Performance Monolithic Catalysts for Hydrogenation Reactions', *Catalysis Today*, 105 (**2005**) 623.

6. A. F. Pérez-Cadenaz, F. Kapteijn and J. A. Moulijn, 'Tuning the Morphology of Monolith Coatings', *Applied Catalysis A: General*, 319 (**2007**) 267.

7. J. J. W. Bakker, W. G. Groendijk, K. M. de Lathouder, J. A. Moulijn, F. Kapteijn, M. T. Kreutzer and S. A. Wallin, 'Enhancement of Catalyst Performance Using Pressure Pulses on Highly Permeable Structured Catalysts', *Industrial & Engineering Chemistry Research*, (**2007**) *submitted*

8. R. J. Berger, E. H. Stitt, G. B. Marin, F. Kapteijn and J. A. Moulijn, 'Chemical Reaction Kinetics in Practice', *CATTECH*, 5 (**2001**) 30.

9. J. A. Moulijn, A. Tarfaoui and F. Kapteijn, 'General Aspects of Catalyst Testing', *Catalysis Today*, 11 (**1991**) 1.

10. M.V.Twigg, 'Catalyst Handbook', 2nd Ed. Oxford University Press (**1997**)

11. R. V. Chaudhari, R. Jaganathan, S. P. Mathew, C. Julcour, and H. Delmas, ‘Hydrogenation of 1, 5, 9-cyclododecatriene in Fixed-Bed Reactors: Down- vs. Upflow Modes’, *AIChE Journal*, 48 (**2002)**, 116.

12. C. R. Wilke, P. Chang, ‘Correlation of Diffusion Coefficients in Dilute Solutions, *AIChE Journal*’ 1 (**1955)**, 264.

6

Summary and Evaluation

1. Background and Motivation

Catalyzed hydrogenation reactions play an important role in the chemical industry and are commonly observed in many processes in crude oil refineries as well as in the production of specialty chemicals. Catalyst performance is usually described in terms of its activity (i.e. the rate of consumption of the reactants per unit amount of catalyst) and product selectivity (ratio of the amount of desired product formed to the reactant consumed). However, the loss of catalyst activity by deactivation is also an important factor to be considered since deactivation is observed in a majority of industrial hydrogenation processes. Though catalyst deactivation is well accepted and documented for the bulk processes in petroleum refining [1], its importance has traditionally been neglected in the fine chemical industry. Even today, only limited literature exists on the catalyst deactivation occurring in the fine chemical industry [2,3]. Due to the high value of the products, the catalyst is usually replaced after a few runs [4]. However, with increasing competition, tighter profit margins and environmental legislations, the focus in the coming years will also be on improving catalyst stability. In this thesis, the hydrogenation of *4*-isobutylacetophenone (Scheme 1) is investigated as a model reaction related to the fine chemicals industry. This reaction is the second step in the multi-step synthesis of Ibuprofen [5], and severe catalyst deactivation was observed after a single batch run. Identifying the cause of deactivation is indeed the first and most important step towards improving the catalyst stability. A major aspect of this research was therefore

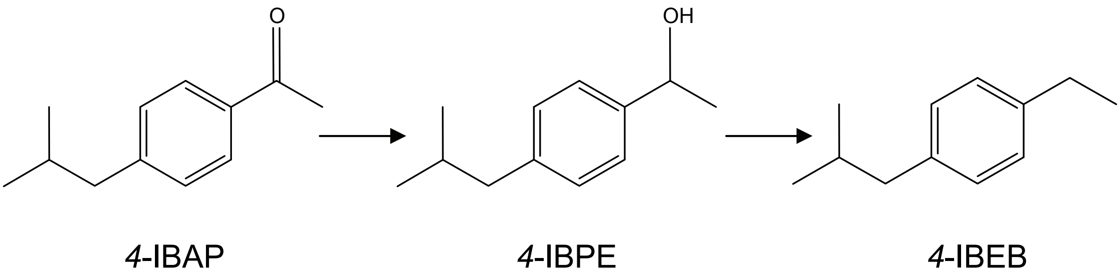

Scheme 1: Reaction scheme for the hydrogenation of *4*-isobutylacetophenone over supported Pd catalysts

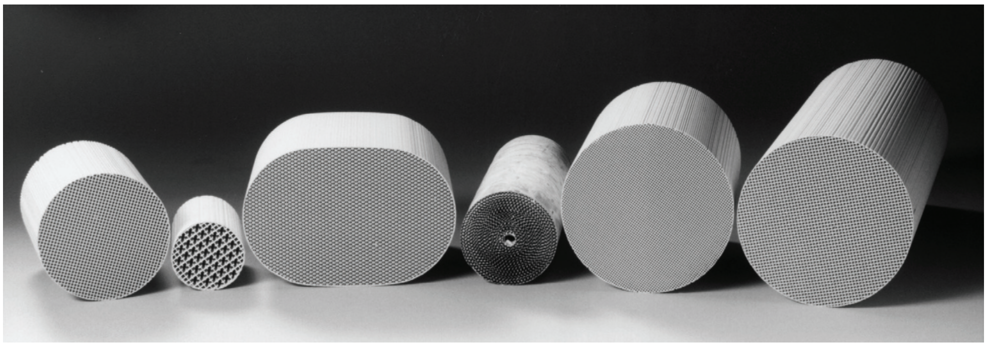

Figure 1: Various available shapes of monoliths

to identify the cause of catalyst deactivation and to study related aspects (elucidation of reaction pathway, kinetic modelling including activity loss due to deactivation) for this industrially important reaction through systematic catalyst characterization and catalyst performance studies.

The combined effects of catalyst activity, selectivity and stability along with the scale of production usually dictate the choice of reactor for any hydrogenation process. The mechanically agitated batch reactor with slurry catalyst particles is still the ‘workhorse’ of the fine chemical industry, since production is on a relatively small scale and different reactions using different catalysts can be performed using the same piece of equipment. Recently, the use of monolithic reactors has been proposed as an alternative to the use of slurry reactors for fine chemicals production [6,7]. Monoliths are macro porous cordierite structures containing many long, straight, parallel channels usually of a square cross-section (Figure 1). Due to the low specific surface area of cordierite ($< 4\ m^2/g$), a high specific surface area catalyst support is washcoated onto the walls of the monolith channels prior to application of the catalytically active metal in order to enhance dispersion of the active metal.

Monoliths perform excellently for processes where mass transfer to the catalyst, and pressure drop are an important aspect. Typically, fast (mass transfer limited) reactions that are performed in slurry reactors fall into this category, since monoliths offer high gas-liquid mass transfer rates as compared to slurry reactors and can ensure an optimum use of the highly active catalyst [8,9].

An externally diffusion limited reaction also suffers from internal diffusion limitations due to the high observed reaction rate ($r_{v,obs}$). As seen from the Wheeler-Weisz criterion (equation 1) to test the presence of internal diffusion limitations,

$$\Phi = \frac{r_{v,obs} \cdot L^2}{D_{eff} \cdot C_s} \left(\frac{n+1}{2} \right) < 0.15 \qquad (1)$$

the effective diffusion length (L) is one of the controllable parameters and plays an important role in the reaction being internally diffusion limited. If the effective diffusion length is sufficiently short, the reaction might not suffer from internal diffusion limitations although it has a high observed reaction rate ($r_{v,obs}$).

The internal diffusion limitations theoretically lower the desired intermediate product selectivity in a consecutive hydrogenation. Coating the bare cordierite monoliths with a high specific surface area support has two important shortcomings (*i*) the high specific surface area support and consequently the active metal enters the macro pores in the channel walls leading to a longer effective diffusion length for the reactants. Furthermore, ignoring the presence of the active metal inside the macropores leads to an overestimation of the catalyst effectiveness (*ii*) the application of the washcoat on the square channels leads to a non-uniform diffusion length at the corners as compared to the edges of the monolith (***Chapter 1***). Thus, another aspect of this research was to develop an improved washcoating technique to plug the macro pores and to obtain a uniform diffusion length, thereby overcoming the detrimental effects of the above mentioned problems.

The most obvious downside to the use of monoliths in comparison to slurry reactors is similar as that for the packed beds, the required long-term catalyst stability. If the catalyst deactivates too quickly, the frequent replacement of the monolith is too costly and renders the alternative use of monoliths unattractive. As a result, the selective hydrogenation of *3*-methyl-*1*-pentyn-*3*-

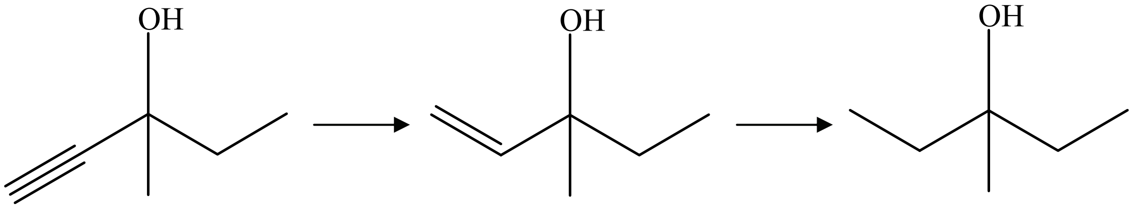

3-methyl-1-pentyn-3-ol 3-methyl-1-penten-3-ol 3-methyl-pentan-3-ol

Scheme 2: Schematic representation of hydrogenation of 3-methyl-1-pentyn-3-ol

ol to 3-methyl-1-penten-3-ol (Scheme 2) over Pd/SiO_2 was chosen as a model reaction system to test the monoliths with optimized channel geometry, since a Pd/SiO_2 catalyst was reported to be stable for this reaction [10,11] and this is an example of a fast, diffusion limited reaction.

2. Summary

2.1. Selective Hydrogenation of 4-isobutylacetophenone

2.1.1. Catalyst and Support Selection

The selective hydrogenation of 4-IBAP involves the selective reduction of the carbonyl functional group to the corresponding alcohol. Pd is known to selectively hydrogenate the carbonyl functional group [12] and hence was the preferred metal. Although a basic support (e.g. $CaCO_3$) would ideally maximize the 4-IBPE selectivity (by preventing the acid catalyzed dehydration to 4-IBEB), its low surface area has a negative effect on the Pd dispersion and correspondingly on the activity (***Chapter*** 3). Moreover, the use of a basic support does not guarantee a full selectivity to the desired alcohol product, since Pd is also known to be a good hydrogenolysis catalyst [13]. The choice of the support between a basic one having a low surface area ($CaCO_3$) and conventional high surface area supports (SiO_2, activated carbon) which are slightly acidic was finally in favour of the 'in-house' prepared Pd/SiO_2. This catalyst showed the highest activity and selectivity during the catalyst screening (***Chapter*** 3).

2.1.2 Reaction Pathway

In a typical 4-IBAP hydrogenation run over Pd/SiO_2, the selectivity to the desired 4-IBPE reached a maximum after which the formation of the undesired 4-IBEB was observed. The formation of the styrene intermediate (by dehydration of 4-IBPE) could not be confirmed by GC analysis. The knowledge of the accurate C-O scission pathway (by direct hydrogenolysis or by dehydration-hydrogenation) of 4-IBPE (Scheme 3) was highly desired because the styrene intermediate could be responsible for the observed catalyst deactivation (discussed later). ***Chapter* 2** deals with identifying the C-O bond scission pathway over three catalysts, Pd/SiO_2, a commercial Pd/C and Pd black.

The power of deuteration experiments in elucidating hydrogenation mechanisms was underlined by the work of Burwell [14]. 4-IBAP was reacted with deuterium under standard reaction conditions (T = 373 K, P_{D2} = 20 bar) and the resulting 4-IBEB was isolated from the reaction mixture and analyzed by multi-nuclear (^1H, ^2H and ^{13}C) NMR spectroscopy. Based on the NMR analyses, it was concluded that the C-O scission of 4-IBPE occurred by direct hydrogenolysis of the C-O bond over Pd/SiO_2, whereas the dehydration-hydrogenation pathway was observed over Pd/C. Experiments performed with unsupported Pd black suggested that the hydrogen dissociated on the metal surface plays the major role in the direct hydrogenolysis on Pd without any involvement of the support.

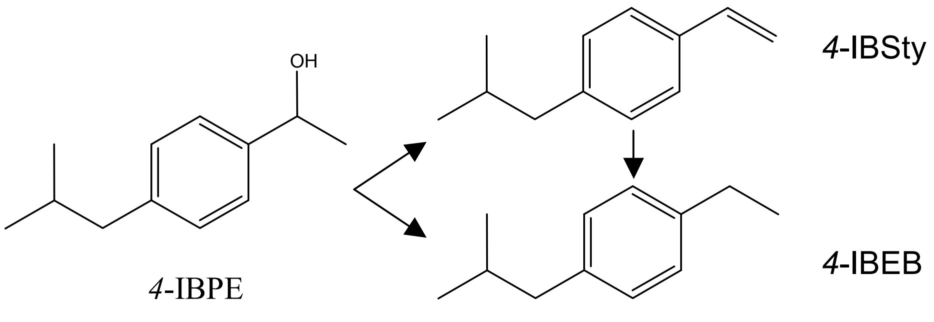

Scheme 3: Possible pathways for C-O bond scission of 4-IBPE

Characterization tests (TPD-MS and Boehm titration [15]) performed on the commercially available Pd/C indicated the presence of carboxylic acid sites, which could be responsible for the dehydration of 4-IBPE. This reasoning is plausible since carbon is usually activated by treatment with mineral acids to increase the surface oxygen complexes prior to impregnation of the active metal [16,17]. The SiO_2 support did not show any desorption of NH_3 when analyzed by NH_3-TPD, indicating the absence of strong acidity. This can explain the reason for not observing the dehydration-hydrogenation pathway on Pd/SiO_2, whereas for Pd/C it plays a role.

2.1.3. Catalyst Deactivation

A severe loss of catalytic activity was observed after a single batch run over Pd/SiO_2 as well as over Pd/C. To enable the use of thermal analysis techniques to study catalyst deactivation, the use of Pd/SiO_2 was preferred for all further studies. Five theoretically possible reasons for catalyst deactivation suggest themselves (Scheme 1) (*i*) polymerization of the styrene intermediate formed by dehydration of 4-IBPE (*ii*) The strong adsorption of the H_2O liberated by hydrogenolysis of 4-IBPE on the catalyst (*iii*) presence of impurities in commercially available SiO_2 support or reactants (*iv*) Pd crystallite growth and (*v*) condensation of 4-IBAP and 4-IBPE molecules to form oligomers. The fresh and spent Pd/SiO_2 catalyst samples were analyzed using a wide range of thermal (TGA, TPO-MS), microscopic (TEM) and spectroscopic (LEIS, DRIFT) techniques (***Chapter* 3**) to investigate the mechanism(s) of catalyst deactivation.

Deactivation due to polymerization of the styrene intermediate can be ruled out based on deuteration studies (***Chapter* 2**). Furthermore, the catalyst was stable for three runs when styrene was used as a feed. The H_2O liberated by the hydrogenolysis of 4-IBPE inhibited the reaction when Pd/SiO_2 was used, obviously due to the hydrophilicity of SiO_2. LEIS analysis of the fresh and spent Pd/SiO_2 as well as the blank SiO_2 support excluded the possibility of any strongly adsorbing conventional feed poisons causing deactivation. The absence of strongly adsorbing feed impurities was also confirmed by GC-MS analysis. Thermal analyses (TGA and TPO-MS) indicated the presence of hydrogen containing deposits on Pd as well as on the support. These findings were supported by CO chemisorption and N_2 physisorption analyses, which also indicated a drop in CO and N_2 uptake capacities of the spent catalyst. The possibility of catalyst deactivation due to condensation of 4-IBPE molecules to form ethers is unlikely, since a maximum of only two 4-IBPE molecules can condense theoretically, which might be insufficient to form oligomers. Ketones are known to undergo condensation type reactions in either acidic or basic medium leading to high molecular weight compounds. Two molecules of 4-IBAP can condense to form an α, β unsaturated carbonyl compound. The carbonyl group of this α, β unsaturated carbonyl compound can further condense with another molecule of 4-IBAP, consequently leading to the formation of oligomers by the aforementioned mechanism. The analysis of the SiO_2 support by DRIFT spectroscopy indicated the presence of isolated silanols, which can impart acidity to the support. Although the acidity was insufficient to catalyze the dehydration of the 4-IBPE (***Chapter 2***), it was apparently sufficient to promote condensation type reactions. The contribution of the support in the catalyst deactivation was also evident from the fact that the catalyst stability was nearly similar for consecutive runs when Pd black was used as a catalyst. Some Pd crystallite growth (as observed by TEM analysis) was also partly responsible for the loss of catalytic activity. However, its contribution to catalyst deactivation was far less significant than oligomerization considering the fact that calcination of the spent catalyst at 873 K resulted in a 30% loss of the metal surface area, whereas the reaction was performed at only 373 K. The deactivation observed on using Pd/C as a catalyst could be attributed to the polymerization of the styrene intermediate (as shown by deuteration studies), in addition to the condensation type reactions. The higher activity drop observed on spent $Pd/CaCO_3$ (compared to spent Pd/SiO_2 and Pd/C) was expected since the strong basic character of $CaCO_3$ would surely catalyze condensation reactions.

The use of a commercially available hydrophobic SiO_2 (in which the surface OH groups are replaced by CH_3 groups, leading to hydrophobicity) as an alternative support was also unsuccessful, because of a limited capacity of the surface for accommodating the Pd complexes during synthesis. The main finding of ***Chapter 3*** is that the acidity/basicity of the support plays an important role in the deactivation of aromatic ketones over Pd supported catalysts. A neutral support would be ideal, but requires further catalyst development.

2.1.4. Kinetic Modelling

Kinetic modelling is usually performed to help scale-up reactors from the lab-scale to a pilot scale and consequently to an industrial scale. The determination of accurate kinetics including loss of catalyst activity due to deactivation is a very challenging task and can only be seen as an empirical solution in majority of cases [18]. This is due to the fact that deactivation is a very complex phenomenon, which involves many uncertain parameters on the catalyst level that can seldom be accurately explained. Nevertheless, we have made an effort to model the kinetics for this industrially important reaction including the loss of activity due to deactivation (***Chapter 4***). The knowledge of accurate reaction pathway (***Chapter 2***) and the deactivation phenomena (***Chapter 3***) helped to reduce uncertainties in our model. A comprehensive model including the effects of different 4-IBAP concentrations, H_2 partial pressures, H_2O concentrations and catalyst concentrations over a wide temperature range (333 – 373 K) was developed.

A Langmuir-Hinshelwood type rate expression that assumed competitive adsorption of the reactants on the same site and the hydrogenolysis of 4-IBPE occurring via an S_N2 mechanism was chosen as the representative model.

It was difficult to decouple the kinetics from the deactivation due to the use of a semi-batch reactor to model deactivation. Nevertheless, we have tried to keep the uncertainties in this kinetic model to a minimum. To develop a more rigorous kinetic model, which can then be used to scale-up reactors, the deactivation parameter should be determined in a continuous flow reactor at low conversion levels. A similar approach as that mentioned in ***Chapter 4*** can then be followed to study the effect of various operating parameters on the catalyst performance and develop the kinetic model.

2.2. Selective Hydrogenation of 3-methyl-1-pentyn-3-ol using monoliths

Since most commercially available monoliths have channels with a square geometry, application of a high specific surface area support usually leads to a non-uniform washcoat thickness. Furthermore, due to the presence of macropores, the catalytically active material might be located deep inside these macropores and not utilized optimally. A technique to obtain a uniform washcoat thickness and prevent the active metal from entering the macropores is presented in ***Chapter 5***. Non-porous α-Al_2O_3 is used as a filler to plug the macropores. The SiO_2 support is then washcoated onto the optimized monoliths followed by impregnation of the active metal. Electron Probe Micro Analysis (EPMA) confirmed the presence of the active metal only in a thin outer layer. FEM calculations indicated that ignoring the presence of active metal inside the macropores leads to an overestimation of the catalyst effectiveness, especially in the Thiele modulus region of unity. The uniform diffusion length of the optimized monoliths led to a higher selectivity and yield of the desired intermediate product during the hydrogenation of *3*-methyl-*1*-pentyn-*3*-ol studied under mass-transfer limited conditions.

3. Evaluation

A systematic and thorough approach has been presented in this thesis to elucidate the catalyst deactivation occurring during the hydrogenation of an aromatic ketone. The hydrogenation of aromatic ketones is an important class of reactions in the fine chemicals industry. The approach presented in this thesis to elucidate catalyst deactivation can also be applied in general for other reaction systems. The use of deuterium as a tracer is very helpful to elucidate the pathway of reactions. A combination of thermal, microscopic and spectroscopic analysis techniques should be employed to get a clear picture about catalyst deactivation. Relying heavily on just one of these techniques might lead to erroneous results. Similarly, as shown for the kinetic modelling of 4-IBAP, it is important to choose a reaction model based on sound chemistry principles, rather than selection only on the basis of the best fit of the experimental data.

The commercially available cordierite monoliths usually have a square channel geometry, which leads to uneven distribution of the active material on washcoating. Although rounding of the square monolith channels will not be necessary if monoliths with such a geometry are commercially available, the negative effects of the presence of catalytic material in the macro pores of the walls still has to be taken into consideration. Thus, a single coat layer of non-porous α-Al_2O_3 might still be advisable to plug macro pores.

4. Structured reactors for deactivating systems in fine chemistry?

An important conclusion of this research is that the catalyst deactivation is an important variable during the hydrogenation of aromatic ketones, an example of an industrially important reaction. In view of the severe catalyst deactivation, the use of a structured (monolithic) reactor as a replacement for conventional slurry reactors seems unattractive. However, a monolithic reactor could still be a viable option by an ingenious attractive reactor design. As shown in Figure 2, an existing stirred tank reactor is equipped with a dual monolithic add-on unit. This retrofitted reactor allows the use of one monolith unit for the reaction, while the other is being regenerated in a swing operation. This allows for the long-term use of the monolithic catalyst for many batches, provided the catalyst is regenerable. The advantages of this design are that the existing infrastructure of a fine chemical production facility can be utilized and that the monolithic reactor concept can be applied even for a deactivating system, thereby eliminating the catalyst separation step as well as simplifying the regeneration step. Further investigations

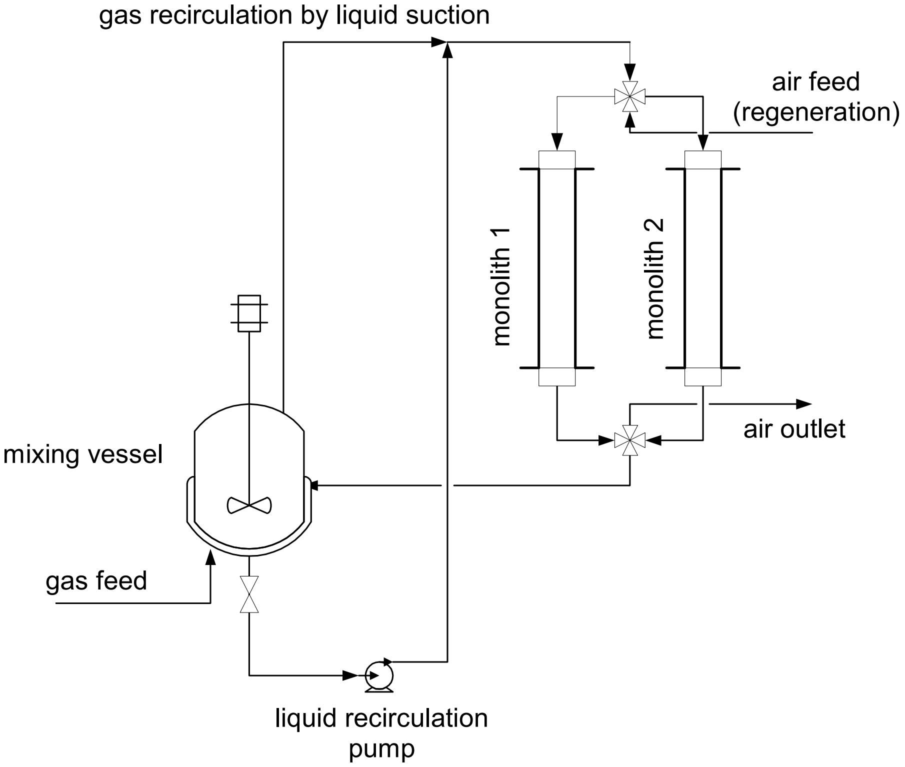

Figure 2: Example of conceptual process design retro fitting an existing slurry batch reactor with monoliths for a deactivating system

regarding efficient catalyst regeneration as well as economic feasibility are necessary before drawing final conclusions.

Another conceptual reactor design for a multistep reaction consisting of

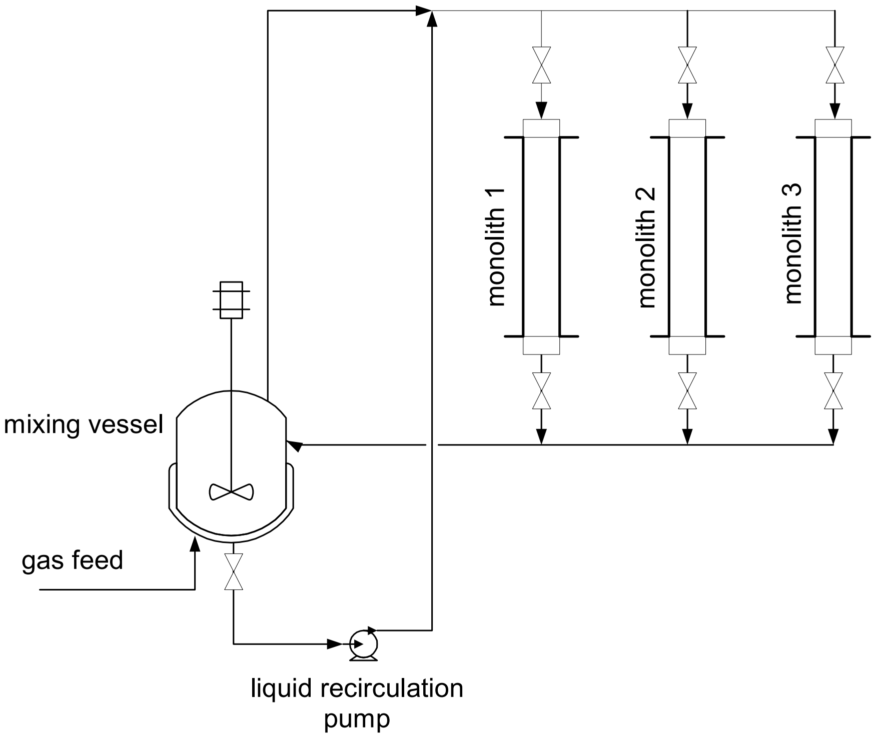

Figure 3: Example of conceptual process design retro fitting an existing slurry batch reactor with monoliths for a multistep reaction system

different catalytic steps is shown in Figure 3. The monoliths coated with the desired catalyst for each individual reaction steps are arranged in series. The existing stirred tank reactor can be used for mixing and for controlling the temperature of the reaction mixture. On attaining the desired conversion level in the first step, the reaction mixture can then be passed through the monolith containing the catalyst for the second step.

This concept is attractive for multistep reaction systems in which the different reaction steps are chemically compatible (e.g. multistep synthesis of Rossitol). An intermediate product purification step would, however, be necessary for multistep reaction systems in which the successive steps are not chemically compatible, e.g. synthesis of Ibuprofen.

Reference List

1. C. H. Bartholomew, 'Mechanisms of Catalyst Deactivation', *Applied Catalysis A: General*, 212 (**2001**) 17.

2. D. Y. Murzin and T. Salmi, 'Deactivation in Liquid Phase Heterogeneous Catalytic Reactions', *Trends in Chemical Engineering*, 8 (**2003**) 137.

3. D. Y. Murzin, E. Toukoniitty and J. Hajek, 'Deactivation in Liquid Phase Hydrogenation', *Reaction Kinetics and Catalysis Letters*, 83 (**2004**) 205.

4. J. A. Moulijn, A. E. van Diepen and F. Kapteijn, 'Catalyst Deactivation: Is It Predictable? What to Do?' *Applied Catalysis A: General*, 212 (**2001**) 3.

5. E. Varadaraj, 'Method for Producing Ibuprofen', EP 0400 892 A2 (**1990**) to Hoechst Celanese Corp.

6. F. Kapteijn, J. J. Heiszwolf, T. A. Nijhuis and J. A. Moulijn, 'Monoliths in Multiphase Catalytic Processes - Aspects and Prospects', *CATTECH*, 3 (**1999**) 24.

7. A. Cybulski and J. A. Moulijn, 'Monoliths in Heterogeneous Catalysis', *Catalysis Reviews - Science and Engineering*, 36 (**1994**) 179.

8. M. T. Kreutzer, P. Du, J. J. Heiszwolf, F. Kapteijn and J. A. Moulijn, 'Mass Transfer Characteristics of Three-Phase Monolithic Reactors', *Chemical Engineering Science*, 56 (**2001**) 6015.

9. M. T. Kreutzer, F. Kapteijn and J. A. Moulijn, 'Shouldn't Catalysts Shape Up? Structured Reactors in General and Gas-Liquid Monoliths in Particular.', *Catalysis Today*, 111 (**2006**) 111.

10. I. Hoek, T. A. Nijhuis, A. I. Stankiewicz and J. A. Moulijn, 'Performance of the Monolithic Stirrer Reactor: Applicability in Multi-Phase Processes', *Chemical Engineering Science*, 59 (**2004**) 4975.

11. T. A. Nijhuis, G. van Koten and J. A. Moulijn, 'Optimized Palladium Catalyst Systems for the Selective Liquid-Phase Hydrogenation of Functionalyzed Alkynes', *Applied Catalysis A: General*, 238 (**2003**) 259.

12. H. U. Blaser, C. Malan, B. Pugin, F. Spindler, H. Steiner and M. Studer, 'Selective Hydrogenation for Fine Chemicals: Recent Trends and New Developments', *Advanced Synthesis and Cataysis*, 345 (**2003**) 103.

13. P. N. Rylander, 'Catalytic Hydrogenation Over Platinum Metals', Academic Press, New York (**1967**).

14. R. L. Burwell Jr., 'Deuterium As a Tracer in Reactions of Hydrocarbons on Metallic Catalysts', *Accounts of Chemical Research*, 2 (**1969**) 289.

15. H. P. Boehm, 'Some Aspects of the Surface Chemistry of Carbon Black and Other Carbons', *Carbon*, 32 (**1994**) 759.

16. M. A. Fraga, E. Jordao, M. J. Mendes, M. M. A. Freitas, J. L. Faria and J. L. Figueiredo, 'Properties of Carbon-Supported Platinum Catalysts: Role of Carbon Surface Sites', *Journal of Catalysis*, 209 (**2002**) 355.

17. F. Rodriguez-Reinoso, 'The Role of Carbon Materials in Heterogeneous Catalysis', *Carbon*, 36 (**1998**) 159.

18. G. F. Froment, 'Modelling of Catalyst Deactivation', *Applied Catalysis A: General*, 212 (**2001**) 117.

Samenvatting

Gestructureerde reactoren voor deactiverende katalysatoren in de fijn-chemische industrie?

1. Achtergrond en Motivatie

Gekatalyseerde hydrogeneringsreacties spelen een belangrijke rol in de chemische industrie en worden veelal toegepast in de raffinage van ruwe olie en de productie van chemische specialiteiten. Het verlies van katalysatoractiviteit door deactivering is een belangrijke factor omdat dit in een meerderheid van de industriële hydrogeneringsprocessen wordt waargenomen. Hoewel dit voor de bulkprocessen in de aardolieraffinage een geaccepteerd en goed gedocumenteerd fenomeen is, is het belang hiervan in de fijn-chemische industrie verwaarloosd en is er slechts beperkte literatuur beschikbaar. In dit proefschrift wordt de hydrogenering van 4-isobutylacetofenon onderzocht als modelreactie met betrekking tot de fijn-chemische industrie. Deze reactie is de tweede stap in de meerstapssynthese van Ibuprofen waarbij aanzienlijke katalysatordeactivering werd waargenomen na één batch run. Het identificeren van de oorzaak van deactivering is de eerste en belangrijkste stap naar het verbeteren van de katalysatorstabiliteit. Een belangrijk aspect van dit onderzoek was daarom het identificeren van de oorzaak van katalysatordeactivering en het bestuderen van verwante aspecten (opheldering van het reactiepad, kinetische modellering inclusief het verlies van activiteit door deactivering) voor deze industrieel belangrijke reactie door het uitvoeren van systematische katalysatorkarakterisering en –testen.

Hoewel de mechanisch geroerde batchreactor met slurry katalysatordeeltjes nog steeds het 'werkpaard' van de fijn-chemische industrie is, is het gebruik van monolithische reactoren voorgesteld als alternatief. Monolieten zijn macroporeuze cordierietstructuren die gewoonlijk vele lange, rechte, parallelle kanalen van een vierkante dwarsdoorsnede bevatten. Door de lage specifieke oppervlakte van cordieriet (< 4 m^2/g), kunnen de wanden van de kanalen worden bedekt met een hoge oppervlakte katalysator voorafgaand aan de depositie van het katalytisch actieve metaal om zo de dispersie van het actieve metaal te verbeteren. Deze 'washcoat'-procedure heeft echter twee belangrijke tekortkomingen:

(*i*) de katalysator met het hoge specifieke drageroppervlak dringt samen met het actieve metaal de macroporiën in de kanaalwanden binnen, wat leidt tot een langere effectieve diffusielengte voor de reactanten. Het negeren van de aanwezigheid van actief metaal in de macroporiën leidt tot een overschatting van de katalysator effectiviteit

(*ii*) het aanbrengen van een washcoat bij vierkante kanalen leidt tot een niet-uniforme verdeling. In de hoeken wordt meer afgezet dan op de vlakke delen van de kanaalwanden van het monoliet (***Hoofdstuk 1***).

Een ander aspect van dit onderzoek was om een betere washcoat-techniek te ontwikkelen die de macroporiën blokkeerde om zo een uniforme afzetting te verkrijgen en de bovengenoemde problemen te vermijden. De selectieve hydrogenering van *3*-methyl-*1*-pentyn-*3*-ol tot *3*-methyl-*1*-penten-*3*-ol over Pd/SiO_2 werd gekozen als model reactiesysteem om monolieten met geoptimaliseerde kanaalgeometrie te testen omdat gerapporteerd is dat deze katalysator stabiel is voor deze reactie. Daarnaast wordt ook de haalbaarheid om gestructureerde reactoren te gebruiken voor deactiverende hydrogeneringssystemen geëvalueerd voor de fijnchemische industrie.

2. Samenvatting

2.1. Selectieve Hydrogenering van 4-isobutylacetofenon

2.1.1. Katalysator en Drager Selectie

De selectieve hydrogenering van *4*-IBAP omvat de selectieve reductie van de functionele carbonyl groep naar de bijbehorende alcohol. Pd staat bekend om het selectief hydrogeneren van deze functionele carbonyl groep en werd daarom geprefereerd als metaal. Hoewel een basische drager (zoals $CaCO_3$) ideaal gezien de selectiviteit naar *4*-IBPE zou maximaliseren (door het voorkomen van zuur-gekatalyseerde dehydratatie naar *4*-IBEB), heeft het lage specifiek oppervlak een negatief effect op de Pd dispersie en de bijbehorende activiteit (***Hoofdstuk 3***). Daarnaast waarborgt het gebruik van een basische drager geen volledige selectiviteit naar het gewenste alcoholproduct, omdat Pd ook een goede katalysator is voor hydrogenolyse. De afweging tussen een basische drager met een laag oppervlak

($CaCO_3$) en de conventioneel hoge oppervlakte dragers (SiO_2, aktieve kool) welke matig zuur zijn, resulteerde uiteindelijk in een zelf bereide Pd/SiO_2 katalysator. Deze katalysator toonde de hoogste activiteit en selectiviteit gedurende het katalysator onderzoek (***Hoofdstuk 3***).

2.1.2. Reactiepad

In een typische 4-IBAP hydrogenering met Pd/SiO_2 bereikte de selectiviteit naar het gewenste 4-IBPE product een maximum waarna de vorming van ongewenst 4-IBEB werd waargenomen. De vorming van een styreen als tussenproduct (door dehydratatie van 4-IBPE) kon niet worden bevestigd door GC analyse. Kennis over het daadwerkelijke C-O splitsingspad (door directe hydrogenolyse of door dehydratatie-hydrogenering) van 4-IBPE was benodigd omdat het tussenproduct styreen verantwoordelijk zou kunnen zijn voor de waargenomen katalysator deactivering (wordt later besproken). ***Hoofdstuk 2*** behandelt de identificatie van het C-O splitsingspad over drie katalysatoren, Pd/SiO_2, een commerciële Pd/C en 'Pd-zwart'. Gebaseerd op (^1H, ^2H, ^{13}C) NMR analyses, werd er geconcludeerd dat de C-O splitsing van 4-IBPE verliep via directe hydrogenolyse van de C-O binding over Pd/SiO_2, terwijl een dehydratatie-hydrogeneringspad werd waargenomen voor Pd/C. Experimenten uitgevoerd met ongedragen Pd-zwart wezen uit dat waterstof op het metaal oppervlak de verantwoordelijk was voor directe hydrogenolyse op Pd zonder enige invloed van de drager.

2.1.3. Katalysatordeactivering

Voor zowel Pd/SiO_2 en Pd/C werd na een enkele batch run al een flink verlies in katalytische activiteit waargenomen. Voor alle verdere studies had Pd/SiO_2 de voorkeur omdat hiervoor thermische analysetechnieken gebruikt kunnen worden om katalysatordeactivering te bestuderen. Vijf theoretisch mogelijke redenen voor katalysatordeactivering zijn: (*i*) polymerisatie van het tussenproduct styreen gevormd door de dehydratatie van 4-IBPE (*ii*) De sterke adsorptie van H_2O, vrijgekomen door de hydrogenolyse van 4-IBPE, op de katalysator (*iii*) de aanwezigheid van onzuiverheden in commercieel verkrijgbare SiO_2 drager of in de reactanten (*iv*) kristalgroei van Pd (*v*) condensatie van 4-IBAP en 4-IBPE moleculen door vorming van oligomeren. De verse en gebruikte Pd/SiO_2 katalysatoren werden geanalyseerd met een verscheidene thermische (TGA, TPO-MS), microscopische (TEM) en spectroscopische (LEIS, DRIFT) technieken (***Hoofdstuk** 3*) om het mechanisme van deactivering te achterhalen. Samenvattend, is de katalysator deactivering gedurende de hydrogeneringvan 4-IBAP over Pd/SiO_2 een gecombineerd effect van (*i*) oligomerisatie van 4-IBAP (*ii*) sterke H_2O remming en (*iii*) Pd kristalgroei. De hoofdconclusie van ***Hoofdstuk 3*** is dat de zuurheid van de drager een belangrijke rol speelt in de deactivering van aromatische ketonen over Pd gebaseerde katalysatoren. De toepassing van een neutrale drager is het meest ideaal, maar vereist verdere katalysatorontwikkeling.

2.1.4. Kinetische Modellering

Over het algemeen wordt kinetische modellering uitgevoerd voor het opschalen van reactoren van laboratoriumschaal naar reactoren op pilot-schaal en later naar industriële schaal. De bepaling van nauwkeurige kinetiek onder katalysatordeactiveringsomstandigheden, is een zeer uitdagende taak en kan in de meeste gevallen slechts als een empirische oplossing worden gezien. Dit is toe te schrijven aan het feit dat deactivering een zeer complex fenomeen is, dat vele onzekere parameters op het katalysatorniveau impliceert die zelden nauwkeurig kunnen worden verklaard. Desalniettemin is getracht om de kinetiek te bepalen voor deze industrieel belangrijke reactie tijdens het verlies van katalysatoractiviteit door deactivering (***Hoofdstuk** 4*). De onzekerheden in het model zijn verminderd door kennis van het exacte reactiepad (***Hoofdstuk** 2*) en de deactiveringsverschijnselen (***Hoofdstuk** 3*). Een uitvoerig model werd ontwikkeld waarin de effecten van concentraties 4-IBAP, H_2 partiaaldruk, H_2O concentraties en katalysatorconcentraties over een temperatuursbereik van 333 - 373 K werden verwerkt. Om een rigoureuzer kinetisch model te ontwikkelen, dat voor opschaling van reactoren kan worden gebruikt, zou de deactivering in een doorstroomreactor op lage omzettingsniveaus moeten worden bepaald. Eenzelfde benadering als beschreven in ***Hoofdstuk 4*** kan worden gevolgd om het effect te bestuderen van de diverse operationele variabelen op de katalysatorprestaties en het ontwikkelen van het kinetische model.

2.2. Selectieve Hydrogenering van 3-methyl-1-pentyn-3-ol met monolieten

Aangezien de meeste commercieel beschikbare monolieten een vierkante kanaal geometrie hebben, leidt het aanbrengen van een dragermateriaal of katalysator gewoonlijk tot een niet-uniforme washcoatdikte. Door de aanwezigheid van macroporiën bestaat er daarnaast de mogelijkheid dat het katalytisch actieve materiaal diep hierin dringt waardoor het niet optimaal wordt gebruikt. ***Hoofdstuk 5*** beschrijft een techniek waarmee een uniforme washcoatdikte verkregen kan worden en welke verhindert dat het actieve metaal de macroporiën binnendringt. Niet-poreus α-Al_2O_3 is gebruikt als vuller voor de macroporiën. Vervolgens werd de SiO_2 drager gewashcoat op deze monolieten gevolgd door de impregnatie van het actieve metaal. Electron Probe Micro Analysis (EPMA) bevestigde dat het actieve metaal alleen aanwezig was in een dunne buitenlaag. FEM berekeningen toonden aan dat het negeren van de aanwezigheid van actief metaal in de macroporiën leidt tot een overschatting van de katalysatoreffectiviteit, en met name de waarde van de Thiele modulus. De uniforme diffusielengte in geoptimaliseerde monolieten leidde tot een hogere selectiviteit en opbrengst van het gewenste tussenproduct tijdens de hydrogenering van 3-methyl-1-pentyn-3 bestudeerd onder transportgelimiteerde condities.

3. Gestructureerde reactoren voor deactiverende katalysatoren in de fijn-chemische industrie?

Een belangrijke conclusie van dit onderzoek is dat de katalysatordeactivering een belangrijke variabele is tijdens de hydrogenering van aromatische ketonen, een voorbeeld van een industrieel belangrijke reactie. Gezien de aanzienlijke katalysatordeactivering lijkt het gebruik van een gestructureerde (monolithische) reactor als vervanging voor conventionele slurry reactoren onaantrekkelijk. Door een ingenieus aantrekkelijk reactorontwerp kan deze monoliet reactor echter nog wel een haalbare optie worden. Bij een aangepast reactorsysteem (***zie hoofdstuk 6, pag. 134***) kan de ene monoliet gebruikt worden voor de reactie terwijl de ander op hetzelfde moment geregenereerd wordt in een swing-`operatie. Dit maakt het gebruik van de monolithische katalysator gedurende een langere periode mogelijk, op voorwaarde dat de katalysator geregenereerd kan worden. De voordelen van dit ontwerp zijn dat de bestaande infrastructuur van een fijn-chemische productiefaciliteit kan worden gebruikt en dat het monolithische reactorconcept zelfs voor een deactiverend systeem kan worden toegepast, waardoor de stap waarin de katalysator wordt geregenereerd, overbodig wordt. Verder onderzoek betreffende efficiënte katalysatorregeneratie evenals economische haalbaarheid is noodzakelijk voor het trekken van definitieve conclusies.

Een ander conceptueel reactorontwerp voor een meerstapsreactie met verschillende katalytische stappen, wordt ook voorgesteld (***zie hoofdstuk 6, pag. 134***). Voor elke individuele reactiestap wordt de monoliet gecoat met de gewenste katalysator en parallel gerangschikt. Het bestaande geroerde vat kan gebruikt worden voor het mengen en controleren van de temperatuur van het reactiemengsel. Bij het bereiken van de gewenste conversie in de eerste stap kan het reactiemengsel vervolgens door de kanalen van de monolietkatalysator voor de tweede reactiestap geleid worden. Dit concept is aantrekkelijk voor meerstapsreactiesystemen waarin de verschillende reactiestappen chemisch compatibel zijn (bijvoorbeeld de multistep synthese van Rossitol). Een tussenstap om het productmengsel te zuiveren zal echter nodig zijn voor meerstapsreactiesystemen waarin opeenvolgende stappen niet chemisch compatibel zijn, zoals de synthese van Ibuprofen.

Dankwoord

This research work culminating in a PhD thesis would not have been possible without the selfless contribution of many people. I take this opportunity to express my gratitude to every individual who has contributed in any possible way towards the completion of this thesis.

Prof. dr. J. A. Moulijn and prof. dr. F. Kapteijn, I thank you two for giving me an opportunity to pursue research work in your world famous group. Prof. Moulijn, I appreciate the trust and confidence you have shown in my abilities, especially considering the fact that I did not have a MSc. degree prior to starting with the PhD research. I hope I have lived up to your expectations. Prof. Kapteijn, I appreciate your patience in dealing with the impatience I might have shown sometimes in submitting research articles for publications. Your decision to appoint me as a teaching assistant for the 'Catalysis and Reaction Engineering' course proved to be very helpful during my job interviews. Finally, I thank you and prof. Moulijn for your efforts in organizing a two-month extension of my contract.

I also thank STW (dr. Chris Marcelis), Quest International (dr. A. J. A. van der Weerdt) and BASF Nederland B.V. (dr. A. E. W. Beers) for providing financial assistance for the research program and useful inputs during the progress meetings.

Els and Elly, thank you for facilitating appointments with prof. Moulijn and prof. Kapteijn. Els, you surely played a motivating role in encouraging me to speak Dutch during the initial years. Bart, thanks for the assistance with the catalyst characterization setups and the discussions about the causes of catalyst deactivation. Harrie, thanks for all your help related to the electronics and data acquisition part of my setup. It would definitely be a difficult task to complete my PhD on time without the assistance of you talented technicians. Sander, thanks for the prompt delivery of results of the catalyst characterization studies. Johan, I enjoyed the innumerable discussions about my thesis and journal co-authorship issues. Good luck with your career!

I also appreciate the contribution of my MSc. students Nadine, Brahim and Akshay. Akshay, although your contribution doesn't figure extensively in this thesis, it was nevertheless an invaluable experience supervising you, as you were my first student. Brahim, I consider myself lucky having the opportunity to supervise a talented student such as you. Your contribution resulted in nearly an entire chapter in this thesis. Thanks for helping me out whenever I had problems with my car. Nadine, it was a great experience working with you. Though you had a seemingly difficult project, I'm happy that your contribution resulted in an article in the Journal of Catalysis.

I would also like to thank the staff members (dr. Michiel Makkee, dr. Guido Mul and dr. Michiel Kreutzer) for their invaluable contribution to my project. Dr. Makkee, your (seemingly endless) critical comments on my work definitely helped me improve its quality. Dr. Kreutzer, thank you for your contribution towards improving the quality of the chapter dealing with monoliths. Dr. Mul, I appreciate your suggestions regarding the ATR-FTIR spectroscopy and deuteration studies.

I would also like to include a word of praise for past and present colleagues for providing a pleasant working atmosphere in the lab. Tilman, thank you for getting me started with my PhD research, and the numerous discussions about scientific and non-scientific issues. The cheerful colleagues in room 0.484 (Jasper, Nari, Asun) also deserve special mention for the innumerable discussions on just about everything. Jasper, I appreciate your efforts to teach me '*useful*' Dutch expressions, though I can probably never use them socially. Nari, I enjoyed eating authentic Japanese cuisine at your place. Asun, thanks for the positive discussions on the catalyst deactivation work and also for proof reading my thesis. I wish you all the best for your future.

My '*bestuursgenootjes*' (Juliet, Fokje, Roel and Mark) at the Delftse Studenten Tennis Vereniging: Obvius, it was a great experience working with all of you. The dinners every Thursday, the tennis activities and the occasional outings were an excellent opportunity for me to experience the Dutch student life.

The regulars at the sports centre (Mahsa, Aylin, Oscar, Jelan and Mark), I am happy that we have become good friends over the last year. I will surely miss the dinners, (table) tennis games, movie marathons, the beach outings in the summers and the Saturday night outs at discotheques. Oscar, Jelan and Aylin, I wish you all the best for your PhD theses.

I would also like to express my gratitude to a few Indian families in the Netherlands (Pandav family and Kulkarni family) for being so hospitable that I rarely felt homesick. I always looked forward to visiting you to enjoy the delicious Indian food. Govert, thanks for being such a kind and helpful landlord. It definitely made life easy for me in the Netherlands.

Last, but not the least, my family deserves a special mention for the successful completion of this thesis. Prachi and Vijay, thanks for the continuous motivation and support for all these years and for your excellent hospitality during my visits to you in Denver. Aai and Baba, thank you very much for your guidance and support in everything that I have done so far. With your blessings and well wishes, I am confident to go on and be an achiever!

Nakul

June 2007
Pune, India

List of Publications and Presentations

Publications

1. "Diffusion- reaction characteristics in monolithic catalysts", N. Thakar, M. T. Kreutzer, B. Daouairi, J. H. L. Voncken, F. Kapteijn and J. A. Moulijn, Submitted to *Industrial & Engineering Chemistry Research*

2. "Modeling kinetics and deactivation for the selective hydrogenation of an aromatic ketone over Pd/SiO_2", N. Thakar, R. J. Berger, F. Kapteijn and J. A. Moulijn, *Chemical Engineering Science* (**2007**) *in press.*

3. "Evaluation of deactivation mechanisms of Pd catalyzed hydrogenation of 4-isobutylacetophenone", N. Thakar, T. J. Schildhauer, W. Buijs, F. Kapteijn and J. A. Moulijn, *Journal of Catalysis* 248 (**2007**) 249.

4. "Deuteration study to elucidate hydrogenolysis of benzylic alcohols over supported palladium catalysts", N. Thakar, N. F. Polder, K. Djanashvili, H. van Bekkum, F. Kapteijn and J. A. Moulijn, *Journal of Catalysis* 246 (**2007**) 344.

5. "Modeling of hydrogenation of maleic acid in a bubble column slurry reactor", N. Thakar, R. Jaganathan, R. V. Chaudhari and P. L. Mills, *AIChE Journal* 49 (**2003**) 3199.

Oral and Poster presentations

1. "On the use of a priming washcoat to improve diffusion-reaction characteristics in structured catalysts", N. Thakar, M. T. Kreutzer, B. Daouairi, F. Kapteijn , J. A. Moulijn and G. Mul, Oral presentation at EUROPACAT-8, Turku, Finland, Aug. 2007.

2. “Towards structured reactors for the selective hydrogenation of an aromatic ketone”, N. Thakar, B. Daouairi, M. T. Kreutzer, F. Kapteijn and J. A. Moulijn, Oral presentation at CAMURE-6, Pune, India, Jan. 2007.

3. “Elucidating catalyst deactivation during hydrogenation of an aromatic ketone using LEIS”, N. Thakar, F. Kapteijn, J. A. Moulijn, A. Knoester and H. H. Brongersma, Oral presentation at 232nd ACS National Meeting, San Francisco, USA, Sept. 2006

4. “Modeling kinetics and deactivation for the selective hydrogenation of an aromatic ketone”, N. Thakar, R. J. Berger, F. Kapteijn and J. A. Moulijn, Oral presentation at NPS-5, Veldhoven, The Netherlands, Oct. 2006

5. “Modeling kinetics and deactivation for the selective hydrogenation of an aromatic ketone”, N. Thakar, R. J. Berger, F. Kapteijn and J. A. Moulijn, Poster presentation at ISCRE-19, Berlin, Germany, Sept. 2006

6. “Utilizing structured reactors for the hydrogenation of an aromatic ketone”, N. Thakar, B. Daouairi, F. Kaptejn and J. A. Moulijn, Oral presentation at NCCC-VII, Noordwijkerhout, The Netherlands, Mar. 2006

7. “Hydrogenation of 4-isobutylacetophenone over Pd/SiO_2: Catalyst performance and stability”, N. Thakar, A. Bueno-Lopez, T. J. Schildhauer, F. Kapteijn and J. A. Moulijn, Oral presentation at the 19th NAM, Philadelphia, USA, May 2005.

Curriculum Vitae

Nakul Thakar was born on 9th March 1980 in Pune, India. After successfully receiving his undergraduate degree of Bachelors in Polymer Engineering from the University of Pune in August 2001, he began work as a research assistant in the group of dr. R. V. Chaudhari at the National Chemical Laboratory (NCL), Pune. The project involved simulating and optimizing the performance of a commercially operated reactor. A short meeting with prof. dr. Jacob A. Moulijn at NCL secured him admission for a PhD program in the Catalysis Engineering group of prof. Moulijn and prof. Kapteijn at the Delft University of Technology, The Netherlands.

He started work on his PhD research in November 2002, focusing on catalyst deactivation occurring during hydrogenation reactions in the fine chemicals industry and the feasibility of using monolithic reactors for similar systems. The results of this research are found in this thesis. This challenging project enabled him to develop technical skills in chemistry as well as in chemical engineering. He also assisted prof. dr. Freek Kapteijn as a teaching assistant for the graduate course of Catalysis and Reactor Engineering and supervised the research projects of three MSc. students during his PhD.

After receiving multiple job offers from leading chemical companies, Nakul is working with BP in London, U.K. since July 2007.